UNIVERSITY OF BELGRADE

FACULTY OF TECHNOLOGY AND METALLURGY

Abdusalam Drah

FUNCTIONALIZATION OF ALUMINIUM OXIDE FOR COMPOSITES BASED ON UNSATURATED POLYESTER RESINS SYNTHESIZED FROM WASTE POLY(ETHYLENE TEREPHTHALATE)

Doctoral Dissertation

Belgrade, 2020

UNIVERZITET U BEOGRADU

TEHNOLOŠKO-METALURŠKI FAKULTET

Abdusalam Drah

FUNKCIONALIZACIJA ČESTICA ALUMINIJUM-OKSIDA ZA KOMPOZITE NA BAZI NEZASIĆENIH POLIESTARSKIH SMOLA DOBIJENIH IZ RECIKLOVANOG POLI(ETILENTEREFTALATA)

doktorska disertacija

Beograd, 2020

Mentor:

        Dr **Aleksandar Marinković**, vanredni profesor,
        Univerzitet u Beogradu, Tehnološko-metalurški fakultet

Članovi komisije:

        Dr **Radmila Jančić-Heinmann**, redovni profesor,
        Univerzitet u Beogradu, Tehnološko-metalurški fakultet

        Dr Vesna Radojević, redovni profesor,
        Univerzitet u Beogradu, Tehnološko-metalurški fakultet

        Dr **Zlate Veličković**, docent,
        Univerzitet odbrane, Vojna akademija

        Dr Tihomir Kovačević, naučni saradnik,
        Vojnotehnički institut, Beograd

Datum odbrane:_____

Functionalization of aluminium oxide for composites based on unsaturated polyester resins synthesized from waste poly(ethylene terephthalate

SUMMARY

The aim of this doctoral dissertation is investigation of physical and chemical properties of composites based on unsaturated polyester resin (UPR) resin, produced from the product of the catalytic depolymerization of poly(ethylene terephthalate) (PET) in the excess of 1,2-propylene glycol (PG), with the reinforcement of nano-/micro-scaled alumina particles. There were two types of alumina fillers: commercial (c-Al_2O_3) and synthesized one doped with Fe (Fe-Al_2O_3). To additionally improve properties of UPR resin, alumina particles were modified by following silanes: Vinyltris(2-methoxyethoxy)-silane (VTMOEO), 3-methacryloxypropyl-trimethoxysilane (MEMO) and 3-(aminopropyl)trimethoxysilane (APTMS) as well as methyl ester of linseed oil fatty acids (biodiesel - BD). The influence of the pristine and modified alumina particles size and loading on the mechanical, dynamic-mechanical and thermal properties of the obtained composites was studied. Synthesized UPR resin is qualitatively characterized by NMR and FTIR analysis, while alumina particles were examined by XRD, FTIR, SEM and Image analysis to obtain their morphological characteristics. The best tensile strength was achieved by incorporating the 1 wt% of VTMOEO modified Fe-Al_2O_3 compared to pure UPR resin, while the micro Vickers hardness was significantly improved in all analyzed samples. The results of DMA showed significant influence of the embedding the alumina particles into UPR matrix. It was remarked that Fe-Al_2O3 possessed higher thermal stability in comparison to c-Al_2O_3.

Three-dimensionally ordered macroporous (3DOM) γ-alumina was synthesized using PMMA as porogen agent. XRD measurements confirmed the γ-alumina crystal phase, while SEM confirmed macro and micro porosity. Synthesized adsorbent was used for Pb^{2+}, Ni^{2+}, and Cd^{2+} removal, and the results showed that pH is an important parameter which control effectiveness of pollutant removal. The quality of the isotherm modelling of adsorption data was proved by the correlation coefficients and error functions, and the best adsorption model was found to be Freundlich isotherm for Pb^{2+} removal and Dubinin-Radushkevich isotherm for Ni^{2+} and Cd^{2+} removal. The ΔH^0 value of 9.59 kJ/mol for Pb^{2+}, 2.45 kJ/mol for Ni^{2+} and 6.20 kJ/mol for Cd^{2+} adsorption onto γ-alumina indicated the dominance of physical adsorption. The kinetic data of the adsorption on all the investigated adsorbents were well fitted with the pseudo-second-order kinetic and Weber-Morris models, suggesting that the rate-limiting step was diffusion rather than chemical sorption. Calculated activation energies, E_a, of 4.60 kJ/mol for Ni^{2+}, 0.58 kJ/mol for Cd^{2+} and 5.71 kJ/mol for Pb^{2+} indicate that the adsorption of all three ions onto γ-alumina is a mainly physical adsorption process.

The presented technological procedures of waste PET and ceramic material utilization, have shown that they can be used to obtain useful products with good mechanical and relatively satisfactory thermal characteristics. Presented innovative technology involves the processing of municipal solid waste, which represents a national interest in favoring this type of technology for the development/implementation of the green and circular economy, as is the case in all developed countries.

Keywords: *waste PET based composites, alumina nano/micro-particles, mechanical properties, thermal properties, silane functionalization, heavy metal ions removal*
Scientific area: Technological Engineering
Scientific sub-area: Material Engineering
UDC number:

Funkcionalizacija čestica aluminijum-oksida za kompozite na bazi nezasićenih poliestarskih smola dobijenih iz reciklovanog poli(etilentereftalata)

REZIME

Cilj ove doktorske disertacije je ispitivanje fizičkih i hemijskih svojstava kompozita na bazi nezasićene smole poliestera (NZPE) sintetisanoj od proizvoda katalitičke depolimerizacije poli (etilen tereftalata) (PET) u višku od 1,2-propilena glikol (PG) sa ojačanjem od nano/mikro čestica alumine. Korišćena su dva tipa alumine: komercijalna (c-Al_2O_3) i sintetizovana dopirana sa Fe (Fe-Al_2O_3). Da bi dodatno poboljšali gore navedena svojstva NZPE smole, čestice alumine su modifikovane sledećim silanima: Viniltris (2-metoksietoksi)silan (VTMOEO), 3-metakriloksipropil-trimetoksisilan (MEMO) i 3-(aminopropil) trimetoksizilan (APTMS) kao metil estri masnih kiselina lanenog ulja (biodizel - BD). Ispitan je uticaj veličine čestica i udela netretiranih/modifikovanih čestica alumine na mehanička, dinamičko-mehanička i termička svojstva dobijenih kompozita. Sintetisana NZPE smola kvalitativno je okarakterisana korišćenjem NMR i FTIR tehnika, dok su čestice alumine ispitivane uz pomoć XRD, FTIR, SEM i analizom slike kako bi se dobile njihove morfološke karakteristike. Najbolja zatezna čvrstoća postignuta je udelom 1 mas% VTMOEO modifikovanog Fe-Al_2O_3 u poređenju sa čistom NZPE smolom, dok je mikro Vickers tvrdoća značajno poboljšana u svim analiziranim uzorcima. Rezultati DMA pokazali su značajan uticaj ugradnje čestica alumine u NZPE matricu. Primećeno je da Fe-Al_2O_3 glinica poseduje veću toplotnu stabilnost u poređenju sa c-Al_2O_3.

Trodimenzionalno orijentisana makroporozna (3DOM) γ-alimina sintetisana je koristeći PMMA kao agens za dobijanje poroznosti konačnog proizvoda. XRD merenja su potvrdila kristalnu fazu γ-alumine, dok su mikro i makro pore potvrđene SEM analizom. Sintetisani adsorbenti su korišćenii za uklanjanje Pb^{2+}, Ni^{2+} i Cd^{2+} jona, gde se pokazalo da pH vrednost predstavlja esencijalni parametar za efikasno uklanjanje navedenih polutanata iz vode. Kvalitet adsorpcije je potvrđen modelovanjem izotermi, gde se najadekvatnijim modelom za uklanjanje Pb^{2+} pokazala Frojndlihova, a za uklanjanje Ni^{2+} i Cd^{2+} Dablin-Raduškevičova izoterma. Vrednosti entalpije od 9.59 kJ/mol za Pb^{2+}, 2.45 kJ/mol za Ni^{2+} i 6.20 kJ/mol for Cd^{2+} ukazuju na dominantnu fizičku adsorpciju. Kinetički podaci adsorpcije na svim ispitivanim adsorbentima su u dobroj korelaciji sa kinetičkim modelima pseudo drugog reda i Veber-Morrisom, što sugeriše da je adsorpcija difuziono kontrolisana. Izračunate energije aktivacije, E_a, od 4.60 kJ/mol for Ni^{2+}, 0.58 kJ/mol for Cd^{2+} and 5.71 kJ/mol for Pb^{2+} dodatno su potvrdile da je adsorpcija navedenih jona na aluminu fizičke prirode.

Predstavljeni tehnološki postupci upotrebe otpadnog PET i keramičkog materijala pokazali su mogućnost dobijanja korisnih proizvoda sa dobrim mehaničkim i relativno zadovoljavajućim termičkim karakteristikama. Predstavljena inovativna tehnologija uključuje preradu čvrstog komunalnog otpada, što predstavlja nacionalni interes davanja prednosti ovoj vrsti tehnologije za razvoj/implementaciju zelene i cirkularne ekonomije, kao što je to slučaj u svim razvijenim zemljama

Ključne reči: *kompoziti na bazi otpadnog PET-a, nano/mikro čestice alumine, mehanička svojstva, termička svojstva, funkcionalizacija silanima, uklanjanje jona teških metala*
Naučna oblast: Tehnološko inženjerstvo
Uža naučna oblast: Inženjerstvo materijala
UDK broj:

LIST OF ABBREVIATIONS AND SYMBOLS

PET - (polyethylene terephthalate)
UPR - Unsaturated polyester resin
MA - Maleic anhydride
c-Al_2O_3 - commercial nano-scaled alumina
Fe-Al_2O_3 - Fe doped alumina
PG - 1,2-propylene glycol
TBT - Tetrabutyl titanate
EG - Ethylene glycol
VTMOEO - vinyl tris(2-methoxyethoxy)-silane
MEMO - 3-methacryloxypropyl-trimethoxysilane
APTMS - 3-(aminopropyl)trimethoxysilane
BD - Methyl ester of linseed oil fatty acids (biodiesel)
DEG - Diethylene glycol
TBBPA - Tertrabromobisphenol A
TMPAE - Trimethylolpropane mono allyl ether
PA - Phthalic anhydride
T_g - Glass transition temperature
AN - Acid number
HQ - Hydroquinone
BHAT - Bis(2-hydroxyalkyl)terephthalate
TEG - Triethylene glycol
[bmim]Br - 1-butyl-3-methylimidazolium bromide
BHET - Bis(2-hydroxyethyl)terephthalate
ANi - Aluminum nitrate
CA - Citric acid
PMC - Polymer matrix composites
PMMA - Poly(methyl methacrylate)
PP-g-MA - Polypropylene grafted with MA
POEGMA - Poly(oligo (ethylene glycol) methyl ether methacrylate)
SI-ATRP - Surface-initiated atom-transfer radical polymerization
APTS - 3-Aminopropyl)triethoxysilane
BIBB - 2-bromoisobutyryl bromide
EVA - Ethylene-vinyl acetate
UTAL - Untreated alumina
TAL - Treated alumina
σ_t - Tensile strength
σ_f - Flexural strength
E - Young's modulus
HDPE - High-density polyethylene
SEM - Scanning electron microscope
TGA - Thermogravimetric analysis
DSC - Differential scanning calorimetry
PAI - poly(amide-imide)
DMA - Dynamic-mechanical analysis
G' - Storage modulus
G" - Loss modulus
$\tan\delta$ - Damping factor
ALC - Commercial alumina

ALS - Synthesized alumina
THF - Tetrahydrofuran
$FeCl_3 \cdot 6H_2O$ - Iron(III)-chloride
$Al_2(OH)_5Cl \cdot 2.5H_2O$ - Locron L
HV - Hydroxyl value
KBr - Potassium(I)-bromide
KOH - Potassium(I)-hydroxide
VH - Micro Vickers hardness
NMR - Nuclear magnetic spectroscopy
XRD -X-ray diffraction
T_{max} - Maximum curing temperature
$T_{0.05}$ - Temperature for weight loss of 5%
ν - Cross-linking density
G'_{RP} - Storage modulus in rubbery plateau
G'_{GS} - Storage modulus in glassy state
C - Coefficient of reinforcement
KPS - Potassium persulfate
PEG - poly(ethylene glycol)
AAS - Atomic adsorption standard
$Pb(NO_3)_2$ - Lead(II)-nitrate
HNO_3 - Nitric acid
$Ni(NO_3)_2 \cdot 6H_2O$ - Nickel(II)-nitrate hexahydrate
Pb^{2+} - Lead ion
Cd^{2+} - Cadmium ion
Ni^{2+} - Nickel ion
MMA - Methyl metacrylate monomer
LDH - Layered double hydroxide
NO^{3-} - Nitrate ion
CO_2 - Carbon(IV)-oxide
Na^+ - Sodium ion
ATR-FTIR - Attenuated total reflactance-Fourier-transform infrared spectroscopy
M_v - Molecular weight determined by viscosity measurements
η - Intrinsic viscosity
3DOM - Three dimensionally ordered macroporous materials
CCT - Colloidal crystal template
PS - Polystyrene
pH_{PZC} - pH values at the point of zero charge
q_e - Adsorbed amount of metal ions per unit weight of the adsorbent at equilibrium
C_e - Equilibrium concentration of metal ions
q_m - Maximum theoretical Pb^{2+}, Ni^{2+} and Cd^{2+} capacity
K_L - Langmuir constant
K_F - Freundlich constant
n - Constant that gives information about the degree of heterogeneity of the surface sites
D-R - Dubinine-Radushkevich isotherm model
K_{DR} - D-R constant
Q_0 - Intercept yields the adsorption capacity
ΔG^0 - Gibbs free energy
ΔH^0 - Entalpy
ΔS^0 - Entropy
R - Universal gas constant

K_{L1} - Non-dimensional constant

R_L - Separation factor

C_0 - Initial adsorbent concentration

PSO - Pseudo-second order

k_w - Intra-particle diffusion rate constant

k_2 - Pseudo-second order rate adsorption constant

k_0 - Temperature independent factor

E_a - Activation energy

LIST OF FIGURES

LIST OF TABLES

TABLE OF CONTENTS

1. INTRODUCTION

Rapid technological development in many fields leads to reducing of non-renewable resources, which demands finding new solutions for satisfy all needs of modern humanity. Tracing that trend, great efforts have been made in development of sustainable and advanced technologies which include usage of alternative energy and raw material resources. Conversely, phenomenon caused by globalization and mass production as a consequence, leads to generating of huge amount of waste materials. The great part in such waste belongs to polymeric materials which possess short applicable time (primarily bottles and food packages). Polymeric waste cause severe problems worldwide, especially in non-developed regions since its proper treatment, including collecting, separation and sorting is expensive and technologically demanded.

Poly(ethylene terephthalate) (PET), among other commercial polymeric materials, is the most used material in textile, food, electronic, automotive and other industries. Such industries and their customers generate huge amount of waste PET, which needs to be subjected to appropriate recycling processes, respecting the principles of green and circular economy. Additionally, various environmental, economic and energetic benefits are achieved by PET recycling which are reflected in preservation of natural resources, lowering the energy consumption as well as reduced disposal of waste [1–3]. There are myriad recycling processes for treatment of waste PET, but the most economically and environmentally promising are the chemical ones (tertiary recycling) [4]. The products obtained by tertiary recycling processes are monomers from which PET consists (total depolymerization) and oligomers (partially depolimerization). Monomers/oligomers, used as obtained or purified, can be employed in synthesis of unsaturated polyester, epoxy or alkyd resins [5–7].

Unsaturated polyester resins (UPRs) with polyurethanes represent a group of the most commonly used thermosetting matrices for obtaining the advanced composite materials [8]. Considering that UPR is a brittle material, the addition of reinforcements is necessary for obtaining the high-performance composites. The remarkable improvement of physical and chemical properties of UPRs can be tuned by addition of various types of organic or inorganic fillers such as: glass fibers, minerals, natural and synthetic polymers etc. [9–11]. The most commonly used reinforcements for UPR matrix are: silicon(IV)-oxide, nanocellulose and carbon nanotubes [12–14].

One of the most promising candidates for UPR matrix reinforcement is alumina. Alumina or aluminum oxide is an amphoteric oxide that exists in nature as the minerals corundum (Al_2O_3); diaspore ($Al_2O_3 \cdot H_2O$); gibbsite ($Al_2O_3 \cdot 3H_2O$); and most commonly as bauxite, which is an impure form of gibbsite. Alumina exists in numerous crystalline structures. Metastable phases may be irreversible translated to α-Al_2O_3 by an adequate thermal or hydroxylation treatments. The crystal structure of alumina consists from hexagonal and octahedral sites [15].

The subject of this study could be divided into three distinctive parts: 1) The synthesis of UPR resin through the reaction between dihydroxyl monomers, obtained by depolymerization of waste PET, and maleic anhydride (MA), 2) functionalization of commercial and Fe doped alumina and 3) preparation of composites based on UPR resin and pristine and/or functionalized alumina. The first step in the producing of UPR resin was obtaining the hydroxyl-terminated precursor (glycolyzate) by catalytic depolymerization of waste PET using 1,2-propylene glycol (PG). PG was used in excess towards waste PET (molar ratio PET:PG=1:1.2). The depolymerization was carried-out in presence of the tetrabutyl titanate (TBT) as a catalyst, without azeotropic removal of ethylene glycol (EG). Further on, the obtained glycolyzate reacted with MA which resulted in producing of UPR resin. The UPR was mixed together with various amount and type of alumina particles to obtain composite

materials. There were two types of alumina: nano-scaled commercial (c-Al$_2$O$_3$) and micro-scaled Fe doped alumina (Fe-Al$_2$O$_3$). The both types of alumina particles were subjected to functionalization by vinyl tris(2-methoxyethoxy)-silane (VTMOEO); 3-methacryloxypropyl-trimethoxysilane (MEMO), 3-(aminopropyl)trimethoxysilane (APTMS) (one step modification) and successive modification with APTMS in the first step followed by methyl ester of linseed oil fatty acids (biodiesel, BD) in the second step.

The influence of alumina type, filler loading and type of functionalization on mechanical and thermal properties of corresponding composites was investigated in this study. Literature data, related to subject of interest, are very scarce which makes this research significant. Data obtained for composites with pristine alumina particles were referent values used for comparative analysis.

The obtaining of the composites with uniformly distributed alumina capable for interaction with polymeric matrix represents unique scientific challenge and motive for experiments included in this thesis. Particles affinity toward agglomeration and heterogeneous distribution within the UPR matrix were overcome by optimization of filler type and loading which resulted in high performance composites. Experimental results broadened the knowledge about alumina functionalization, its application as a reinforcement in polymeric matrix, as well as mutually influence and connection of functional groups upon filler surface. Moreover, the contribution in thorough understanding of interactions between pristine and modified alumina with UPR matrix, reflected in greater compatibility and thus better composite performance, was achieved.

2. THEORETICAL SECTION

2.1. Literature review of procedures for synthesis of unsaturated polyester resins

Technologies for production of UPRs have been known since 1930s and recently have reached the maximum level. UPRs are one of the most used thermosetting polymers with a wide range of applications due to their low cost, versatility and ability to undergo various post-polymerization reactions [16]. In general, UPRs are condensation products of unsaturated acids or anhydrides and two-functionalized alcohols (diols). The synthesis of UPR resin could be performed by bulk or azeotropic polycondensation giving plausible results at both, laboratory and industrial level [17]. Such obtained product is polyester which should be distinguished from UPR resin. Polyester is a rigid material at room temperature and is not suitable for further processing, which is the reason for its dissolving in the vinyl type monomer, whereupon a viscous liquid is obtained - UPR resin. The double bonds within the UPR resin represent the anchoring sites for creation of a three-dimensional structure with the same ones from vinyl monomers, which is promoted by using of activator and initiator.

Cured UPR resins represent inherently brittle material which limits their applicability value, *i.e.* their mechanical and thermal properties are very poor. These performances can be significantly improved by incorporation of myriad types of additives within UPR matrix [5,18,19]. The main group of ingredients used for UPR resins production are monomers for their synthesis and vinyl monomers. Table 2.1 shows monomers for the production of UPR resins. The most commonly used glycols are ethylene and 1,2-propylene glycol.

Polyesters based on unsaturated diols can be prepared by the transesterification of diethyl adipate with unsaturated diols, e.g., *cis*-2-butene-1,4-diol, and 2-butyne-1,4-diol. The transesterification method is a suitable procedure for the preparation of unsaturated polyesters in comparison to the direct polycondensation [20].

Table 2. 1. Monomers for synthesis of UPRs [17]

Saturated alcohols	Remarks
1,2-Propylene glycol (PG)	Most common glycol
Ethylene glycol (EG)	Less compatible with styrene then PG
Diethylene glycol (DEG)	Good drying properties
Neopentyl glycol	Good hydrolysis resistance
Glycerol	Trifunctional alcohol for branched UPR; danger of cross-linking during reaction
Tertrabromobisphenol A (TBBPA)	Flame retardant
Trimethylolpropane	Trifunctional alcohol, cheaper than glycerol
Trimethylolpropane mono allyl ether (TMPAE)	Weather resistant for coatings
Undecanol	Used as chain stopper
Saturated acids and anhydrides	**Remarks**
Phthalic anhydride (PA)	Most common anhydride
Isophthalic acid	Good hydrolysis resistance
Terephthalic acid	Superior hydrolysis resistance
HET acid	Flame retardant systems
Tetrabromophthalic anhydride	Flame retardant systems
Adipic acid	Soft resins
Sebacic acid	Soft resins
Unsaturated acids and anhydrides	**Remarks**
Maleic anhydride (MA)	Most common
Fumaric acid	Copolymerizes better with styrene than maleic anhydride
Itaconic acid	-

The synthesis of general purpose UPR resins is performed using PG, phthalic anhydride and maleic anhydride. If AMK is used without AFK, a resulting UPR resin has high unsaturation density per the macromolecule unit, which contributes to significant rigidity of final product. Therefore, to decrease product reactivity, the unsaturated component has been diluted with a saturated, non-polymerizing component. During the synthesis of the UPR resin, MA partially converse to its isomer, fumaric acid. Fumaric acid shows remarkable reactivity towards vinyl monomer (styrene), but is more expensive than MA. Another aspect for selecting the MA before fumaric acid is a lower amount of reaction water, 2 mol in comparison to 1 mol when MA is used, which has to be removed from reaction mixture to achieving the high polyester yield. Anhydrides are preferred over the corresponding acids due to their higher reactivity. Figure 2.1 shows structural chemical formula of acids and anhydrides used in UPRs synthesis.

To obtain UPR resin the synthesized polyester is dissolved in the vinyl monomer, which additionally serves as a curative, i.e. cross-linking agent. The most commonly used vinyl monomer is styrene. Conversely, styrene exhibits high volatility and carcinogenicity, which requires seeking for an adequate replacement for it. Other vinyl monomers commercially used as a curative for UPR resins are: vinyl pyridine, α-methyl styrene, vinyl and divinyl ethers, acrylates and methacrylates.

During the curing, the vinyl type monomer can evaporate, which causes the changes in material structure reflecting in shifting the glass transition temperature (Tg) of end-product [22]. The addition of waxes can prevent this phenomenon by formation the physical barrier which disables curative evaporation. Conversely, the wax incorporation causes deterioration of resin characteristics and due to that the more appropriate additives for such purpose are polyethers/their copolymers, alcoxylated fatty acids or polysiloxanes, with superb bonding performances [8].
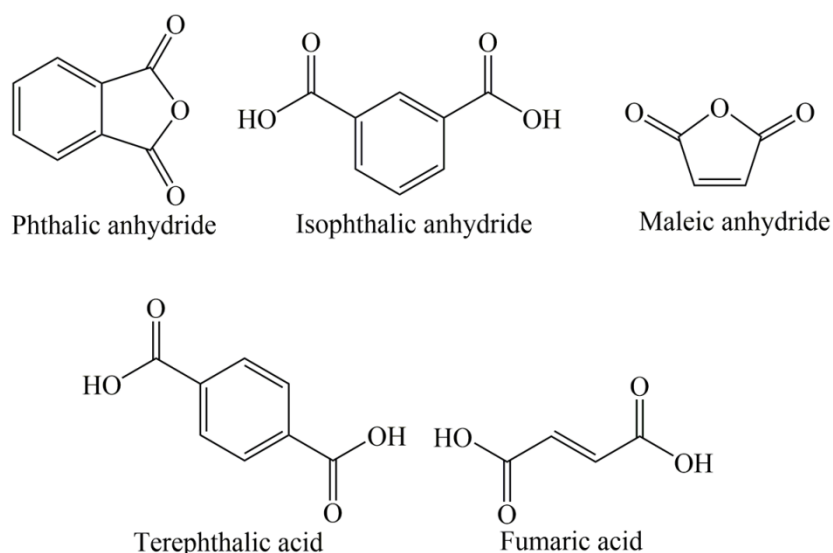
Figure 2. 1. Structural chemical formula of acids and acid anhydrides used in synthesis of UPRs [8,21]

The synthesis of UPRs has been performed by polycondensation in batch reactor, whereby the main products is polyester and the water as a by-product, which is removed from reaction mixture. In the reactor equipped with stirrer, condenser and water cooling jacket, the low molecular weight diol component (glycol - the most frequently PG) is charged, in small excess, to compensate losses resulting from its volatility and for preventing occurring the side reactions. Then, unsaturated acid or anhydride simultaneously with saturated one are added in reactor, whereby the molar ratio between glycol, unsaturated and saturated components is adjusted to be 1.1:1:1, respectively. The reaction is carried-out in inert atmosphere which is provided by removing the remained air with nitrogen blow.

The polymerization starts at about 90 °C, which is followed by remarkably heat release (exothermic reaction). Afterwards, a catalyst is added into the reaction mixture to affect the curing kinetics and prevents color change of the targeted product [23]. The most commonly used catalysts are lead dioxide, *p*-toluenesulfonic acid and zinc acetate. Further on, the reaction temperature is gradually increased to 220 °C, taking into account that steam temperature never goes over 150 °C, to hinder glycol evaporation. At 150 °C, the esterification reaction starts, which is manifested in water generation. There are several approaches for water removal, but the most convenient is using of toluene or xylene to create azeotropic mixture. Reaction water is collected in a particular container, while azeotropic agent refluxes into the reactor. Traces of water, glycol and other low-molecular substances are removed from final product using vacuum distillation technique.

The esterification progress is monitored via quantity of obtained water, but that method is not suitable for accurate determination of reaction stage. The best available technique for such purpose is the calculation of acid number (AN) by sampling of reaction mass, its dissolving in toluene/isopropyl alcohol mixture and titration with an alcohol solution of potassium(I)-hydroxide. When the AN value is 30-40 mg KOH/g of the resin, the reaction is finished which demands the addition of HQ before polyester cooling and dissolving in styrene. The polyester dissolving is a crucial moment in UPR synthesis whereby the temperature must be lower than styrene boiling point. There are two problems which may occur if that condition is not fulfilled:

- If the temperature of polyester is too high, the gelatinization can occur upon styrene addition,

5

- If the polyester temperature is too low, its viscosity is too high which disables good homogenization with styrene.

After homogenization of polyester and styrene, the obtained pale yellow UPR resin is cooled to room temperature and packed in tin cans or jars. The mass ratio of polyester towards styrene is very important for preventing phase separation and the ideal one is 60:40. Figure 2.2 shows UPR synthesis as well as it curing with styrene.
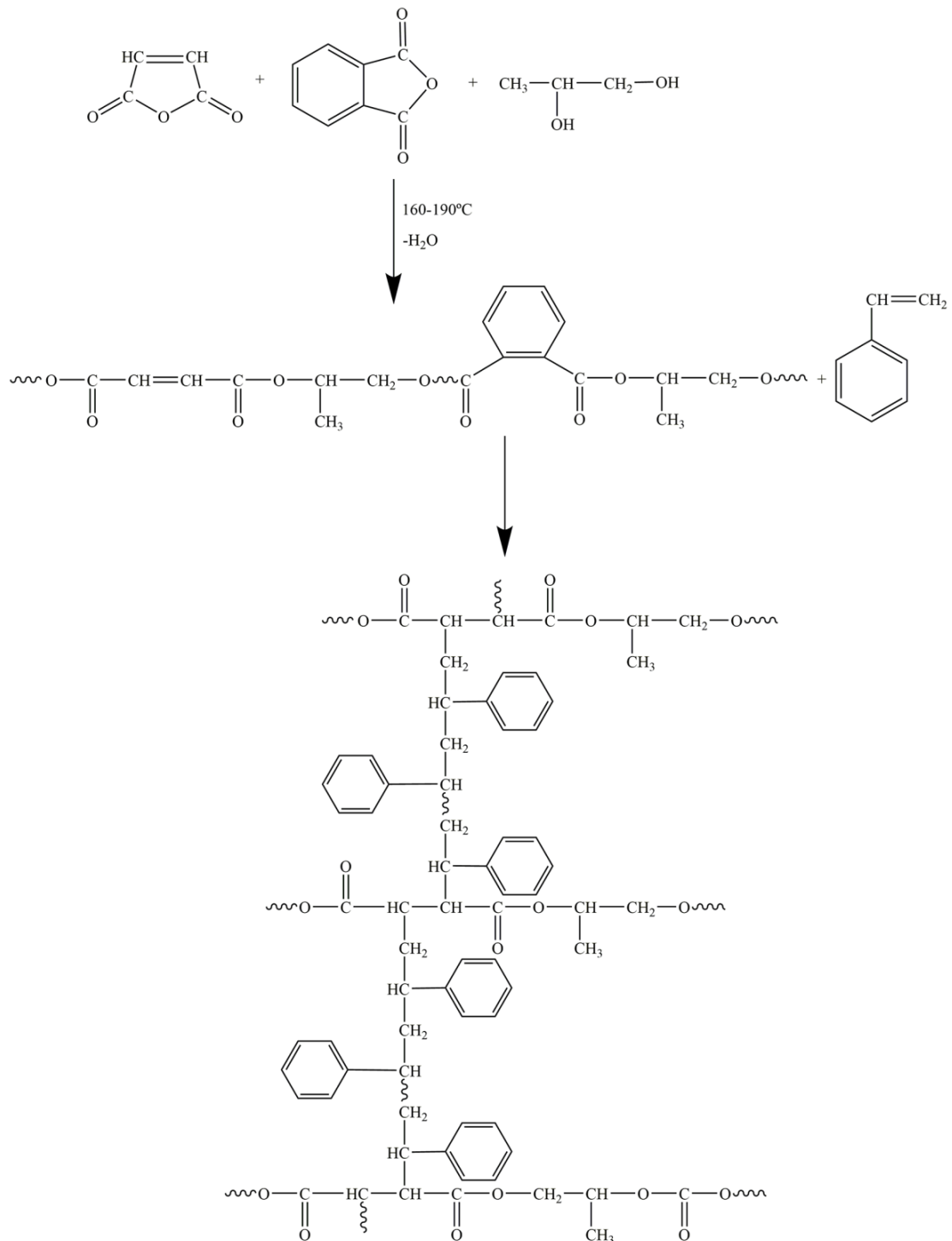
Figure 2. 2. Synthesis and curing of UPR [24]

2.1.1 The UPR synthesis from waste poly(ethylene terephthalate) (PET)

PET is semi-crystalline, linear, saturated polyester, obtained in reaction between ethylene glycol and terephthalic acid (Figure 2.3). PET possesses superb mechanical characteristics, high resistance towards acids and mineral oils and barrier properties (impermeability for moisture and gases) which makes it suitable for myriad application: food and beverage packaging, audio and video tapes and so on [25].
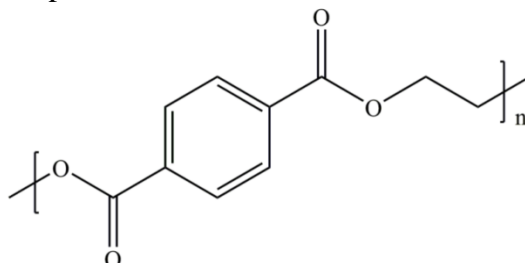
Figure 2. 3. Chemical structure of PET

Increased worldwide consumption and short life-time of PET products together, with human negligence, lead to generation of huge amount of waste in recent decades [26]. That is the reason why the waste PET has to be properly treated using one of the four distinct recycling techniques:

- Primary - involves the use of pre-consumer industrial scrap;
- Secondary - physical processing (washing, grinding, melting, reforming);
- Tertiary - subject waste PET to chemical treatment;
- Quaternary - incineration of PET waste to obtaining of energy [3].

Among all the mentioned techniques, tertiary (chemical) recycling processes, as the economically and environmentally more suitable, are emphasized. The products obtained by tertiary recycling processes are raw materials (monomers) from which PET consists (total depolymerization) and oligomers (partially depolimerization).

2.1.1.1 Catalytic depolymerization of waste poly(ethylene terephthalate)

Chemical recycling of PET is provided thanks to presence of ester group within the PET structure which can react with various type of reagents. In such reactions, ester bonds along the macromolecules structure are cleaved using an appropriate chemical agents. Depending on type of used reagents, chemical recycling is divided on following procedures:

- Alcoholysis (alcohols),
  - Methanolysis (methanol)
  - Glycolysis (glycols)
- Hydrolysis,
  - Alkaline
  - Acidic
  - Neutral
- Other processes,
  - Aminolysis
  - Ammonolysis [3].

The most commercially applied process for PET recycling is glycolysis, which represents structural degradation of PET network in presence of the trans-esterification catalysts. In such a way, the cleavage of the ester bridges results in obtaining of hydroxy terminated product, *i.e.* oligoester diols [8]. The most commonly used glycols for such purpose are EG, PG, DEG

7

and so on [27]. Glycolysis requires using of an adequate catalyst to achieve complete depolymerization of PET to bis(2-hydroxyalkyl)terephthalate (BHAT). Conversely, the reaction is very slow and incomplete, resulting in low yield of BHAT, mixed with other by-products, which makes difficult its recovering. to cannot be achieved. Thus, significant research efforts have been directed toward increasing the reaction rate and BHAT yield by developing highly efficient catalysts. Besides, the optimization of the reaction conditions (e.g. temperature, time, PET/EG ratio, PET/catalyst ratio) are also taken into consideration [3]. Figure 2.4 shows scheme of PET glycolysis and possible application of obtained products.
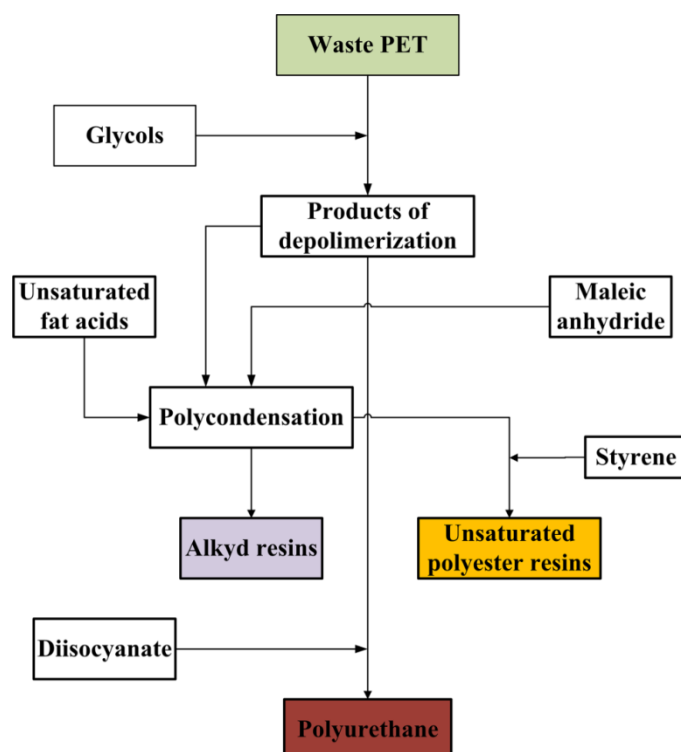
Figure 2. 4. Schematic review of processes from waste PET to useful products [8]

Glycolysis is carried out over a wide temperature range, from 180 to 240 °C, for 30 min to 8 hours [28]. The influence of used glycol is essential for efficacy of PET glycolysis, which is evaluated through determination of its remaining quantity in the reaction mixture, *i.e.* how much is spent on the glycolysis process [29]. It has been shown that PG exhibits the highest efficacy in PET depolymerization, in comparison to the other glycols.

Khoonkari and co-workers have investigated the PET glycolysis by EG in the presence of different catalysts as following: ionic liquids (1-butyl-3-methylimidazolium bromide ([bmim]Br)), metal salts (zinc acetate) and hydrotalcites [4]. The usage of zinc acetate brings good yield, but takes more time to starts reaction, compared to (bmim)Br and hydrotalcites. Moreover, the required amount of zinc acetate and reaction temperature for successfully performing of PET glycolysis is higher than for other two catalysts. The purity of obtained product is low, requiring catalyst recovery, which is quite expensive since that operation is technologically demanded. The PET glycolysis reaction rate is fast when (bmim)Br is employed, in comparison to zinc acetate, and product yield at elevated temperature (zinc acetate temperature condition) is near 100%. If a high yield is to be achieved, there is a problem with temperature sensibility of the catalyst which disables its recovery. The utilization of hydrotalcites enables higher reaction rate, although the reaction takes a little bit more time compared to using of metal salts and ionic liquids. Conversely, the reaction needs

a lower temperature range and the recovery of hydrotalcites is easy, which provides high purity of the final products.

López-Fonseka and co-workers have studied PET depolymerization in excess of EG, added, catalyzed by different metal salts: zinc(II)-acetate, sodium(I)-carbonate, sodium(I)-bicarbonate, sodium(I)-sulfate and potassium(I)-sulfate [30]. The highest yield of bis(2-hydrocyethyl)terephthalate (BHET) (about 70% and 50%, respectively) is achieved by employing the zinc(II)-acetate and sodium(I)-carbonate at 196 ℃ and PET/catalyst molar ratio 100:1. In comparison with the activity of zinc (II)-acetate, other metal salts do not show such high degree of conversions. The lowest conversion rate is remarked in the case of sodium- and potassium(I)-sulfate, due to low solubility of these catalysts in EG.

The severe problems occur with the use of metal salts as catalysts due to their toxicity and non-biodegradability as well as the non-selectivity. Although zinc (II)-acetate has been proven to be the most active catalyst, the small difference in the activity of zinc(II)-acetate and sodium(I)-carbonate indicates the potential of using sodium(I)-carbonate as a catalyst that has no adverse environmental impact.

Besides metals salts, tetrabutyl titanate (TBT) is one of the most commonly employed catalyst for PET depolymerization. TBT exhibits high activity, good solubility in organic solvents and easy separation from the product by rinsing with distilled water [31]. Lu and coworkers [32] have examined the catalytic depolymerization of PET with PG and TBT, where the PET/PG ratio has been varied. The glycolysis is performed at two temperatures, first at lower temperature, 190 °C for 5 hours, and second for 1 hour at 210 °C. They conclude that the degree of depolymerization is increased with amount of PG in reaction mixture, which is in great accordance with the results presented by Abdelaal and co-workers [29].

2.1.1.2. Polycondensation of PET glycolyzate with maleic anhydride

There are different types of products, which can be obtained from PET glycolizate, as can be remarked from Figure 2.4. One of the main product is UPR resin, which is obtained in reaction between PET glycolyzate with saturated/unsaturated dicarboxylic acids or anhydrides [25]. The structure and properties of UPR can be tailored by PET/glycol ratio, reaction time and temperature, type of catalyst and PET/catalyst ratio [33].

Dugue-Ingunza and co-workers has studied the catalytic PET depolymerization using EG and metal salts as well as parameters for obtaining of the UPR resin in reaction between BHET and MA [34]. The BHET:MA molar ratio was 1.1:1.0 in all cases. They showed that as the reaction temperature and time increased, the molar mass of the UPR resin raised, which irreversibly affected the viscosity raising. The optimal polyesterification conditions were 180 ℃ and 4 hours, where the obtaining of processable UPR resin was achieved (acceptable viscosity). The synthesized resin had a mean molar mass with a numerous distribution of 1460 g/mol, which was in accordance with the molar mass of commercial resins. In the synthesis of UPR resins, the mean value of the molar mass should be taken into account, since in the case of too low molar mass, the cross-linked resins have significantly lower physical-mechanical characteristics, and in the case of too high, the processability of the resin is hindered [8].

Lu and Kim [35] investigated the synthesis and cross-linking of UPR, obtained by polycondensation of waste PET glycolyzate by PG and MA, and compared to a commercial resin synthesized from MA, FA, and PG. Based on the KB values and the duration of the polycondensation reactions, it was concluded that the polycondensation of the PET glycolyzate and MA occurred faster than polycondensation in the case of commercial resin.

2.2 Alumina as filler in polymer matrices

Alumina or aluminum oxide is a natural-based material, which appears in various shapes: corundum (Al_2O_3); diaspore ($Al_2O_3 \cdot H_2O$); gibbsite ($Al_2O_3 \cdot 3H_2O$); and most commonly as bauxite, an impure form of gibbsite. Alumina exhibits numerous crystalline structures, which can be converted one to each other using an appropriate thermal of chemical treatment [15]. Figure 2.5 shows several different forms of alumina. Nanoscale γ- and α-alumina are thermally stable at higher temperature, but are difficult to produce due to grain growth promotion caused by heating, which hinders obtaining of the such fine alumina powder [36].
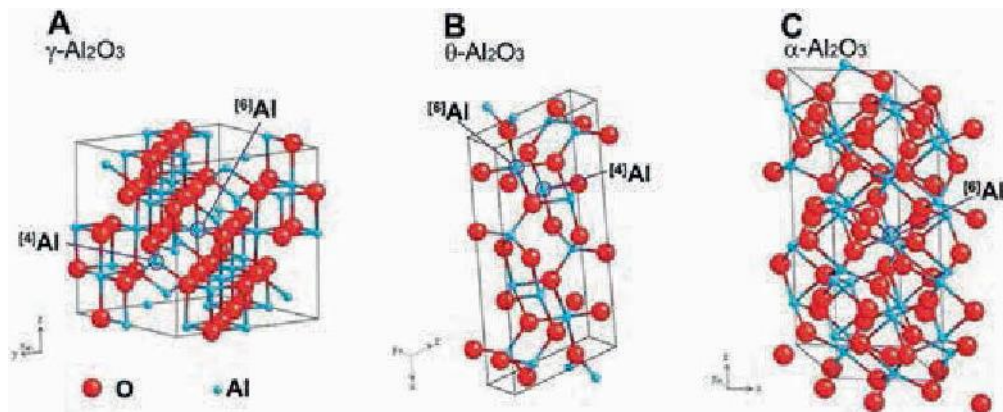
Figure 2. 5. Some structural forms of alumina [37]

Al_2O_3 has superb physical and chemical properties such as high hardness, strength, elastic modulus and remarkable resistance to chemical impact. Due to that, Al_2O_3 have extensive applications in various fields such as: electronics, metallurgy, composites, wear protection, refractories, catalysis, automotive emission control and hydrogenation [38–40]. Kovačević and co-workers. demonstrate that the significant increase in mechanical properties can be achieved by incorporation of pristine Al_2O_3 filler into UPR resin with respect to neat polymer [41]. However, its application shows some constraints due to poor toughness and inferior thermal resistance [42].

There are several approaches for synthesis of nano-scaled alumina which generally can be divided to physical or chemical. The physical methods involve mechanical milling or flame spray, while chemical implies co-precipitation, combustion, sol-gel methods and so on [43–45]. The properties of nano alumina particles depend on their size, morphology, and phase distribution, which can be tailored by selecting a proper synthesis method.

The mentioned methods have some disadvantages; mechanical synthesis needs extensive mechanical ball milling, vapor phase reaction requires high temperature, while the precipitation method is complicated and lasts a long time. The combustion method is used to yield nano-scaled α-Al_2O_3 particles, which exhibit somewhat degree of agglomeration. The sol–gel method is based on polymeric precursors usually formed from metal alkoxides [46].

2.2.1 Sol-gel technique for alumina obtaining

The sol-gel method represents one of the most promising approach for alumina synthesis due to yielding homogeneous powder with high purity at low processing temperature and great reproducibility [37]. The main disadvantages are the moisture sensitivity of the precursors (alkoxides), which demands special and costly handling. There are several factors for designing the needed properties of targeted product such as: raw materials, an adequare

process parameters (solvents, stirring time, pH value), water content and type of surfactants. Figure 2.6 shows the block diagram of the sol-gel method.

The sol-gel techniques use a variety of inorganic and organic precursors, commonly nitrate and chloride salts of aluminum and aluminium isopropoxide. Rogoja et al. obtained nano-scaled α-Al_2O_3 at $1000\,°C$ starting with aluminum chloride as an inorganic, and aluminium triisopropylate as an organic precursor [47]. Such calcination temperature was suitable for designing proper means for obtaining alumina powder with superb properties, compared to those synthesized at different temperatures. The nano-scaled α-Al_2O_3 can also be obtained by aqueous sol-gel technique using cheap $AlCl_3 \cdot 6H_2O$ and Al powder, as raw materials [48].

In sol-gel technique, solvent has an essential role in increasing contact between precursors, and thus increasing of end-product yield. The most commonly used solvents are alcohols, ethers and glycols. Beside solvent, the special additives such as urea and citric acid also have important role in obtaining the desired properties of alumina powder through control of complex formation, hydrolysis and reactants condensation [37].
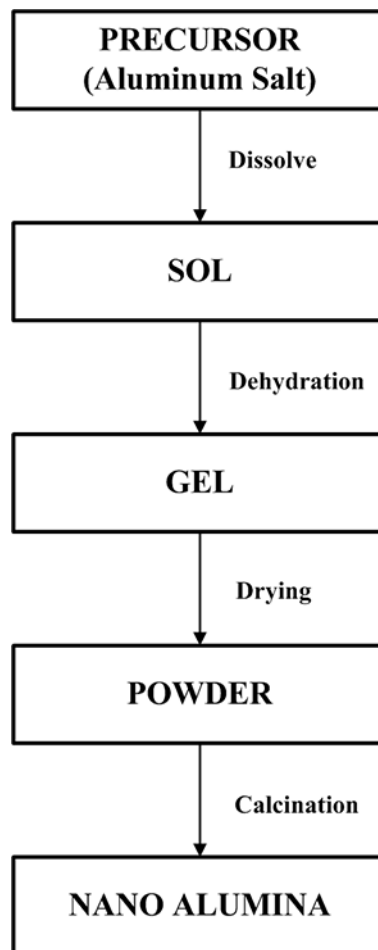
Figure 2. 6. Flowchart of sol-gel technique [37]

Li et al. obtained ultrafine α-Al_2O_3 by an aqueous sol–gel method using a citrate polymeric precursor prepared from various molar ratio of aluminum nitrate (ANi) and citric acid (CA). The increasing molar ratio of CA/ANi favored phase transition of γ- to α-Al_2O_3, whereas the precursor with CA/ANi = 1 yielded an ultrafine α-Al_2O_3 powder with particle size of 200 nm [49].

To reduce particles agglomeration, surfactans, which postpone crystals growth, are introduced into precursor mixture solution. The commonly used surfactants for such purpose are: sodium dodecyl sulfate, sodium bis-2-ethylhexylsulfosuccinate and hexadecyl trimethyl ammonium bromide. The addition of sodium dodecylbenzene sulfonates and sodium bis-2-ethylhexylsulfosuccinate into the precursor solution, makes from aluminum isopropoxide and aluminum nitrate hydrate, impacts the alumina particle size, shape as well as degree of their aggregation [50].

2.3. Composites based on UPR resin and alumina particles

2.3.1 Polymer composite materials

Since the needs of modern humanity demand high-performance materials, composites attract more attention due to the capability to answer to such requirements. They possess superb properties suitable for wide fields for application. Composites contain two or more components with unique characteristics that, when are combined, give materials with properties quite different from the particular constituents. Composite materials are generally classified by the matrix into ceramic, metal and polymer composites. Polymer matrix composites (PMC) became the material of interest in recent years as they provide easy processability and tuning the desired properties of end-products.

PMC are composed of a reinforcements, shaped as a short/continuous fibers or nano/micro filler particles, which are uniformly distributed in polymeric matrix. These reinforcements bring an improvement of physical, chemical and thermal properties of pure polymeric matrix making it suitable for usage in advanced applications. The mentioned properties strongly depend on (1) the characteristics of the individual components; (2) the amount and mass ratio of matrix and reinforcements; (3) the orientation of incorporated fiber reinforcements and intensity of the bonding strength between the matrix and the reinforcements and (4) the size, morphology and distribution of the reinforcements [51]. Polymer matrix as well as reinforcements, through offering their particular characteristics, participate in creating of the properties of final products. Fillers provides remarkable mechanical properties reflecting in high resistance to bending and breaking under applied load. Conversely, the polymer matrix absorbs stress by its transfer to the filler particles. The second role of polymer matrix is providing the protection of reinforcements towards abrasion and moisture impact [52].

Combination of type and amount/particle size of filler particles provides designing the composites with desired properties. Generally, smaller filler particles give higher improvements of pure polymeric materials. The reinforcement loading needs to be carefully selected to avoid formation of clusters, which deteriorate the quality of end-product [18,19]. Accordingly, the optimization of each aforementioned aspect has to be fulfilled in composite preparation process to obtain a product with superb characteristics.

Unlike traditional polymer composites containing micro-scaled fillers, the integration of nano-scaled materials into a polymer matrix results in obtaining the superb properties of targeted products. Therefore, the properties of composites can be successfully tailored even using low amounts of filler [53]. To obtain material with superb properties, it is important to uniformly disperse filler particles into the polymer matrix, using several available techniques suitable, such as: blending solution, *in situ* polymerization, sol-gel and so on.

2.3.1.1 Blending solution technique

One of the most promising way for preparing the polymer/Al$_2$O$_3$ composites is solution blending technique. This method includes three-step procedure for homogenization of filler into polymeric matrix: mechanical and magnetic stirring/mixing and sonication [15]. There are several advantages of such method: simplicity and applicability for great assortment of inorganic fillers as well as easy control of polymer and reinforcement concentration in the solution [54]. Johan et al. investigated the impact of nano-scaled alumina to ionic conductivity of solution contained poly(ethylene oxide) matrix, lithium triflate and ethylene carbonate [55]. The results suggest that the 15 wt% of alumina within the composite provides the highest conductivity which is potentially related to the presence of Lewis (Al$^+$) and Bronsted (Al-OH) acid sites onto alumina surface which promotes high mobility of ions. Besides, in such a way is possible to prepare hybrid material based on PET and nano alumina with loading 1-10 wt% by batch mixing under the inert atmosphere [56]. Moreover, latex/alumina films were also prepared by combining aqueous colloidal suspensions of alumina and nanolatex polymer beads. To attain better interaction between the polymeric particles and inorganic filler, small amounts of acrylic acid was previously incorporated in the latex [57].

2.3.1.2 In situ polymerization

In situ polymerization is an efficient method to uniformly distribute filler particles in a polymer matrix. This method implies mixing of filler particles with organic monomers, either in the presence or absence of a solvent, afterwards polymerization is occurred. The polar nature of filler surface enables creation of radicals, cations or anions to initiate the polymerization of the monomers, as well as its anchoring to polymer chains via covalent bonding [15].

This method is suitable for preparation of laminate composite containing epoxy vinyl ester matrix strengthened with chemically modified alumina [58]. Alumina/poly(methyl methacrylate) (PMMA) nanocomposites, synthesized by in situ polymerization, showed substantially drop of glass transition temperature (T$_g$) in comparison to pure polymer [59]. Such effect was evidenced by incorporation of very low amount of alumina particles (less than 0.5 wt.%), while further addition had no influence on T$_g$.

Moreover, other characteristics of *in situ* polymerized materials, such as mechanical and thermal, can also be improved by introducing the alumina particles within their structure. The *in situ* prepared nanocomposites fabricated from vinyl ester matrix and silane functionalized nano-scaled alumina displayed significantly increased mechanical and thermal properties in comparison to neat resin [60]. This technique was also suitable for obtaining the adsorbent for Pb^{2+} from aqueous solution [61]. For such purpose, two poly(acrylic acid)/alumina nanocomposites, with various polymer loadings, were prepared via *in situ* polymerization of acrylic acid. When the quantity of PAA in a nanocomposite sample was lower, there was higher Pb^{2+} sorption capacity due to higher availability (higher active surface) of alumina pores, *i.e.* their lesser clogging with polymer chains.

2.3.1.3 Sol-gel

In this process, organic species and inorganic precursors are combined in the non-aqueous or aqueous solutions where form networks between at moderate temperature. In sol–gel method, using the polymer with suitable functionality, can be achieved the good compatibility and linkage between the organic and inorganic moieties in targeted end-

product. One procedure for the synthesis of composites using this technique is shown in Figure 2.7, wherein polypropylene grafted with MA (PP-g-MA) is reacted with aluminum isopropoxide, promoting crosslink formation [62]. The preparation of composites based on acrylic acid and alumina, previously obtained by sol-gel method, is described in following publication [63]. The storage modulus, T_g, tensile strength, tensile modulus, and thermal stability of the corresponding composites increased considerably, even with a very small amount of embedded alumina, in comparison with pure acrylic resin, but did not change significantly with rising alumina content.
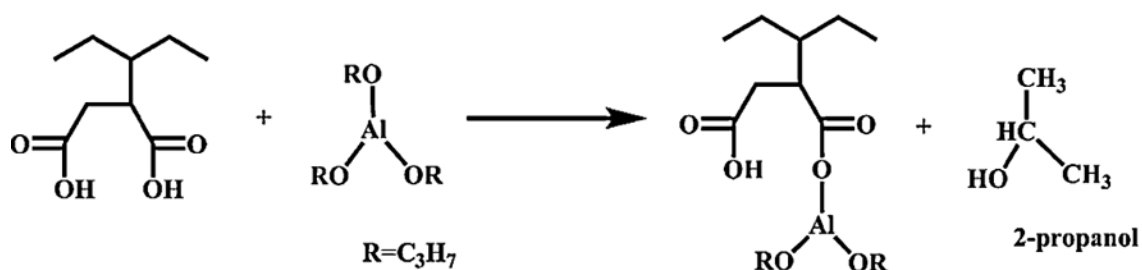
Figure 2. 7. Simplified scheme of PP-g-MA aluminum isopropoxide reaction [64]

2.4 Compatibility between polymeric matrix and filler particles

There are some drawbacks related to achieving of great miscibility/compatibility between polymer matrix and embedded reinforcements which are primarily due to the hydrophilic nature of the reinforcements towards the hydrophobic polymer matrices. To achieve good interactions between the reinforcements and the polymer matrix, reflected in satisfactory wetting and adhesion, the additional actions need to be come into play. These actions implies surface modification/functionalization through reaction between modifying agent and myriad of hydroxyl groups within the reinforcements structure [65,66].

The using of surface modifiers is the best approach to lowering the surface tension between reinforcement and matrix which results in improving of final properties of polymers. The most commonly mechanism how modifiers work is reaction between functional groups within modifier and reinforcement structure, whereas the loose organic parts from the modifier is inserted into the free space among macromolecule chains in polymer matrix [67]. If these organic tails contain reactive groups they are able to chemically interact with similar ones from the polymer matrix, even during curing process. In addition, reinforcement surface modification changes the intensity of interactions between the particles/fibers themselves, especially if their surface is charged. In that case, competition occurs between electrostatic repulsion and establishment of intermolecular hydrogen bonds, which results in preventing of filler agglomeration [68].

Commonly way to design filler/polymer surface is chemical modification. Generally, chemical modification represents chemical bonding of the modifier/coupling agents or polymeric chains on the filler surface. By adequate surface or molecular modification of fillers, it is possible to uniformly distribute them throughout the polymer matrix resulting in establishment of better interaction between reinforcement and matrix. In such a way, the significant improvement of polymer material properties with simultaneous decrease of the final product price is achieved [69]. After the appropriate surface modification, filler particles become hydrophobic, which decreases their surface tension and leads to better miscibility and compatibility with the hydrophobic polymer matrix [70]. Moreover, surface functionalization causes changing in the surface charge which is manifested in competition between electrostatic reflection of the particles themselves and formation of the intramolecular hydrogen bonds [71].

14

2.4.1 Chemical modification of alumina particles

The hydrophilic nature of alumina nanoparticles leads to high moisture absorption, formation of agglomerates and incompatibility with hydrophobic segments of polymeric matrices. These disadvantages are most frequently overcome by surface modification of alumina nanoparticles, using silane coupling agents. The obtained structures enable the establishment of a great linkage with polymeric matrices, especially with those which contain double bond segments.

Employing the coupling agents to overcome these drawbacks is the best available technique covered in literature and praxis. Organosilanes have bifunctional structure suitable for their usage in treatment of natural fiber and inorganic fillers since both bear reactive hydroxyl groups onto the surface [14,21]. These functional groups enable anchoring of hydrophobic segments capable for creation of linkage with polymeric chains. Mechanism of silane grafting onto filler particle is depicted in Figure 2.8. Table 2.2 shows the most commonly used silanes as coupling agents: amino, vinyl, acryl, methacrylate and azido. Aminosilanes are, according to literature data, the most suitable for natural fibers in combination with both, thermoplastic and thermosetting, polymers [72]. Methacrylate treated fillers display high reactivity towards UPRs, azido are extensively used for modification of inorganic fillers to react with thermoplastic matrices, while vinyl and acryl need peroxide based initiators for establishing of linkage between matrix and reinforcements [73].
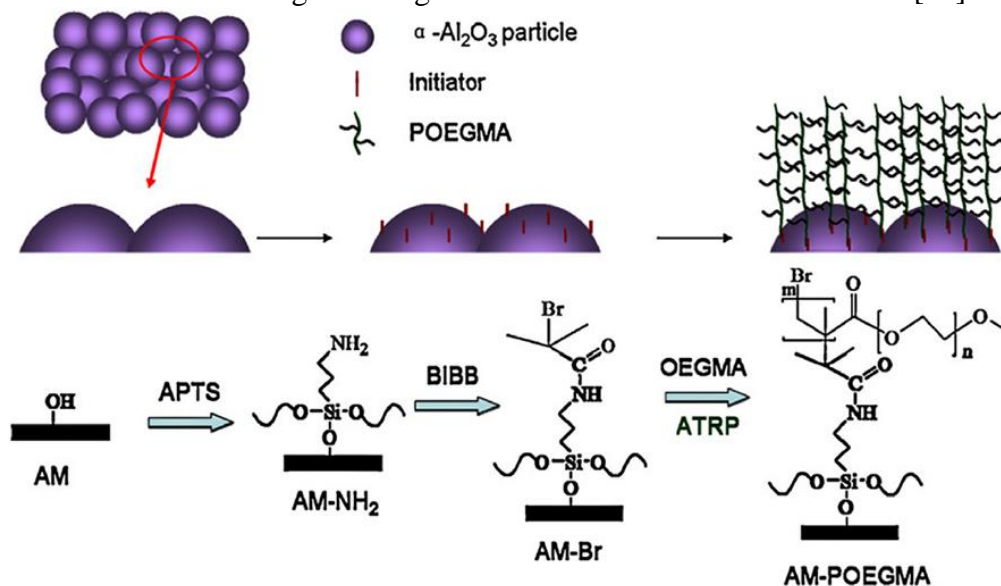
Figure 2. 8. Schematic presentation for grafting Al_2O_3 membranes with poly(oligo (ethylene glycol) methyl ether methacrylate) (POEGMA) brushes via surface-initiated atom-transfer radical polymerization (SI-ATRP) [*APTS - 3-Aminopropyl)triethoxysilane, BIBB - 2-bromoisobutyryl bromide] [74]

Jin et al. [75] prepare the nanocomposites based on ethylene-vinyl acetate (EVA) and modified nano-scale Al2O3. Tensile strength, elongation at break and viscosity of EVA/Al2O3 nanocomposites are significantly improved with respect to pure EVA. Zunjarrao and Singh [76] investigate the effects of particle size and silane treatment on the fracture toughness for epoxy resin reinforced with nano- and micro-scaled rigid aluminum particles. They observe that fracture toughness of epoxy reinforced with as-received 20–100 nm aluminum particles is higher than that reinforced with as-received 3-4.5 μm particles. Furthermore, it is remarked that, although silane treatment of both nanometer and micrometer particles leads to a better particle-matrix bonding, agglomeration issues limit the

enhancement achieved in fracture toughness of the composites with nanometer sized particles. Mallkpour and Dinari [77] report the modification of Al2O3 with KH550 coupling agent. The obtained results indicate that Al2O3 nanoparticles form aggregates of several hundred nanometers in diameter. On the contrary, KH550-modified Al2O3 are finely dispersed in the polymer matrix.

Table 2. 2. Silanes used for the natural fiber/polymer composites: chemical structures, functionalities and target polymer matrices [73]

Structure	Functionality	Abbreviation	Target matrix
$(RO)_3Si-(CH_2)_3-NH_2$	Amino	APS	Epoxy Polyethylene Butyl rubber Polyacrylate PVC
$(RO)_3Si-CH=CH_2$	Vinyl	VTS	Polyethylene Polypropylene Polyacrylate
$(RO)_3Si-(CH_2)_3-OC(CH_3)C=CH_2$	Methacryl	MPS	Polyethylene Polyester
$(RO)_3Si-(CH_2)_3-SH$	Mercapto	MRPS	Natural rubber PVC
$(RO)_3Si-(CH_2)_3-O-CH_2CHCH_2O$	Glycidoxy	GPS	Epoxy Butyl rubber Polysulfide
$R_2-Si-Cl_2$	Chlorine	DCS	Polyethylene PVC
VTS grafted plastics	Vinyl	VSPP	Polypropylene Polyethylene
$(RO)_3-Si-R''-N_3$	Azido	ATS	Polypropylene Polyethylene Polystyrene
$(RO)_3Si-(CH_2)_{15}CH_3$	Alkyl	HDS	Polyethylene Natural rubber

Rashid et al. investigated the influence of pristine and modified alumina on flexural properties of epoxy based composites [78]. They added up to 50 wt% of both, untreated (UTAL) and treated (TAL) alumina and found that the flexural strength decreased with 10 wt% of introduced reinforcement and gradually increased until 50 wt% (Figure 2.9). The strength of the material depends not only on the dispersion of the filler in the matrix, but also on the presence of voids and holes within the material structure as well as the quality of the interface between the reinforcements and polymeric matrix [78].

Figure 2.9 shows that the alumina loading up to 30 wt% reduces the flexural strength of corresponding composites in comparison to neat epoxy resin, whereas the presence of TAL in composites structure displays better results. By further increasing the alumina content, flexural strength for both, UTAL and TAL, raises, respecting the same trend remarked for lower filler loading. The lower amount of alumina is probably not well dispersed in epoxy matrix which suggests that interaction established between reinforcement and matrix is poor. Conversely, these phenomena are improved by embedding more alumina particles, where higher interactions are established between TAL and epoxy matrix in relation to UTAL/epoxy system.
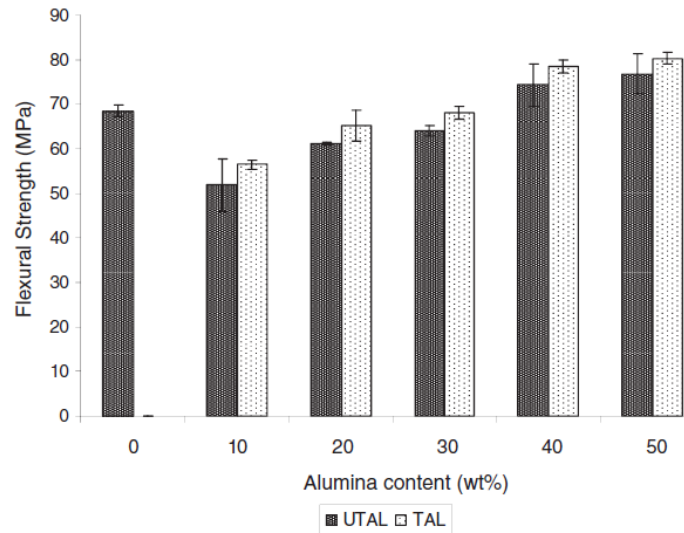
Figure 2. 9. Variation of flexural strength of the UTAL and TAL composites as a function of the alumina content in wt% [78]

2.5 Mechanical properties of polymer/alumina based composites

Hardness, tensile and flexural strength (σ_t, σ_f) are the most important indicators for mechanical properties of composite materials, which need to be tested before their application. During the material being subjected to external force, micro cracks start to create and moving further on, causing deterioration of structural integrity of the composite. Parameters, obtained by examination of mechanical characteristics of composites are: Young modulus, stress and strain, Poisson's coefficient and so on [8]. Standard specimens, cut from bigger boards or casting into mold, are used for determination of above mentioned performances of composites. The load and the corresponding longitudinal and transverse deformations shall be continuously recorded during the test. The device used for this purpose is testing machine which works at a wide range of speeds, 1-500 mm/min, depending on type of the material. On the basis of data about the sample condition before and after test, a stress-strain curve is constructed which gives tensile/flexural strength, elongation at break and Young modulus, E [8]. Conversely, hardness represents the resistance of the material to local deformation caused by the effect of external force. There are a various of standard methods for determination of composite hardness, such as: Vickers, Brinell, Knoop, Shore, Rockwell and so on.

Lins and co-workers have investigated the influence of alumina on mechanical and thermal properties of high-density polyethylene (HDPE) based composites [79]. The loading of alumina in corresponding composites were varied from 5 to 10 wt% with respect to HDPE matrix. They found that the tensile strength of alumina-HDPE composite decrease due to weak adhesion between filler particles and polymer matrix evidenced in Figure 2.10 as well as a slight degree of fiber detachment. Low adhesion (Figure 2.10 (a) and (b)) combined with the particle clustering results in low surface area and formation of voids between filler and matrix, which can act as crack initiation points.
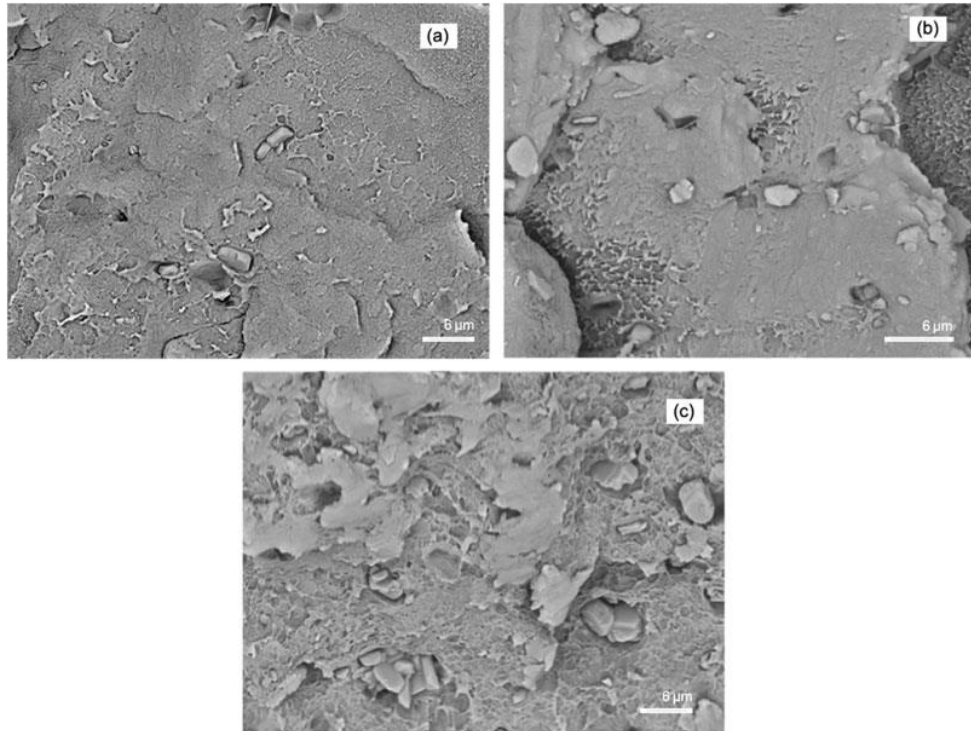
Figure 2. 10. Micrographs of the fractured surfaces of HDPE-alumina composites: Al_2O_3-5% (a), Al_2O_3-7.5% (b) and Al_2O_3-10% (c) [79]

Mohanty and Srivastava used nano alumina in the short glass/carbon fiber reinforced epoxy based composites to improve their flexural and impact properties [80]. They tested alumina/epoxy composites with and without glass/carbon reinforcements and the results revealed that the incorporation of 2 and 3 wt% of alumina increased the impact and flexural strength for 84% and 20% in comparison to pure epoxy matrix, respectively. Besides, the 2 wt% of alumina nanoparticles loading, combined with amount of 5 wt% of glass/carbon fibers within the composites structure showed the highest enhancement of flexural and impact strength compared to pure epoxy resin. Such trend can be observed from Figure 2.11(a).
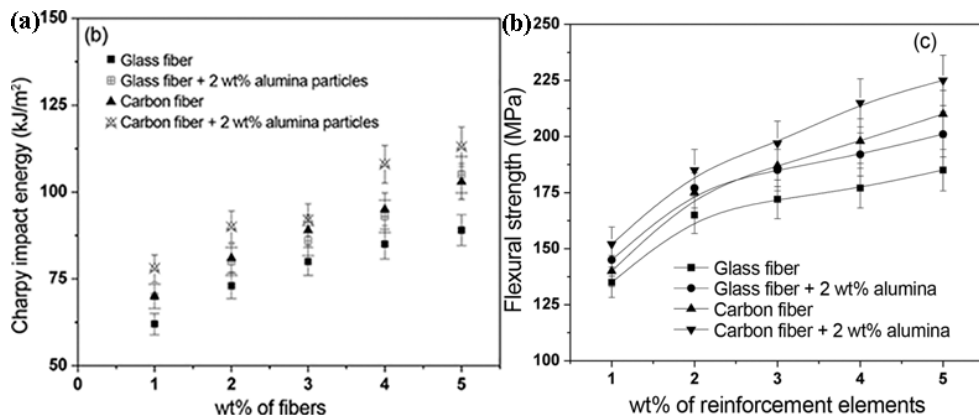
Figure 2. 11. Effect of the addition of the glass/carbon fibers along with/without alumina particles over the range of weight fraction for the (a) Charpy impact energy and (b) flexural strength of epoxy based composites [81]

With an increase in alumina nanoparticles loading in epoxy matrix, the impact energy increased up to a marked concentration and drastically decreased thereafter. The slope decrease in absorption of impact energy is due to the heterogeneous particle distribution in

bulk matrix, *i.e.* appearance of the filler agglomerates which causes fracture initiation, fast growth and thus material collapse [5,19].

Somewhat similar trend showed changes in flexural strength and modulus when alumina was introduced within the composites structure. Figure 2.6(b) showed that flexural strength raised until critical concentration and thereafter slightly decreased. The explanation for such phenomenon is the same as for the impact strength, *i.e.* higher filler loading leads to particles clustering which represents the weak spots into the material.

Baskaran et al. were also examined mechanical properties of UPR/alumina based composites and found that the critical filler concentration was 5 wt%, *i.e.* the maximum increase of tensile, flexural and impact strength was achieved with mentioned loading of alumina particles [82]. The presence of fine particles, well dispersed within the composite structure, enhances the material mechanical integrity making plastic deformation easier. Such phenomenon is the result of good matrix/filler adhesion capable for bearing the applied load and thus delaying the material collapse. Further addition of alumina in UPR matrix deteriorated mechanical properties, mostly due to agglomeration of fine filler nano-scaled particles (Figure 2.12). The agglomerated particles represent rigid spots within the material where stress concentration occurs, resulting in decrease of mechanical properties [8,21].
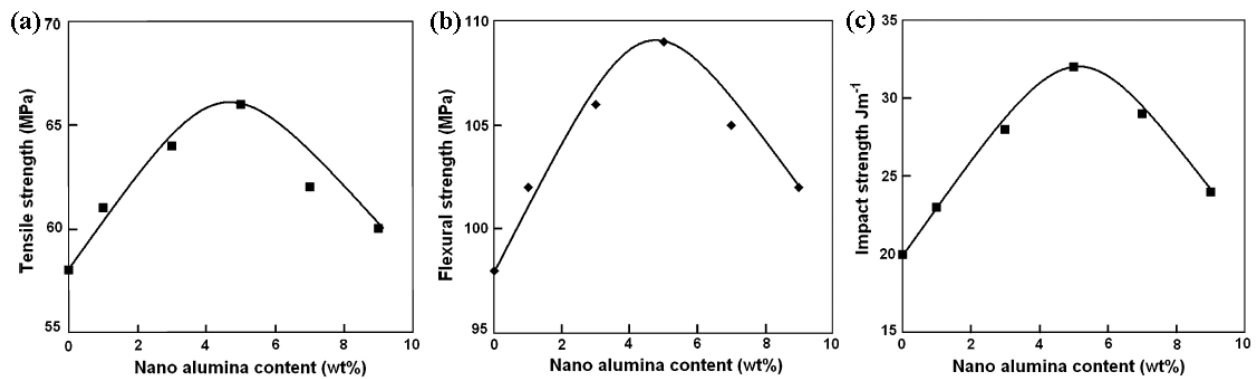
Figure 2. 12. Mechanical properties of UPR/alumina based composites: (a) Tensile, (b) Flexural and (c) Impact strength [82]

As mentioned above, poor compatibility between reinforcements and polymer matrix leads to failure of mechanical properties, which can be improved by chemical functionalization of filler particles. The obtained surface architecture, most frequently created by silane coupling agents, is suitable for establishment of a great linkage with polymeric matrices. Moreover, the aggregation of filler particles is prohibited in this manner, which can cause the mechanical deterioration of composites. Nevertheless, some drawbacks, such as loading and size of filler particles, as well as the viscosity of the polymer matrix have to be overcome to achieve uniform dispersion of reinforcements. Guo et al. evaluated the effect of addition functionalized alumina on the mechanical properties of vinyl ester resin using a tensile test [60]. Figure 2.13 displays stress-strain curve of neat resin and corresponding composites contained 1 an 3 vol% of functionalized nano-alumina.

It can be remarked the significant improvement of tensile strength, 20.8 and 76.4 for the addition of 1 and 3 vol% of nano-alumina in comparison to neat resin, respectively. Such observation is a consequence of great adhesion established between alumina particles and vinyl ester resin, enabled by hydrophobization of filler surface using silane.
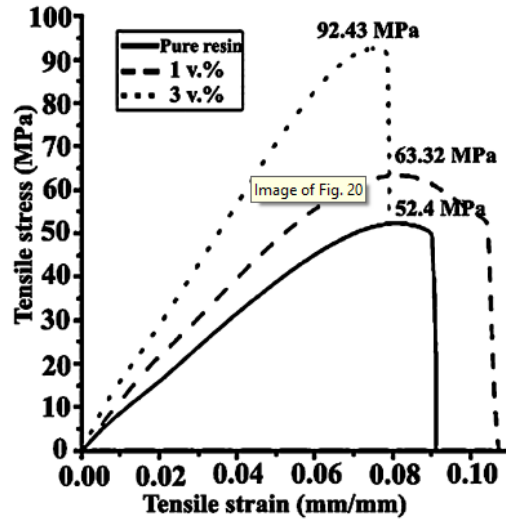
Figure 2. 13. Stress–strain curves of the cured pure resin, 1 vol%, and 3 vol% of functionalized alumina in nanocomposites [60]

Moreover, alumina nanoparticles can be effectively applied in powder coatings to their improve corrosion and wear behavior [83]. Golgoon and co-workers added 10 and 20 wt% of nano alumina to polyester based powder and obtained composites were cured in two regimes by microwave and oven. The obtained results suggested that the samples contained 10 wt% of nano alumina possessed the highest corrosion and wear resistance with respect to pure sample. That is clearly evidenced from SEM micrographs of pure and coatings with alumina nanoparticles cured by two abovementioned regimes (Figure 2.14). It can be remarked that the surface of pure polyester coatings displayed myriad pores and cracks within their structure which deteriorated protective characteristics of these materials. Furthermore, the samples which were subjected to curing by microwave regime showed better corrosion and wear resistance in comparison to those cured in oven (Figure 2.14).
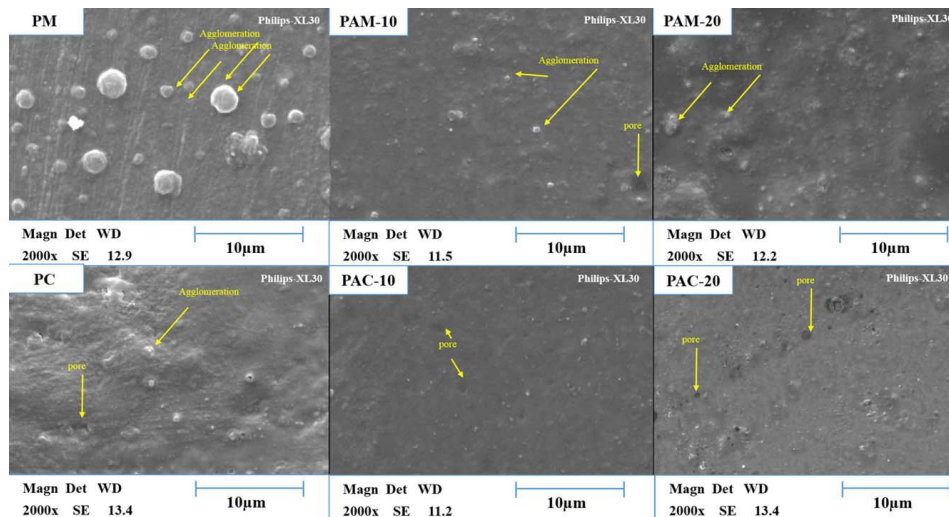
Figure 2. 14. The SEM micrographs from upper surface of cured coating in oven and microwave [84]

2.6. Thermal properties of polymer/alumina based composites

Thermal properties of composite materials have been investigated using two most commonly methods: thermogravimetric analysis (TGA) and differential scanning calorimetry (DSC) [85]. Thermal analysis determines the physical and chemical properties of the material as a function of temperature and/or time, with the sample being exposed to a particular temperature regime in a suitable atmosphere. The results of thermal analyzes are used to evaluate the stability of the material over a given temperature interval, as well as for quantitative and qualitative determination of the presented phases [21].

TGA is a dynamic method of continuously determining the change in mass of a test specimen as a function of temperature, at a constant heat rate or temperature as a function of time. Using the TGA method, it is possible to determine the following parameters: moisture content and easily volatile substances, inorganic fillers content, thermal stability of the test sample under different conditions (N_2, O_2, air) and so on [86].

The DSC method is based on the measurement of the energy that must be brought to the material to keep the temperature difference of the test and reference sample at zero throughout the course of the experiment. The measurement is performed by placing the reference and measuring samples in thermally insulated pots of the measured furnace cell whereby the samples are heated with a linear change in temperature over time. The instrument measures the amount of heat supplied per unit of time, mJ/s, and the thermogram shows the results as a dependence of mJ/s, mW/mg or cp on temperature or time.

The thermal properties of composites depend on myriad factors, including the filler type, amount, particle size and surface nature, *i.e.* interfacial interaction with polymer matrix. It was shown that reinforcing of HDPE with alumina and combination of alumina and glass fibers significantly improved thermal stability of corresponding composites (Figure 2.15) [79].
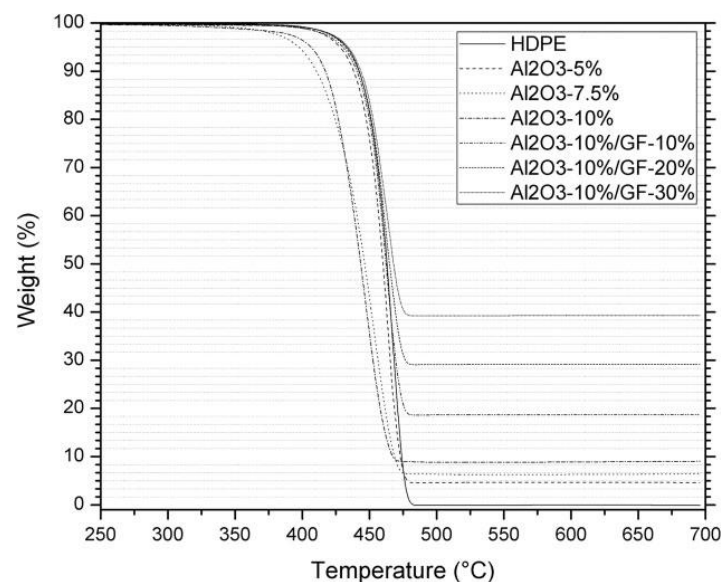
Figure 2. 15. TGA curves of the pure HDPE and corresponding composites [79]

The presence of glass fibers additionally improve thermal stability of examined composites since the content of inorganic materials were increased. The used filler exhibit barrier and catalytic effect, which are in antagonism since the first one is responsible for protecting the material for further exposing to heat flux and thus causes higher thermal stability while the latter promotes premature degradation of the polymer [79].

The onset temperature, end temperature and degradation temperatures at 10% weight loss obtained from the TGA data of pure UPR and corresponding composites are tabulated in Table 2.3 [87]. Shown results indicate that introducing the alumina particles within the polymer structure increases its thermal stability. For pure UPR, the maximum degradation temperature is 344 ºC, while for the composites it increases from 32 to 41 ºC in comparison to neat polymer. The improvement of thermal stability by embedding of alumina can be attributed to its homogeneous distribution into the polymer matrix as well as the tortuous path in the composites that hinders diffusion of the volatile decomposition products compared to that in pure UPR [87].

Table 2. 3. TGA data of pure UPR and UPR/alumina nanocomposites [87]

Composition	Onset temperature [ºC]	End temperature [ºC]	T_{max} [ºC]	T_{10}% [ºC]	Weight residue [%]
UPR	165	422	344	263	3.0
UPR/1 wt% nano alumina	168	425	376	279	4.9
UPR/3 wt% nano alumina	168	430	379	283	1.0
UPR/5 wt% nano alumina	170	433	381	285	2.8
UPR/7 wt% nano alumina	173	436	383	286	5.8
UPR/9 wt% nano alumina	178	438	385	289	6.7

Mallakpour and Dinari investigated thermal properties of neat poly(amide-imide) (PAI) and composites contained 5, 10 and 15% of nano-scaled alumina [88]. The testing was performed by TGA at a heating rate of 10 ºC in nitrogen atmosphere. Figure 2.16 and Table 2.4 exhibit the TGA profiles and the corresponding thermoanalysis data, including the T_5 and T_{10} temperatures degradation occurs and char yield at 800 ºC. The pure PAI gave the T_5 of 415 ºC, which gradually increased by raise of alumina content up to 493 ºC corresponding to 15% of filler amount.

Table 2. 4. Thermal properties of the PAI and different alumina nanoparticles [88]

Samples	Decomposition temperature [ºC]		Char yield [%]
	T_5	T_{10}	
PAI	415	450	54
$Al_2O_3$5%	453	474	58
$Al_2O_3$10%	476	497	62
$Al_2O_3$15%	493	511	67

Besides, the char yields for corresponding composites exhibited the same increasing pattern as the change of T_5, in comparison to neat PAI. The remarked enhancement was from 7.4 to 24.1% compared to pure PAI. This enhancement in the char formation can be ascribed to the high heat resistance exerted by the Al_2O_3. In addition, the nano-scaled alumina offers a larger surface area responsible for the improving of thermal covering/protection effect. The loose tails of coupling agents at alumina surface potentially may interact with the PAI macromolecule, establishing hydrogen bonds. These bonds hindered the thermal motion of PAI segments, enhanced the breaking energy during the heating process and thus improved the thermal stability of corresponding composites.
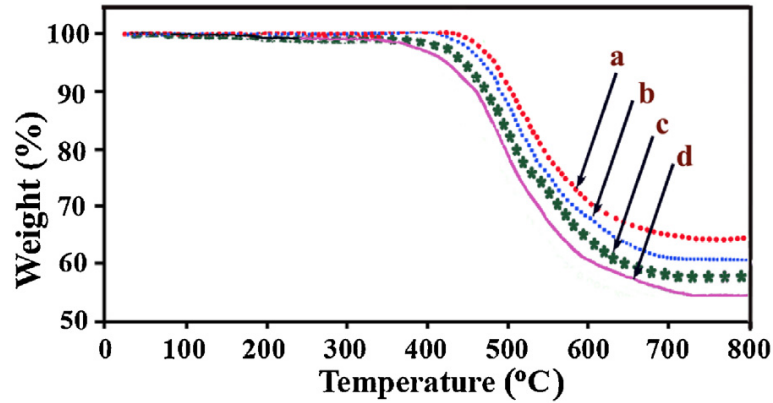
Figure 2. 16. TGA thermograms of (a) PAI/Al$_2$O$_3$ (15 wt%), (b) PAI/Al$_2$O$_3$ (10 wt%), (c) PAI/Al$_2$O$_3$ (5 wt%) and (d) pure PAI [88]

Edhikari et al. prepared UPR based composites strengthened with jute fibers and metal oxides, Al$_2$O$_3$ and ZrO$_2$, and studied their thermal properties [89]. Weight loss of different composites was observed between 32 °C and 460 °C. Thermal stability, degradation temperature for weight loss of 50 wt% (T$_{50}$), , weight change between mentioned temperatures and residue content at 600 °C is shown in the Table 2.5. It is clearly that corresponding composites exhibit better thermal stability in comparison to neat UPR resin. Thermal stability was found to be highest for UP/jute/ZrO$_2$ composites, while the influence of alumina is obvious but slightly lower.

Table 2. 5. Thermal properties of different UP based composites with 20 wt% filler content

Sample	Thermal stability [°C]	T$_{50}$ [°C]	Weight loss at 460 °C [wt%]	Residue content [%]
UPR/jute	32.5	346.18	97.195	1.135
UPR/jute/ZrO$_2$	37.07	352.12	94.025	2.001
UPR/jute/Al$_2$O$_3$	36.14	349.26	96.745	1.775

2.7. Dynamic-mechanical properties of polymer/alumina based composites

Dynamic-mechanical analysis (DMA) is one of the most accurate and widely used methods for analyzing the viscoelastic behavior of polymeric materials. The principle of this technique is based on measuring the viscoelastic response of the test sample to the effect of cyclic (sinusoidal) stress [90]. Stress or deformation changes periodically, most often as a time depending sinusoidal function. In the case of a viscous body, the impact of the sinusoidal stress leads to a strain that delays behind the stress by 90°. In viscous bodies, the rate of deformation is proportional to the stress, not the deformation. In the case of polymers, the effect of sinusoidal stress leads to deformation which is delayed by the stress by an angle δ (0 - 90°). This delay is caused by the relaxation of the polymer chain segments. To separate the elastic and viscous response of the viscoelastic material, the stress vector can be represented as the sum of the components, one in phase and the other out of phase, *i.e.* delays for 90° to the deformation. The relation between the stress in phase with the deformation and the deformation itself is called the modulus of the stored energy, G'. The ratio of the component of stress that is not related to the deformation, *i.e.* phase shifted by an angle of 90° and the deformation itself is called the lost energy modulus, G". The relationship between the two modules is called the loss angle tangents, tanδ [8].

One of the main parameters, which is determined by the DMA method, is the T$_g$ of the polymer. T$_g$ represents a narrow temperature interval where the changing of the following properties: specific volume, specific heat, viscoelastic properties, thermal conductivity, etc. is

occurred [90]. Below T_g, the polymeric material is in the glassy and above in the rubbery state [91]. In the glassy state, the segments of the macromolecular chain only vibrate around the established equilibrium positions. As the temperature increases, the amplitude of the mentioned vibrations increases, so that the polymer chain segment motions are triggered at T_g. Above T_g, the segments can produce rotational, translational, and diffusive motion, while at sufficiently high temperatures in linear polymers, viscous flowing occurs as irreversible deformation.

The parameters that affect the T_g of polymeric materials are: structure and polarity, molar mass, network density, fillers, etc. The presence of a filler reduces or increases T_g, depending on the type and intensity with the polymer matrix. This is explained by the occurrence of complementary relaxation processes related to the filler-polymer matrix interaction. Some studies show an increase in T_g after the addition of char, SiO_2 or other fillers, while others indicate no change in T_g. The nature of the interfacial interactions between the polymer and the filler particles may explain some of the different results related to the effect of the filler on T_g. DMA investigations are often used to study the influence of filler particles on T_g of polymers, where conclusions are brought based on the position of the temperature depending tanδ peak remarked in the glass transition region.

The influence of different loadings of nano alumina on dynamic-mechanical properties of UPR base composites is presented in the following publication [87]. They found that the addition of alumina up to 5 wt% increases T_g, afterwards slightly decrease is remarked, by further incorporation of the filler particles. The maximum achieved value for Tg was 120 ℃ which is evidenced in Figure 2.17.
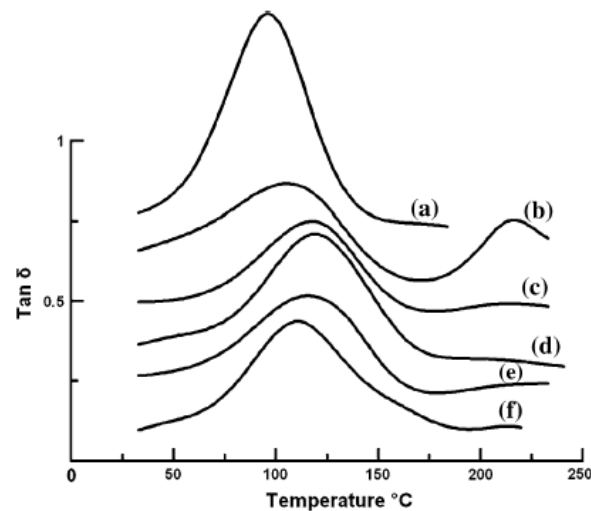
Figure 2. 17. Temperature dependence of tanδ of UPR/alumina nanocomposites, (a) Pure polyester, (b) UPR/1% nano alumina, (c) UPR/3% nano alumina, (d) UPR/5% nano alumina, (e) UPR/7% nano alumina, (f) UPR/9% nano alumina [87]

The increase in T_g is potentially related to enhancing the interfacial interaction between UPR matrix and nano alumina particles, which causes restriction the motion of macromolecule segments within the resin structure [92]. Higher filler loading causes particles clustering, which deteriorates the material homogeneity, weakens the polymer matrix/alumina adhesion and thus decreases mechanical and dynamical properties of end product. The same trend is depicted at storage modulus, where the maximum value, 51% higher in comparison to neat UPR resin, is obtained for composite that contains 5 wt% of alumina.

Conversely, Arimateia et al. show that the addition of two types of alumina, commercial and synthesized (ALC and ALS, respectively), have no significant effect to dynamic-mechanical properties of PMMA based composites [93]. The addition of ALS and ALC to polymer matrix does not cause shifting the tanδ peak to lower or higher temperatures, suggesting that the presence of the alumina has no influence to segmental motion of PMMA macromolecule chains (Figure 2.18b). Contrary to this, there is a slightly increase of E', observed for composite containing 3 wt% of ALC, which is evidenced in Figure 2.18a.
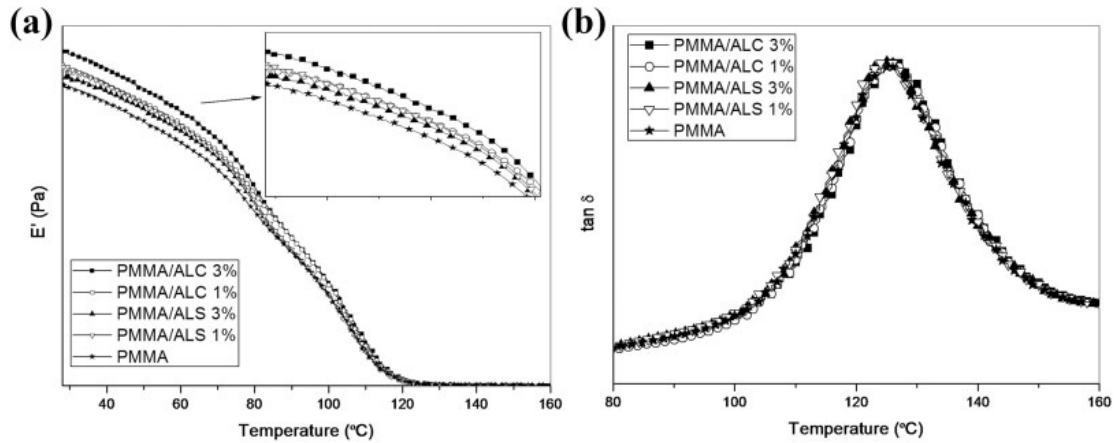
Figure 2. 18. Temperature dependence of E' and tanδ: (a) E' versus temperature and (b) tanδ versus temperature [93]

2.8. Usage of alumina based composites as adsorbents for heavy metal ions removal

Environmental pollution, caused by releasing of toxic substances from industries, such as heavy metal ions (lead, cadmium, nickel) has attracted much concern in recent years [94]. These heavy metal ionic are classified as carcinogen elements linked to myriad forms of skin, lung, liver, bladder and kidney cancers [95]. Moreover, their toxic effect is caused by replacing metal ions naturally presented in biological systems (calcium, zinc, magnesium etc.) followed with modification of active biological molecule conformations and blocking of essential functional groups [96,97].

Therefore, it is important to develop a highly efficient, reliable and economically cost-effective technique for heavy metal ion removal from natural and wastewaters. Various treatment methods such as ultrafiltration, ion exchange, coagulation/precipitation, membrane filtration, reverse osmosis, and adsorption have been used for wastewater purification. Among the above technologies, adsorption is classified as promising technology due to its simplicity in design, ease of handling and ability to overcome secondary pollutants [98]. Many adsorbents have been reported in the literature for the removal of heavy metal ions such as amino-modified nanocellulose impregnated with iron oxide [99,100], amino modified and oxidized multi-walled carbon nanotubes [101], cerium supported porous carbon [102] and iron-oxide-coated eggshell and porous wollastonite as natural based adsorbents [95,103].

Moreover, three dimensionally ordered macroporous materials (3DOM) with ordered arrays of pores of diameters from tens to hundreds of nanometers and high specific surface area are well promising candidates to be used as adsorbents [104]. The colloidal crystal template (CCT) method is a very effective way to prepare 3DOM materials with well-ordered packed structure of silica, polystyrene (PS), or poly(methyl methacrylate) (PMMA) microspheres [105].

Alumina is, among other applications, widely used for a broad range of adsorbents [106]. To achieve high adsorption capacity and faster kinetics, comprehensive studies were performed specifying the high adsorption capability of γ-alumina either in the form of activated alumina [107] or nanoparticles [108]. For successful adsorption, it is necessary to adjust/optimize the various parameters such as contact time, adsorbent dosage, and temperature.

3. EXPERIMENTAL PART

3.1 Materials and chemicals

Waste PET flakes, obtained by crushing of obsolete PET bottles previously liberated from impurities and adhesives, were procured from RKS Kompoziti Ltd. Propylene glycol, tetrabutyltitanate (TBT), styrene, sodium hydroxide, toluene, pyridine, methyl ethyl ketone peroxide, cobalt octoate, maleic anhydride, hydroquinone (HQ), methanol, absolute ethanol, tetrahydrofuran (THF), commercial alumina, c-Al$_2$O$_3$, and iron(III)-chloride (FeCl$_3 \cdot$6H$_2$O), potassium persulfate (KPS) were obtained from Sigma-Aldrich. Monomer methyl methacrylate (MMA) (M55909, Sigma Aldrich) was distilled to remove inhibitor just prior to use. Locron L (Al$_2$(OH)$_5$Cl$\cdot$2.5H$_2$O), used for alumina synthesis, was supplied by Clariant. The 3-(aminopropyl)trimethoxysilane (APTMS), vinyl tris(2-methoxyethoxy)-silane (VTMOEO) and 3-methacryloxypropyl-trimethoxysilane (MEMO) were supplied by Dynasylan, Evonik Industries (Figure 3.1). Poly(ethylene glycol) (PEG), used as a dispersing agent, was procured from Lipoxol 6000, Sasol. Atomic adsorption standard (AAS) solutions of metal ions: Pb^{2+} (Pb(NO$_3$)$_2$ in HNO$_3$ 0.5 mol/L, Merck, Darmstadt, Germany), Ni^{2+} (Ni(NO$_3$)$\cdot$6H$_2$O in HNO$_3$, Accu Standard, New Haven , CT, USA), Cd^{2+} (AppliChem Panreac ITW Companies, Darmstadt, Germany) were further diluted to the required concentration.
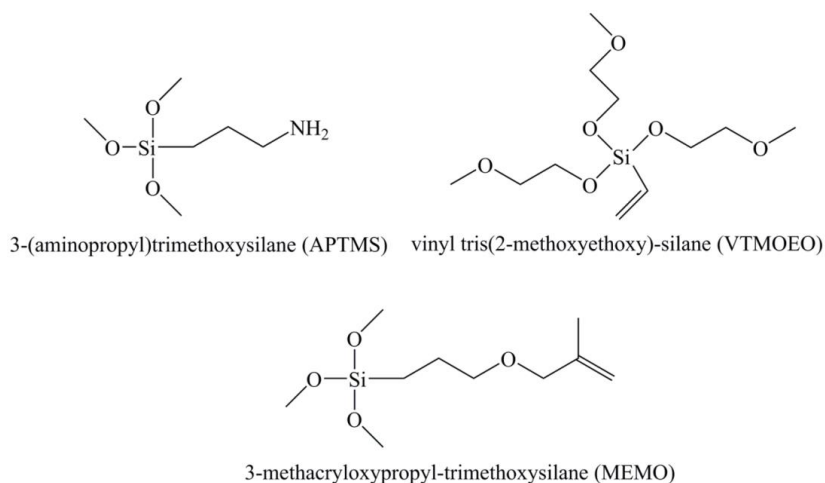
Figure 3. 1. Silanes used for chemical functionalization of commercial and Fe doped alumina particles

3.2 Synthesis of unsaturated polyester resin from waste poly(ethylene terephthalate)

The UPR synthesis was carried-out through two-stages procedure: (i) catalytic glycolysis of waste PET by PG and TBT (molar ratio PET:PG was 1:0.65) and (ii) polycondensation of previously obtained polyol with MA. Pilot-scale synthesis of UPR resin (molar ratio PG:MA was 1:0.95) was performed in accordance with previous publication [14] in a custom-made pressure reactor (8 l of reactor volume) equipped with mechanical stirrer, nitrogen inlet system, reflux condenser, Dean-Stark azeotropic separator, temperature and pressure controllers, and indicators. 4 kg of PET flakes was carefully placed into 1.54 l of PG, previously preheated at 190 ℃ for 3 h, to provide controlled depolymerization. The glycolysis lasted for the next 6 h at 220 ℃, without removal of ethylene glycol (classical glycolysis method). Afterwards, the reaction mixture was cooled down to 90 ℃ and the first

portion (0.015 wt%) of HQ was added. The temperature was increased from 90 to 210 ℃ at heating rate 15 ℃/h. When the reactor temperature reached 150 ℃, the MA ring opened and the polycondensation reaction started, which was manifested by the formation of water as a by-product. To separate water from system and favor the polycondensation reaction, 2 wt% of toluene was added to the reactor. After completion of the reaction, the reaction mixture was cooled to 120 °C and the second portion of HQ was added to the reactor. Vacuum distillation was performed to remove residual water, toluene and other easily volatile components. The resulting resin was then dissolved in styrene (33 wt.% of styrene in relation to the total amount of the mixture) with vigorous stirring to homogenize the system. A styrene reserve of 7 wt% (final weight ratio of polyester and styrene is 60:40 in UPR resin) is left for easier preparation of composite materials, *i.e.* dispersion alumina particles. The prepared UPR resin had the following characteristics: acid value (AV) 12 and hydroxyl value (HV) 41.

3.3 Synthesis of alumina doped with iron(III)-oxide

Alumina particles doped with iron(III)-oxide have been prepared by sol‑gel technique, accordingly to the published procedure [109]. The $Al_2Cl(OH)5·2.5H_2O$, demineralized water and 1.5 wt% $FeCl_3·6H_2O$ were placed into the reactor and left to gel. Hence, the such obtained material was thermally treated at 900 ℃ for the next 2 h.

3.4 Surface modification of alumina reinforcements

Firstly, 1 g of both alumina particles, c-Al_2O_3 and Fe-Al_2O_3, were dispersed in 75 ml of toluene using ultrasonic bath (Bandelin electronic, Berlin, Germany, power 120 W, frequency 35 kHz) for 10 min. Obtained slurry was introduced in reactor equipped with condenser, dropping funnel, heating system and thermometer. Afterwards, 1 g of VTMOEO/MEMO was step-wise added in reactor and reaction was carried-out for the next 22 h at 25 ℃. After completion of reaction, the targeted particles, c-Al_2O_3VTMOEO, Fe-Al_2O_3VTMOEO, c-Al_2O_3MEMO and Fe-Al_2O_3MEMO, were separated by filtration, purified with hexane and dried under the low pressure at 40 °C for 12 h [110].

The described process gave the successfully performed laboratory modification pattern, which was used in semi-industrial level using following reagents: (i) APTMS (one-step modification) and (ii) APTMS modified Al_2O_3 was subsequently modified with methyl ester of linseed oil fatty acids (biodiesel of linseed oil−BD) synthesized according to the previously published method (two-step modification) [5]. Modification procedure was carried-out in the following manner:

a) *First step −modification with APTMS*. Alumina particles, c-Al_2O_3 or Fe-Al_2O_3, (0.1 kg) were dispersed in 2 l of toluene using ultrasonic probe for 1 h. Obtained suspension was poured in reactor, which was used in above described procedure. Afterwards, 20 ml of APTMS was added and the reaction was lasted for the next 48 h at 25 ℃ under inert atmosphere. After the reaction was finished, the excess of solvent was removed by vacuum filtration, while the targeted products, c-Al_2O_3APTMS or Fe-Al_2O_3APTMS, were purified by vigorously washing with toluene and dried. Such products were further used in composite production or subjected to second modification step.

b) *Second step—modification with BD*. The amino-terminated alumina was dispersed in 2 l of THF. Then, 160 g of BD was charged into the four-necked glass reactor (5 l), equipped with a mechanical stirrer, temperature measurement unit, condenser with calcium chloride protection tube and nitrogen inlet tube. The reaction

took place for 12 h at room temperature and then, the temperature was increased to 60 ℃ for the next 2 h. The final products, c-Al$_2$O$_3$APTMS-BD and Fe-Al$_2$O$_3$APTMS-BD, were filtered under the low pressure, thoroughly purified two times with THF and absolute ethanol, and dried at 40 ℃ for 12 h.

The pristine, c-Al$_2$O$_3$ and Fe-Al$_2$O$_3$, as well as the modified fillers were used in composites production as a reinforcements in UPR matrix.

3.5 Preparation of composites based on UPR and alumina reinforcement

Composites have been prepared via the solution blending method by compounding the defined amount of UPR resin and pristine or functionalized alumina filler. The general formula for composites is UPR/a-Al$_2$O$_3$N(n), where specific letters have a following meanings:

- a - the type of alumina particles (commercial or Fe doped);
- N - alumina modification type (c-Al$_2$O$_3$VTMOEO, Fe-Al$_2$O$_3$VTMOEO, c-Al$_2$O$_3$MEMO, Fe-Al$_2$O$_3$MEMO, c-Al$_2$O$_3$APTMS, Fe-Al$_2$O$_3$APTMS, c-Al$_2$O$_3$APTMS-BD and Fe-Al$_2$O$_3$APTMS-BD);
- n - the amount of added filler into UPR matrix: (a) 0.1, (b) 0.25, (c) 0.5, (d) 1.0, and (e) 2.5 wt%.

All ingredients, binder, fillers and the curing system (cobalt octoate/methyl ethyl ketone peroxide), were placed into a vacuum molding device, equipped with mechanical stirrer, where homogeneous slurry was obtained by vigorous blending, which was further injected into the mold. The cured samples were taken out from the mold and subjected to post-curing at 50 ℃ for an additional 2 h. Schematic view of UPR synthesis, semi-industrial alumina modification and composite preparation is presented in Figure 3.2.
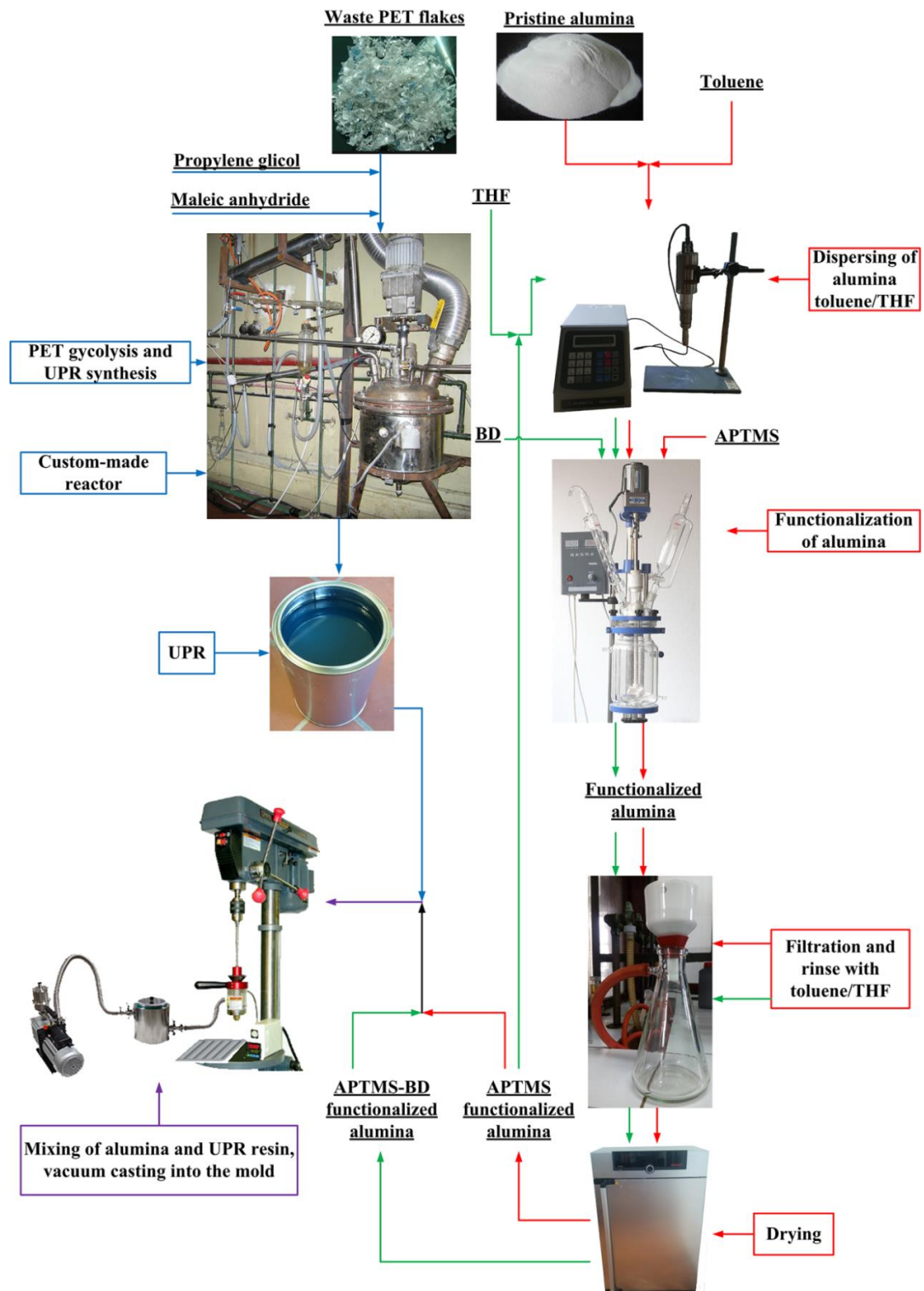
Figure 3. 2. Schematic overview of the procedure for the production the UPR/alumina-based composites

3.6 Synthesis of ultra-fine PMMA microspheres in methanol-enriched aqueous media

The PMMA microspheres were synthesized according to emulsifier-free emulsion polymerization [111]. The procedure was carried out in a 500 mL round-bottomed flask with a mechanical stirring at 100 rpm under a inert atmosphere at 70 °C. Firstly, 200 g of methanol and 80 ml of water were placed into the reactor and then 10 g of MMA was added. When the reaction mixture reached 70 °C, an aqueous solution of KPS (0.075 g KPS/20 mL H_2O) was added as initiator. The polymerization was carried out for 1 h, afterwards the mixture was cooled, filtrated and purified with the mixture of cold methanol and water. The excess of solvent, ethanol and water was removed by centrifugal purification at 4500 rpm. The purified PMMA microspheres were dried and used as pattern for manufacturing the highly ordered alumina.

3.7 Synthesis of highly ordered alumina adsorbent

The highly order alumina (3DOM alumina) was prepared by a CCT method using an aqueous solution of $Al_2Cl(OH)_5 \cdot 2.5H_2O$ as the precursor (15:20 wt/wt). 2 g of PMMA microspheres were added in the mixture solution consisting of 0.98 mL PEG and 3.34 mL aluminum hydroxide. The obtained mixture was vigorously stirred at 800 rpm for 1 min. Such material was kept at room temperature for 5 h to allow the self-assembly of the PMMA microspheres followed by a drying at 40 °C for 48 h. The dried samples were calcined in a tubular furnace, with a heating rate of 1 °C/min to 800 °C and kept for 5 h at this temperature.

3.8 Adsorption and kinetics experiments

Batch experiments for adsorption of Pb^{2+}, Ni^{2+} and Cd^{2+} ions were applied to evaluate the effect of diffusion processes on the performance of the highly ordered γ-alumina-based adsorbents. Various suspensions of the adsorbent material with large range of densities (200, 300, 400, 500, 600, 800, 1000, 2000, 2500 and 300 mg/L), were introduced in vials containing 25 mg/L of standard solutions of Pb^{2+}, Ni^{2+} or Cd^{2+} ions. The adsorption and kinetic experiments were performed at 25, 35 and 45 °C. The kinetics measurement conditions were as follow: the contact time of adsorbent and ions of interest was in the range 0 - 24 h, ions concentration was 5 mg/L, density 200 mg/L, while the was pH 6.5 for Pb^{2+}, 6 for Ni^{2+} and Cd^{2+} ions. The average value from the three iterations was used for processing the experimental data. The amount of adsorbed Pb^{2+}, Ni^{2+} and Cd^{2+} ions was calculated using Eq. (3.1):

$$q = \left(\frac{C_i - C_f}{m} \right) \cdot V \quad (3.1)$$

where q is adsorption capacity in mg/g of adsorbent, C_i and C_f are the initial and final concentrations of Pb^{2+}, Ni^{2+}, and Cd^{2+} ions in mg/L, respectively, V is the volume of solution in L and m is the mass of the adsorbent in g.

3.9 Characterization methods for filler particles, polymer matrix and corresponding composites

3.9.1 Determination of acid value and gel time

The AV value was determined according to the standard ASTM D3644 method. AV is the mass of KOH expressed in mg, required to neutralize the free acid groups per gram of sample. The measured sample was dissolved in 50 ml of isopropanol/toluene mixture (50/50 v/v), afterwards a few drops of phenolphthalein dissolved in ethanol (10 g/L) were added. Further on, the titration with standard solution of KOH (0.5 mol/L) was performed until the solution became pale pink. Conversely, the gel time was determined according to standard ASTMD 2471-99 method.

3.9.2 Nuclear magnetic spectroscopy (NMR)

The ^{1}H NMR spectra of the UPR resin was recorded in deuterated chloroform (CDCl$_3$) on a Varian-Gemini 200 spectrometer. ^{1}H NMR spectrum was recorded at 200 MHz and 50 MHz, respectively.

3.9.3 X-ray diffraction (XRD) of alumina particles

XRD analysis was performed using a Bruker D8 Advance diffractometer in Bragg-Brentano transmission mode θ/θ with the primary germanium (Ge (111)) monochromator of Johannson type (CuKα1 radiation). Anodic voltage and anodic current were 40 kV and 30 mA, respectively. The diffraction data were collected by using scintillation counter of NaI (TI) type and the scan-step method in the range of 2θ diffraction angle from 10-90º, with step size of 0.05º and counting time of 6 s per step. The corundum structure of the alumina particles is confirmed by comparison of the XRD data to the standard card 93096-ICSD.

3.9.4 Infrared spectroscopy with Fourier transformation (FTIR)

FTIR spectroscopic is a non-destructive method suitable for determination of chemical composition, microscopic structure and intensity of interactions between organic and inorganic materials [8]. Fourier transform infrared spectra (FTIR) of pristine and modified alumina particles, UPR resin and corresponding composites as well as synthesized PMMA microspheres were recorded in transmission mode, between 400 and 4000 cm^{-1}, at 4 cm^{-1} resolution, using an FTIR Bomem spectrometer (Brown & Hartmann). Samples were ground and mixed with potassium(I)-bromide (KBr) and compacted on a laboratory hydraulic press.

3.9.5 Scanning electronic microscopy (SEM) and image analysis

Microstructural characterization of the modified alumina particles, the corresponding composites and PMMA microspheres was obtained using a Field Emission Gun Scanning Electron Microscopy device with field emission gun TESCAN MIRA3 electron microscope at an accelerating voltage of 20 kV. Prior to the observation, the samples were degassed and sputter coated with gold using a Polaron SC 502 Sputter Coater (Fison Instruments, UK). The obtained SEM images of both types of pristine alumina partisles as well as VTMOEO and MEMO modified ones were used for detailed morphology analysis using Image ProPlus software.

3.9.6 Thermogravimetric analysis (TGA) and differential scanning calorimetry (DSC)

Thermogravimetry analysis and differential scanning calorimetry of pristine/modified particles as well as corresponding composites were performed using SDT Q600 instrument. Samples were heated at 10 °C min^{-1} to 800 °C in a flow of nitrogen (100 cm^3 min^{-1}).

The thermal stability of the alumina/PMMA composites was investigated by non-isothermal thermogravimetric analysis using a SETARAM SETSYS Evolution 1750 instrument. The measurements were conducted at a heating rate of 10 °C/min in a dynamic argon atmosphere (flow rate 20 cm^3/min) in the temperature range of 30 – 800 °C.

3.9.7 Dynamic-mechanical analysis (DMA)

Dynamical-mechanical properties of composites were obtained using Discovery Hybrid Rheometer HR2. The DMA was conducted in a torsion rectangular mode (sample dimensions: 6x1x0.2 mm^3) from 25 to 250 ℃ at a fixed strain amplitude of 0.1% and angular frequency of 1 Hz. The glass transition temperature, determined by the dynamic mechanical measurements, was estimated as the maximum value at the temperature dependence curve of the loss factor, tanδ [112].

3.9.8 Uniaxial tensile measurements

Uniaxial tensile measurements of standard cured samples were performed using an AG-X plus Universal testing machine, Shimadzu Corporation according to ASTM D882-12 standard method. All the tests were performed on three replicates for each sample at room temperature and crosshead speed of 0.5 mm/min.

3.9.9 Micro Vickers hardness (VH)

The hardness of the composites was measured using micro Vickers hardness (VH) tester Leitz, Kleinharteprufer Durimeti with a load of 4.9 N according to ASTM E384-16 standard method. A pyramidal indenter with a penetration angle of 136º was used. To obtain credible results, the indenter injection time was up to 25 s (usually 10-15 s). The average VH value is expressed as the average value obtained from three points, while the standard deviation was calculated in Microsoft Office Excel software.

3.9.10 Determination of molecular weight of synthesized PMMA microspheres

The molecular weight of the synthesized PMMA microspheres was determined from the results of viscosity measurements. The sample was dissolved in chloroform by mixing at ambient temperature for 24 h, and then thermostatically controlled at 25 °C before conducting the viscosity measurement in an Ubbelohde viscometer at 25 °C. Five solutions of PMMA microspheres, from 0.00275 to 0.00500 kg/L, were used.

3.9.11 Adsorption spectrometry (AAS)

The concentrations of Pb^{2+}, Ni^{2+}, and Cd^{2+} ions were measured by atomic adsorption spectrometry (AAS) using a Perkin Elmer PinAAcle 900T instrument according to the standard method 3111B [111]. A laboratory pH meter, InoLab Cond 730 precision conductivity meter (WTW GmbH), with an accuracy of $\pm$ 0.01 pH units, was used for the pH measurements. The pH values at the point of zero charge (pH_{PZC}) were measured using the pH drift method, before and after metal adsorption [113].`

4 RESULTS AND DISSCUSION

4.1 Structural analysis of UPR and pristine/modified alumina particles

4.1.1 NMR structural analysis of UPR resin

^{1}H NMR analysis of synthesized UPR indicates that reactive fumaric moiety, necessary for achieving high cross-linking reactivity, is present within the resin structure. Results of the analysis of ^{1}H NMR spectrum of UPR resin (Figure 4.1) are: ^{1}H NMR (CDCl$_3$): 1.15-1.42 (*m*, 6H, C$\underline{H}_3$), 3.99-4.54 (*m*, 6H, C$\underline{H}_2$C$\underline{H}$–), 4.33-4.67 (*m*, 4H, –O–C$\underline{H}_2$C$\underline{H}_2$–O–), 5.24-5.47 and 6.69-6.77 (*m*, 2H, fumaric moiety), 8.05 (*s*, 4H, H$_{Ph}$-terephthaloyl moiety).

The ^{1}H NMR spectra show that the dominant products of glycolysis are glycol esters of terephthalic acid: *bis*(2-hydroxylpropyl) terephthalate,(2-hydroxyethyl)(2-hydroxypropyl) terephthalate and glycols [14]. Results of NMR analysis confirm successful synthesis of UPR resin.
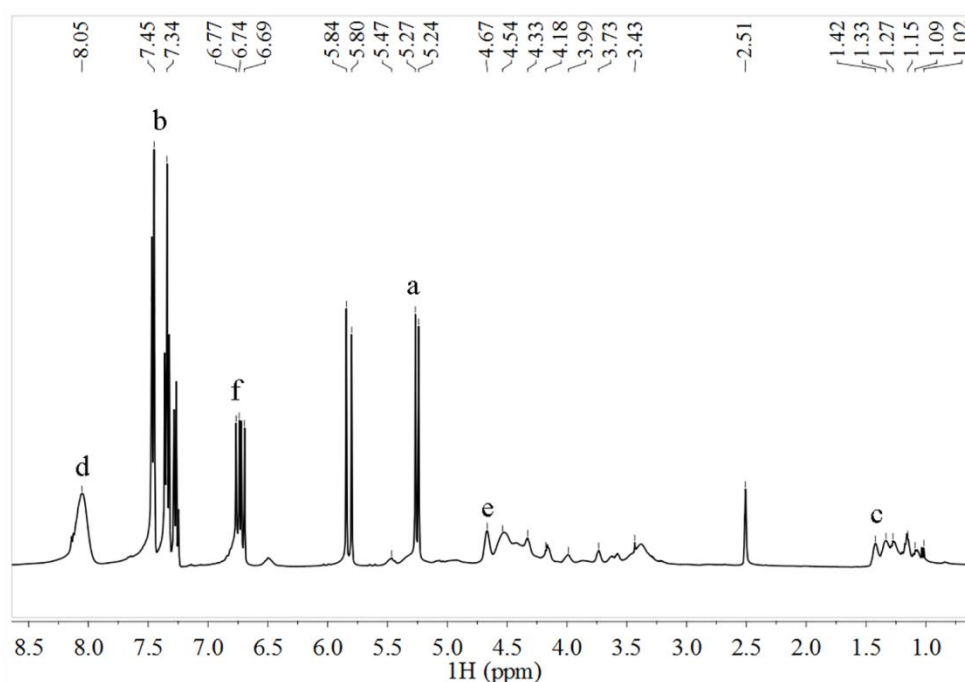
Figure 4. 1. ^{1}H NMR spectra of UPR resin

4.1.2 XRD analysis of alumina reinforcement

The XRD diffractogram of calcined alumina particles doped with iron oxide at 900 °C is shown in Figure 4.2. The alumina based particles with the addition of FeCl$_3$ had dominant η-Al$_2$O$_3$ (39.4%, PDF-2 77-0396), κ-Al$_2$O$_3$ (35.1%, PDF-2 73-1199) and α-Al$_2$O$_3$ phases (25.5%, PDF-2 74-1081) after heat treatment at 900 °C. Detailed study of the influence of processing parameters on the formation of crystalline form of Fe-Al$_2$O$_3$ has been recently published [109].
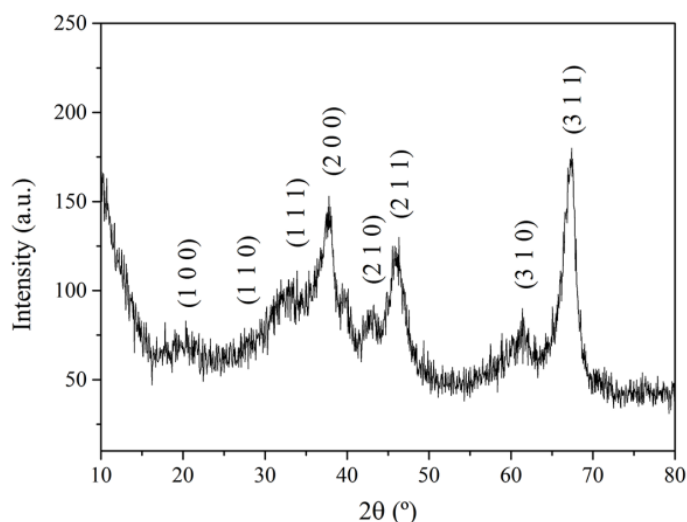
Figure 4. 2. XRD diffractogram of synthesized alumina particles doped with iron oxide – Fe-Al_2O_3 with crystalline planes

The addition of ferrous ion promotes the formation of the corundum crystalline form (α-Al_2O_3). The establishment of dense order in α-Al_2O_3 through alumina phase transition leads to the diminishing of porous structure within the basic material reflecting in lowering the specific surface area as the particle size increases [114]. The synthesized Fe-Al_2O_3 particles were of submicron size [115] while the c-Al_2O_3, γ phase were of diameter <50 nm.

The transition of sol-gel mixture of Al and Fe precursors to final product takes place in following manner: the crystalline single phase γ-(Al, Fe)$_2O_3$ of spinel structure is established from starting material, which is followed with directly transformation to α-(Al, Fe)$_2O_3$ solid solution. It is interesting to remark that there is no nucleation of ferric oxide seeds before mentioned transformation. The formation of α-Al_2O_3 is favored at lower temperatures due to segregation of Fe-rich clusters within the γ-(Al, Fe)$_2O_3$ matrix which act as seeds for nucleation and growth of α-Al_2O_3 [116].

Moreover, the interaction between γ-Al_2O_3 and α-Fe_2O_3 occurs at the temperature of 900 °C [116]. The width of the miscibility gap in the Fe_2O_3-Al_2O_3 system at 900 °C is between ~8 wt% Al_2O_3 in hematite (*ss*) and ~8 wt% Fe_2O_3 in corundum (*ss*). According to the calculated lattice parameter of obtained alumina particles by PowderCell 4.3 software (Fe-Al_2O_3, a = 4.673 Å), the introduced iron ion was effectively incorporated into the η-Al_2O_3 lattice.

The presence of corundum in Fe-Al_2O_3 particles can physically improve hardness of UPR based composites, but the γ c-Al_2O_3 provides better interfacial interactions with the polymer matrix due to the higher specific surface area, resulting in overall superb mechanical properties [109].

4.1.3 FTIR analysis of pristine/modified alumina and corresponding composites

The FTIR spectra of pristine, APTMS and APTMS-BD modified c-Al_2O_3 and Fe-Al_2O_3, are presented in Figure 4.3. The influence of utilized functionalization processes in tailoring of filler surface characteristics is studied.
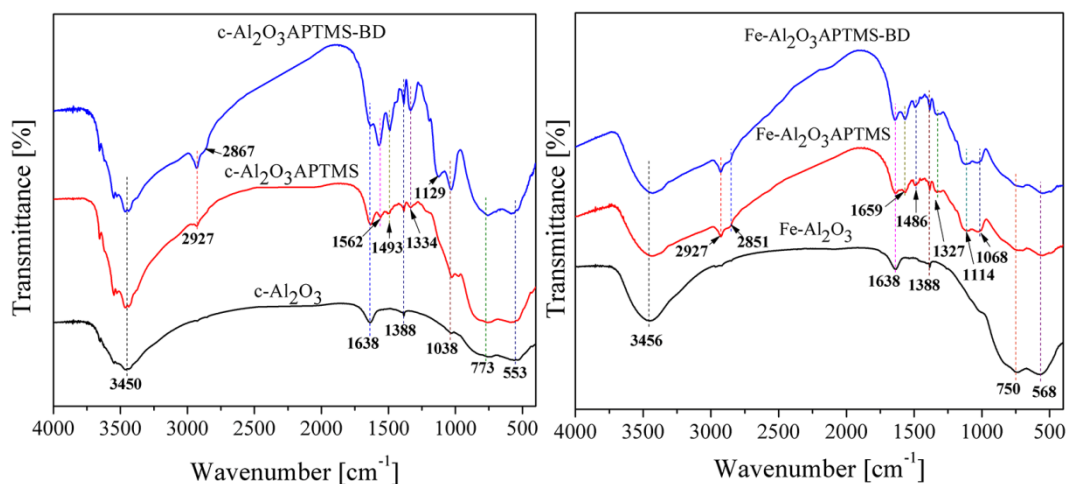
Figure 4. 3. FTIR spectra of pristine and APTMS and APTMS-BD modified alumina particles

The specific peaks of c-Al_2O_3 and Fe-Al_2O_3 particles, remarked at about 3450 cm^{-1} and 1638 cm^{-1} are attributed to hydroxyl group stretching and bending vibrations, respectively [38,117]. This suggests that most of OH groups are on the alumina surface, which points to surface affinity for adsorption of ambient moisture [118]. Moreover, pristine alumina shows characteristic broad bands in the range 550-750 cm^{-1} originated from Al-O-Al and Al-O vibrations [119]. The contribution of introduction the Fe atom within the alumina structure is expressed in shifting the band around 553 cm^{-1} of c-Al_2O_3 to the higher value (568 cm^{-1}) at the Fe-Al_2O_3 spectrum (Fe-O bending vibration) [120].

The peaks for modified alumina, observed at 2927, 2867 and 2851 cm^{-1}, originate from CH_3 and CH_2 groups stretching vibrations, respectively. The stretching ν(N-H) vibrations, which are overlapped with OH vibrations are remarked at ~ 3400 cm^{-1}. The peaks displayed at 1638 (amide I) at 1562 cm^{-1} (amide II) (Figure 3.3(a)) are associated with the C=O stretching vibration and N-H bending vibration coupled with the C-N stretching vibration of amide group, respectively [121]. In the range 1650-1600 cm^{-1} ethylenic double bonds, originated from BD, give the intensity to corresponding peaks. Moreover, these groups are overlapped with the ones corresponding to OH bending vibrations. Symmetrical C-H deformation vibrations of CH_3 groups are observed at 1493 and 1486 cm^{-1} (Figure 3.3(a) and (b), respectively). Stretching vibrations of N-H mixed with δN-H, from amino and primary amide bond present in c-Al_2O_3APTMS-BD are observed at 1129 cm^{-1} (Figure 3.3(a)). Two overlapped asymmetric bands at 1114 and 1068 cm^{-1} belong to Si-O stretching vibrations [122,123].

The FTIR spectra of UPR and chosen composites, UPR/Fe-Al_2O_3, UPR/Fe-Al_2O_3VTMOEO and UPR/Fe-Al_2O_3MEMO are shown in Figure 4.4.
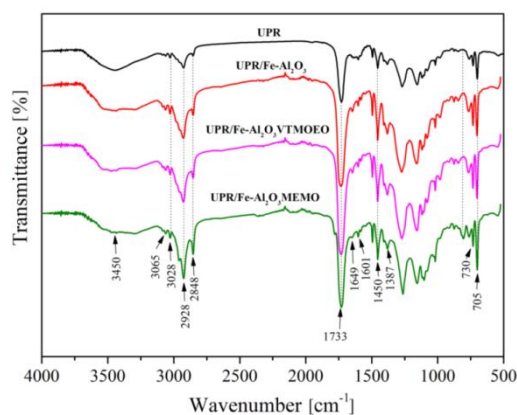
Figure 4. 4. FTIR spectra of UPR and composites reinforced with 1 wt% of pristine and modified Fe-Al$_2$O$_3$ particles

The wide band at $\approx$3450 cm^{-1} originates from the stretching vibrations of the hydroxyl groups present in UPR resin and corresponding composites. The two narrow peaks remarked at 3065 cm^{-1} and 3028 cm^{-1} are ascribed to =C–H stretching vibrations of reactive vinyl groups and aromatic ring in the terephthaloyl moiety. In addition, two pair of peaks, at 2928 cm^{-1} and 2848 cm^{-1} and at 1450 cm^{-1} and 1387 cm^{-1}, are corresponded to the stretching and bending vibrations of methyl and methylene groups, respectively. The intensive band at 1733 cm^{-1} belongs to the stretching vibrations of carbonyl C=O ester groups in the terephthaloyl moiety. The two peaks at 1649 cm^{-1} and 1601 cm^{-1} represent the skeletal C=C vibrations related to the phenyl core. The narrow adsorption peaks at about 730 cm^{-1} and 705 cm^{-1} are associated to the skeletal γ(CH) vibrations of the substituted benzene rings [19].

4.1.4 Curing kinetics of composites containing pristine and VTMOEO/MEMO modified alumina particles

The FTIR technique was also used in a kinetics measurements during the cross-linking reaction between ethylenic segments from UPR resin and vinyl moiety from styrene through the consumption of the characteristic styrenic C=C peak (Figure 4.5). The styrene consumption was quantified by the peak area change at 909 cm^{-1} and the obtained kinetics kinetic data were processed according to Beer's law [124]. The styrene conversion (α) was calculated in the manner shown by the Eq. 4.1:

$$\alpha = \frac{I_0 - I}{I_0} \quad (4.1)$$

where I_0 and I are the normalized transmittances of the characteristic peak before the reaction and at an appropriate reaction time, respectively.

Figure 4.5 shows that after 20 min, styrene conversion for all specimens, excluding UPR/Fe -Al$_2$O$_3$MEMO, reaches more than 75% of conversion. After 2 h, further increase of styrene conversion, above 80% is remarked, whereas the highest value is displayed for UPR/c-Al$_2$O$_3$ and UPR/Fe-Al$_2$O$_3$VTMOEO composites (higher than 90%). To achieve complete conversion of styrene into polymer network, the additional heating at 50 ºC for 2 h is performed. The highest value for styrene conversion of 99.5% upon additional heating is achieved for UPR/Fe-Al$_2$O$_3$VTMOEO, while for the another composites is in range 88 – 97%. This means that the part of styrene is evaporated during heating, while some quantity is captured within the composites.
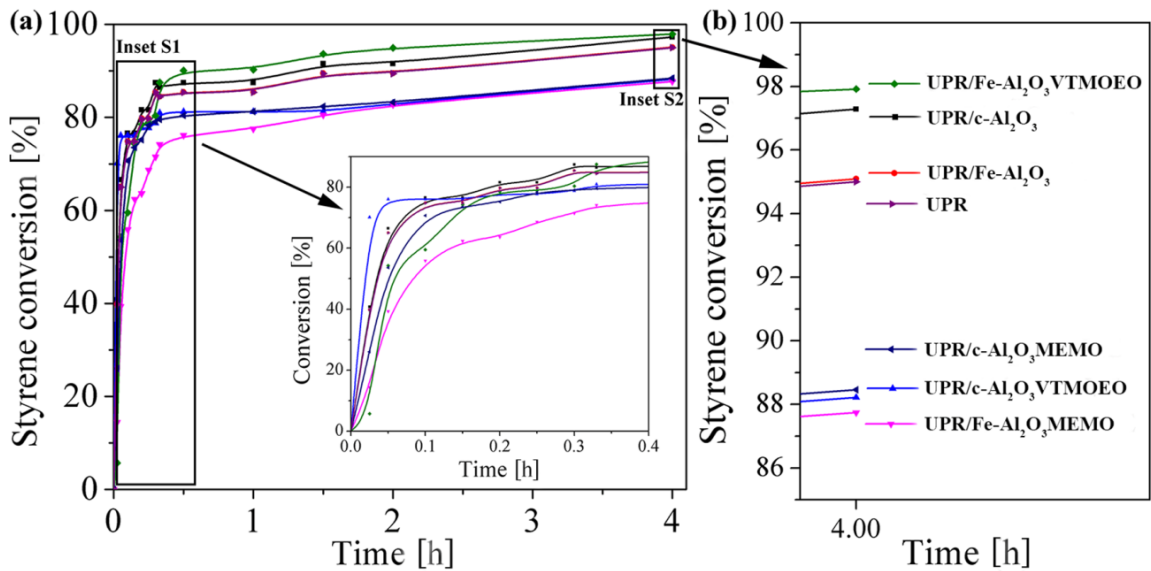
Figure 4. 5. Styrene conversion during curing of UPR resin and composites reinforced with APTMS/APTMS-BD modified alumina particles determined by FTIR method

These results approves the influence of alumina surface vinyl functionalities on cross-linking reactions during the curing process. It has been known that neat alumina particles ((c, Fe)-Al$_2$O$_3$) exhibit slight accelerating effect on curing process [125]. Silane domains onto alumina generally shows the negative influence on styrene depletion, except for Fe-Al$_2$O$_3$VTMOEO, causing slower cross-linking reactions. It seems that the steric hindrance caused by larger size of modified alumina overcomes the mutual affinity of reactive vinyl and methacryloyl functionalities involved in cross-linking reactions. The introduction of functionalized particles, especially Fe doped and MEMO functionalized alumina, reduces the free volume needed operative orientation of surface functionalities towards reactive ethylenic moieties present in UPR resin and styrene structure. Further on, embedding the large Fe-Al$_2$O$_3$ particles into polymer matrix increases the viscosity of corresponding composites, which limits the movement of macromolecule segments and thus, hinders diffusion process [126]. Lower mobility disables effective occurring of the free radical reaction (radical transfer reaction). Moreover, once the chain radical transfer takes place, it generates lower reactivity center due to steric hindrance of neighboring groups and lower mobility of filler particle. The consequence of all mentioned phenomena is the lower degree of styrene conversion. Another factor that control reactivity of the system originates from the potential for establishing of chemical interactions: dipole/dipole, dipole/induced dipole, Lewis acid/base between alumina and styrene. Considering that, a particular quantity of styrene/resin is anchored onto the alumina particle surface resulting in the reduction of available reactive centers. The large consumption of styrene at the first period of the curing substantially changes the conversion rate (Figure 4.5). Vinyl modification of the alumina increases the preferred compatibility with styrene which is reflected in the highest styrene conversion of UPR/Fe-Al$_2$O$_3$VTMOEO composite. Conversely, the low reactivity remarked for UPR/Fe-Al$_2$O$_3$MEMO composite is a consequence of incompatibility between methacryloyl and vinyl functionality which decreases the possibility for establishing the strong chemical interactions among them.

4.1.5 Curing kinetics of composites containing pristine and APTMS/APTMS-BD modified alumina particles

Curing kinetics of UPR resin and composites, containing 1 wt% of pristine and APTMS/APTMS-BD modified fillers is also measured by FTIR technique (Figure 4.6). Figure 4.6 shows that styrene conversion in the initial stage of curing (first 20 min - inset S1) is in range 77 - 87%. Composites reinforced with pristine alumina exhibit somewhat higher degree of styrene conversion (about 5%) in comparison to the ones strengthened with modified fillers. Further on, the prolonged heating for 2 h at 50 °C rise up styrene consumption for the additional 8 - 11% for all composites excluding the one reinforced with alumina modified with APTMS. The reason for such phenomenon is the inhibitory effect exhibited from amine functionalities which could participate in radical transfer reactions with peroxy radical (initiator) or alkyl radicals (chain transfer radical-propagation). This leads to formation of aminoxyl radicals of lower chain transfer capability which further could participate either in propagation or could return to their amino form. Another factor which define the system reactivity represents the potential for establishing the hydrogen bonds between amino groups from APTMS and carbonyl groups from UPR resin. Decreased flexibility of macromolecule segments causes reduced efficacy of radical transfer between ethylenic segments from UPR resin and styrene which slow down the cross-linking reaction [127].
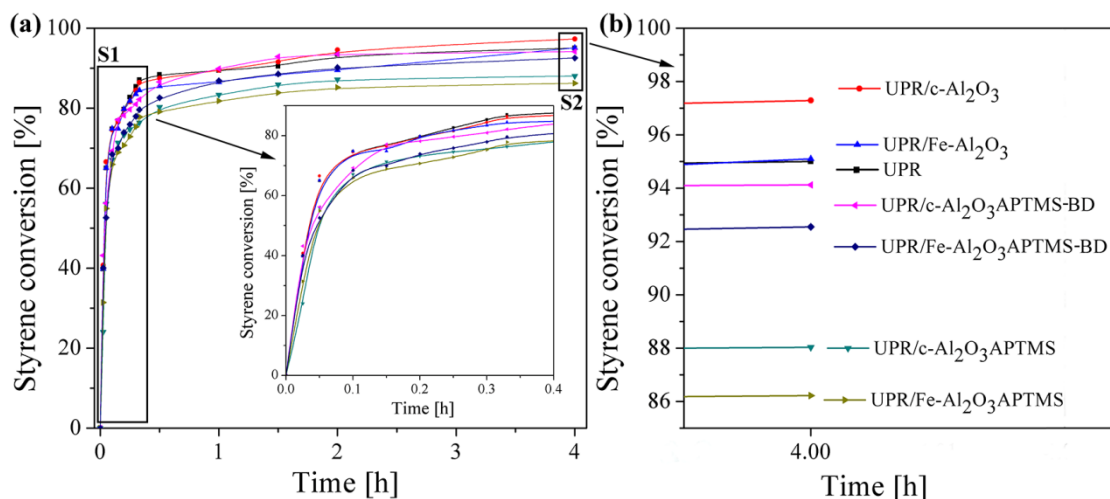
Figure 4. 6. Styrene conversion during curing of UPR resin and composites reinforced with APTMS/APTMS-BD modified alumina particles determined by FTIR method

Conversely, APTMS-BD modified alumina contains approximately six double bonds per molecule (equivalent number) capable to react with ethylenic segments from UPR resin and styrene. Figure 4.6 shows that the styrene consumption is higher, comparing to UPR/(c, Fe)-Al_2O_3APTMS composites, regardless of geometry/size of BD structure which could hinder effective approach of the reactive centers. The equivalent number for APTMS-BD is sufficient to overcome the influence of flexible/coiled BD structure, leading to obtaining higher end-value of styrene conversion (Figure 4.7).

The embedding of pristine alumina ((c, Fe)-Al_2O_3) enables auto-acceleration of curing reaction and thus higher values for styrene conversion [128]. A lower value is obtained for Fe-Al_2O_3 due to increased viscosity which causes obtaining the lazy system, *i.e.* material with decreased reactivity [129]. Those results approve that system reactivity significantly depends upon filler surface properties.
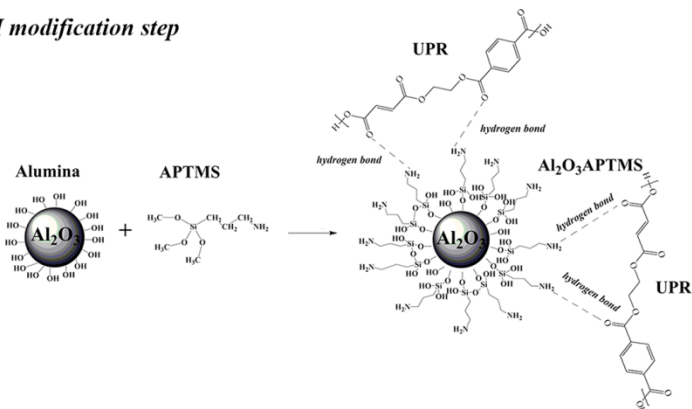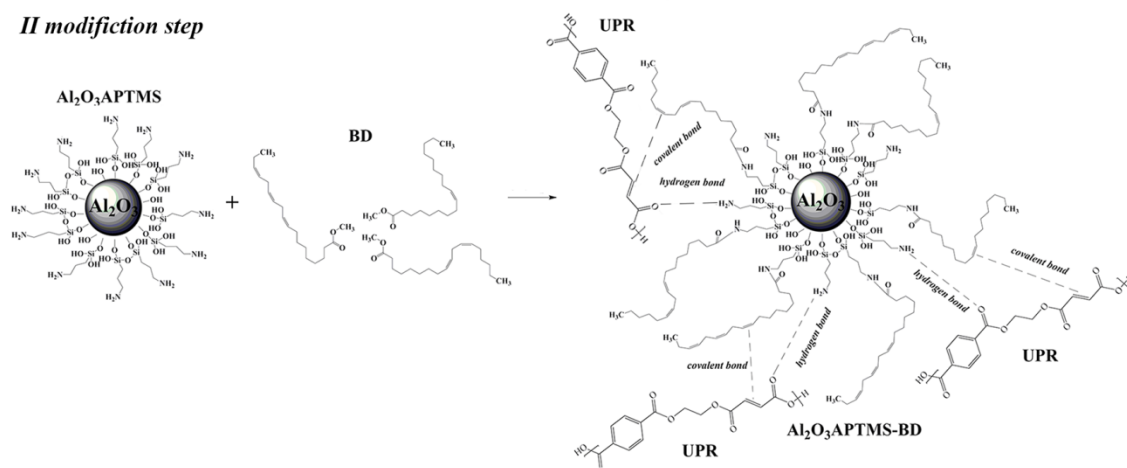
Figure 4. 7. Modification paths of alumina particles together with interactions between modified fillers and UPR resin

4.2 The gel time and maximum curing temperature of UPR resin and corresponding composites

The gel times and maximum curing temperatures, determined from curing exotherms, of UPR resin and composites with 1 wt% of filler particles are shown in Table 4.1. The results suggest that addition of pristine alumina decreases the gel time compared to pure UPR resin, while the maximum curing temperature is slightly increased. The remarked phenomenon is potentially related to a catalytic effect exhibited from nano/submicron-scaled alumina when the radical polymerization reaction is done [130]. The incorporation of larger functionalized alumina particles (Figure 4.7) prevents the approaches of vinyl moieties from UPR resin and fillers, causing the decrease of T_{max} [5]. The composites containing BD modified alumina have slightly higher gel time and maximum curing temperature compared to samples with APTMS modified reinforcements due to unsaturation segments present in BD capable to react with vinyl moieties from UPR resin/styrene. Moreover, amino group show low retardation effect to system reactivity which is reflected in lower T_{max}. Table 4.1 shows that the best compatibility between ethylenic segments from applied modifiers and UPR resin, *i.e.* system reactivity, is displayed in composites containing VTMOEO modified alumina. On the other hand, composites reinforced with MEMO functionalized alumina show the highest gel time and the lowest T_{max}. A steric hindrance of methyl group present in the MEMO silane causes poor availability for radical attack during curing and thus significantly lower

41

reactivity. These results are in fully accordance with trend obtained by FTIR curing kinetics measurements.

Table 4. 1. The gel time and maximum curing temperature of UPR resin and analyzed composites

Sample	Gel time, min	T_{max}, °C
UPR	11.75	95.6
UPR/c-Al$_2$O$_3$(d)	11.50	97.8
UPR/c-Al$_2$O$_3$APTMS(d)	12.25	92.1
UPR/c-Al$_2$O$_3$APTMS-BD(d)	11.75	95.3
UPR/c-Al$_2$O$_3$VTMOEO(d)	11.00	100.8
UPR/c-Al$_2$O$_3$MEMO(d)	13.50	98.2
UPR/Fe-Al$_2$O$_3$(d)	11.25	97.1
UPR/Fe-Al$_2$O$_3$APTMS(d)	12.75	91.3
UPR/Fe-Al$_2$O$_3$APTMS-BD(d)	12.00	93.8
UPR/Fe-Al$_2$O$_3$VTMOEO(d)	11.50	101.2
UPR/Fe-Al$_2$O$_3$MEMO(d)	15.25	84.7

4.3 Microstructural analysis of alumina particles

The microstructural properties of pristine and alumina particles modified with APTMS and APTMS-BD are determined using FEG-SEM technique (Figure 4.8). The nano-sized commercial alumina exhibit high affinity toward the ambient moisture resulting in forming of the micro-scaled, regularly shaped aggregates (Figure 4.8(a)). Conversely, the Fe doped alumina creates smaller, irregular shaped agglomerates [109] (Figure 4.8(d)). The modification of c-Al$_2$O$_3$ resulting in breakage of large agglomerates to smaller ones (Figure 4.8(b, c)). It can be remarked that the agglomeration degree is higher for APTMS-BD modified c-Al$_2$O$_3$ due to establishing dipole-dipole and hydrogen chemical bonding interaction [5,14]. Slightly larger agglomerates of Fe-Al$_2$O$_3$APTMS are noticed, compared to the c-Al$_2$O$_3$APTMS (Figure 4.8(e)), while similar morphology of c- and Fe-Al$_2$O$_3$APTMS-BD fillers is dispayed (Figure 4.8(f)).

The FEG-SEM technique combined with Image ProPlus 6.0 software was utilized to analyze the microstructure of the alumina particles before and after surface modification using VTMOEO and MEMO. The surface modification of c-Al$_2$O$_3$ with VTMOEO designs hydrophobic surface of filler suitable for good its dispersibility throughout the polymer matrix and thus enabling good contact/wetting between two phases (Figure 4.9a) [131].

The usage of MEMO silane provides obtaining of a smooth filler surface, due to the affinity of silane towards alumina. Another phenomena occurred in this case is particle coupling through condensation/polymerization of silane (Figure 4.9b). Surface modification with VTMOEO contributes to deterioration the cluster structure, increasing filler potential to have uniform distribution within the UPR matrix. Consequently, a higher number of reactive groups could be involved in the cross-linking reaction.
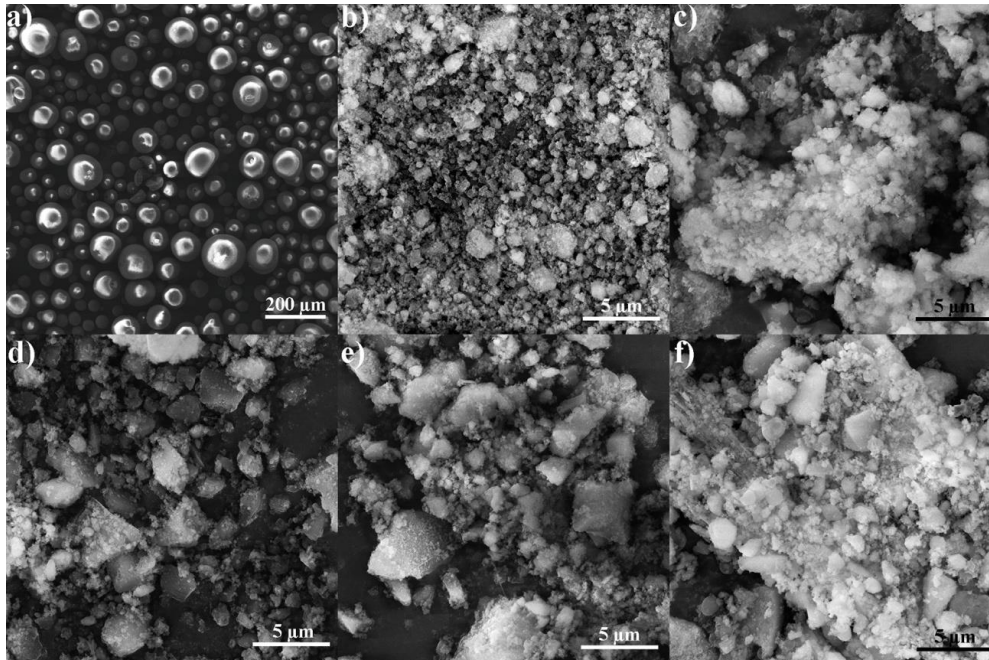
Figure 4. 8. SEM micrographs of pristine/modified alumina particles: a) c-Al_2O_3, b) c-Al_2O_3APTMS, c) c-Al_2O_3APTMS-BD, d) Fe-Al_2O_3, e) Fe-Al_2O_3APTMS, f) Fe-Al_2O_3APTMS-BD
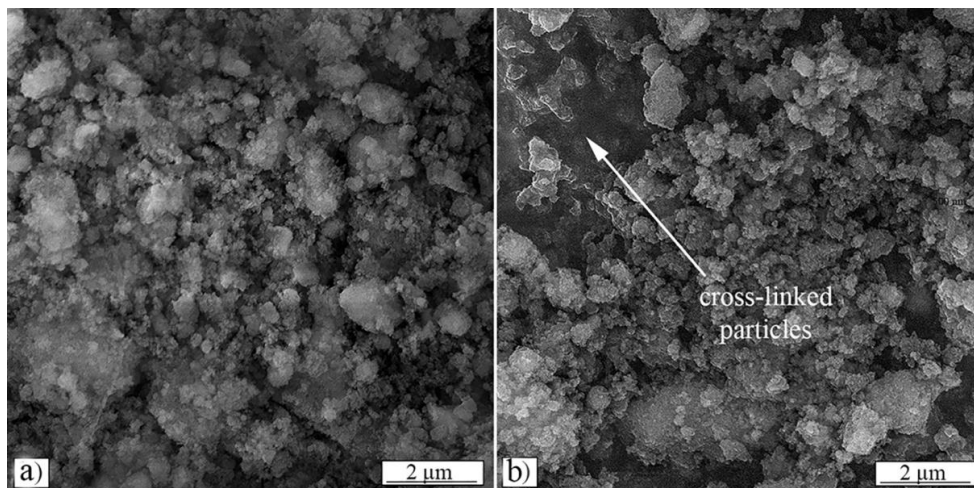
Figure 4. 9. FEG-SEM images of alumina based particles: a) c-Al_2O_3VTMOEO and b) c-Al_2O_3MEMO

4.4 Mechanical properties of composites based on UPR resin and pristine/modified alumina particles

To monitor the effect of pristine and functionalized alumina particles on the mechanical properties of UPR resin, the comparative analysis of tensile strength and micro Vickers hardness was performed. The influence of the physicochemical properties of the above mentioned fillers, *i.e.* the particle amount, particle size and geometry, on the specific properties of the corresponding composites was examined.

4.4.1 Tensile properties of composites with pristine VTMOEO and MEMO modified alumina particles

The tensile strength depends on the morphological properties of alumina, the type of introduced functionalities *via* modifications and distribution within the UPR matrix. The particles incorporated into the inner layer of the formed aggregates are insufficient wetted/wrapped by UPR resin, resulting in lower σ_t, ε_t and E_t of the corresponding composites [19,132]. The composite structure is mainly heterogeneous and capability for efficient load transfer from the polymer matrix to filler particles significantly depends on these factors.

It can be remarked that the incorporation of the both pristine and modified alumina particles, in the range of 0.1 to 1 wt%, resulting in improving of the σ_t and ε_t for corresponding composites (Table 4.2). The addition of 2.5 wt% of fillers deteriorate tensile properties due to the impossibility for uniformly distribution of reinforcement within the UPR matrix. Such phenomenon is the most obvious for UPR/Fe-Al_2O_3(e) and UPR/Fe-Al_2O_3MEMO(e) composites.

The presence of vinyl domains onto filler particles generally provides the highest improvement of tensile properties of UPR matrix. The influence of Fe doped alumina modified by VTMOEO and MEMO on tensile properties of corresponding composites is more pronounced in comparison to using of commercial alumina. These enhancement is 35% and 27%, for UPR/c-Al_2O_3(VTMOEO, MEMO) (d), and 62% and 50%, for UPR/Fe-Al_2O_3(VTMOEO, MEMO)(d), respectively. Such results indicate higher accessibility of vinyl groups, capable to establish myriad covalent bonds with ethylenic domains in UPR resin. The created bonds additionally strength the material providing an adequate conditions for a successful load transfer from the polymer matrix to the fillers, which is reflected in the substantially improvement of tensile properties [133].

To thoroughly explain previous conclusions, the SEM analysis of the fracture surface of the composites with 1.0 wt% alumina particles is performed (Figure 4.10). The both pristine alumina show a higher tendency to form agglomerates due to their higher surface energy whereas the Fe-Al_2O_3 particles produces smaller clusters (Figure 4.10(a, d)). It can be remarked that macromolecule segments penetrate into the clusters (Figure 4.10a), which indicates good compatibility between the two phases. Figure 4.10d shows the appearance of pronounced crack front which is the consequence of the lack of adhesion between the polymer matrix and the reinforcement (enlargement of Figure 4.10d) [134].

Likewise, the UPR/c-Al_2O_3 composite exhibits defects (cavities) inside the agglomerates, formed by stress concentration originated from the high attractive forces between the particles. Figure 4.10b shows a fracture surface of the UPR/c-Al_2O_3VTMOEO composite indicating that deformation of particle aggregates represents the response to the applied load. The reinforcing effect is more pronounced for the UPR/Fe-Al_2O_3VTMOEO composite, Figure 4.10e where filler particles act as a physical barrier which changes the crack spreading mechanism by deflecting the direction of deformation. That is allowed by strong bonding of particles with polymer matrix which gives a great endurance to impact of external force resulting in an increased toughness of the composites. On the other hand, the presence of the Fe-Al_2O_3MEMO clusters on the edge of the crack represents defects for stress concentration and crack initiation (Figure 4.10f). That is the reason for the lower mechanical properties of UPR/Fe-Al_2O_3MEMO composites.

Table 4. 2. Tensile properties of UPR/(c, Fe)Al$_2$O$_3$ and composites with modified particles

Sample	σ_t [MPa]	ε_t [%]	E_t [GPa]
UPR	31.23±0.73	3.06±0.13	0.96±0.07
UPR/c-Al$_2$O$_3$(a)	31.14±1.34	3.80±0.14	0.84±0.07
UPR/c-Al$_2$O$_3$(b)	35.09±1.48	4.31±0.15	0.82±0.08
UPR/c-Al$_2$O$_3$(c)	36.59±1.64	3.55±0.14	1.06±0.12
UPR/c-Al$_2$O$_3$(d)	41.65±1.13	4.81±0.13	0.96±0.05
UPR/c-Al$_2$O$_3$(e)	30.54±1.55	3.04±0.13	0.96±0.11
UPR/c-Al$_2$O$_3$VTMOEO(a)	34.81±1.46	4.32±0.16	0.90±0.06
UPR/c-Al$_2$O$_3$VTMOEO(b)	39.22±1.31	4.57±0.16	1.00±0.07
UPR/c-Al$_2$O$_3$VTMOEO(c)	40.99±1.71	4.55±0.11	1.03±0.10
UPR/c-Al$_2$O$_3$VTMOEO(d)	42.04±1.78	4.81±0.18	1.00±0.08
UPR/c-Al$_2$O$_3$VTMOEO(e)	27.38±1.09	3.55±0.10	0.98±0.07
UPR/c-Al$_2$O$_3$MEMO(a)	26.58±0.88	1.99±0.11	1.71±0.14
UPR/c-Al$_2$O$_3$MEMO(b)	28.08±1.03	2.79±0.14	1.59±0.10
UPR/c-Al$_2$O$_3$MEMO(c)	36.75±1.35	2.99±0.13	1.62±0.11
UPR/c-Al$_2$O$_3$MEMO(d)	39.64±1.21	3.78±0.17	1.60±0.09
UPR/c-Al$_2$O$_3$MEMO(e)	19.03±1.17	1.59±0.15	1.68±0.12
UPR/Fe-Al$_2$O$_3$(a)	30.85±1.60	3.80±0.13	0.87±0.11
UPR/Fe-Al$_2$O$_3$(b)	36.56±1.42	4.05±0.14	0.99±0.07
UPR/Fe-Al$_2$O$_3$(c)	38.58±1.13	4.56±0.13	1.04±0.06
UPR/Fe-Al$_2$O$_3$(d)	39.69±1.34	4.81±0.17	1.01±0.08
UPR/Fe-Al$_2$O$_3$(e)	23.99±1.85	2.23±0.14	1.08±0.12
UPR/Fe-Al$_2$O$_3$VTMOEO(a)	35.51±1.32	7.10±0.17	0.62±0.08
UPR/Fe-Al$_2$O$_3$VTMOEO(b)	40.26±1.53	6.82±0.19	0.76±0.07
UPR/Fe-Al$_2$O$_3$VTMOEO(c)	44.53±1.44	9.54±0.23	0.75±0.11
UPR/Fe-Al$_2$O$_3$VTMOEO(d)	50.74±1.74	11.18±0.25	0.72±0.09
UPR/Fe-Al$_2$O$_3$VTMOEO(e)	32.13±1.27	7.08±0.21	0.83±0.09
UPR/FeAl$_2$O$_3$MEMO(a)	33.69±1.22	4.09±0.25	1.03±0.14
UPR/FeAl$_2$O$_3$MEMO(b)	39.94±1.47	5.46±0.23	0.82±0.08
UPR/FeAl$_2$O$_3$MEMO(c)	44.07±1.54	9.28±0.28	0.78±0.07
UPR/FeAl$_2$O$_3$MEMO(d)	47.00±1.88	6.55±0.31	0.84±0.10
UPR/FeAl$_2$O$_3$MEMO(e)	33.07±1.31	4.10±0.19	1.00±0.11
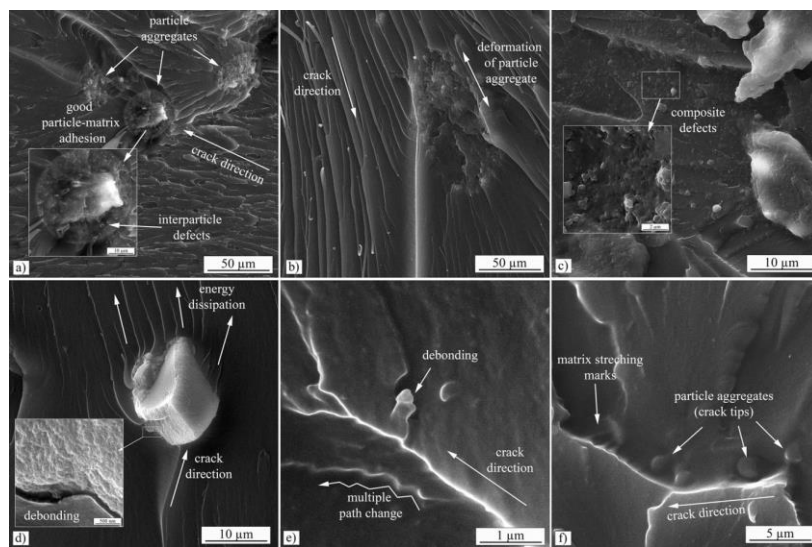
Figure 4. 10. FEG-SEM images of composite containing 1 wt% of reinforcements: a) UPR/c-Al$_2$O$_3$, b) UPR/c-Al$_2$O$_3$VTMOEO, c) UPR/c-Al$_2$O$_3$MEMO, d) UPR/Fe-Al$_2$O$_3$, e) UPR/Fe-Al$_2$O$_3$VTMOEO, and f) UPR/Fe-Al$_2$O$_3$MEMO

These results reflect the contribution of the type of functionalization, physico-chemical interactions between filler and polymer matrix (compatibility) and filler content and size on improvements of the tensile properties of composites [19]. It can be concluded that the primary factor which impacts the tensile properties of the analyzed composites is the interfacial adhesion between the filler particles and the polymer matrix. This implies that higher loadings of filler contribute to the creation of a myriad potential sites responsible for crack initiation and growth. The mechanism of fracture propagation are mainly controlled by the UPR matrix resistance [19].

The Energy absorption of UPR/Fe-Al$_2$O$_3$VTMOEO composites, with the highest tensile strength, is determined from the area under the curves from tensile stress-strain diagrams (Figure 4.11). The best fracture toughness, defined by tensile modulus E_t (Table 4.2) exhibits UPR/FeAl$_2$O$_3$VTMOEO(d) composite. The toughness of this composite is increased for ~477%, compared to neat UPR resin. The addition of filler in the range from 0.1 to 0.5 wt%, also cause the increasing the composite toughness (the increase is in a range of 135-234%). The addition of 2.5 wt% of reinforcement improves UPR resin toughness, but quite lesser (96%) due to non-uniform distribution of alumina into polymer matrix, resulting in higher brittleness of corresponding composite. Still, this result is a quite remarkable when compared to neat UPR matrix.
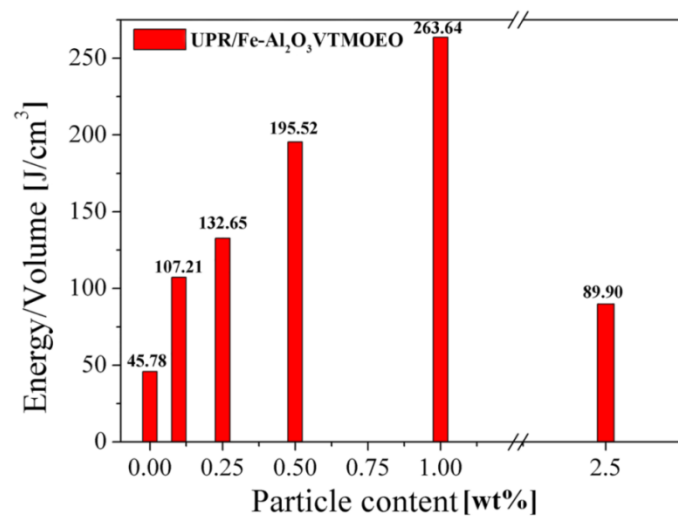
Figure 4. 11. Toughness of Fe-UPR/Al$_2$O$_3$VTMOEO composites represented as energy absorption (area under tensile stress-strain diagram) *versus* Al$_2$O$_3$ Fe–VT particle content

4.4.2 Mechanical properties of the composites based on UPR resin and APTMS/APTMS-BD modified alumina

The tensile strength, determined *via* σ_t, ε_t and E, is shown in Table 4.3. These properties gradually increase up to 1.0 wt% of filler loadings, while the mechanical properties dramatically decrease by further addition of reinforcement. The main reason for such trend is the appearance of particle aggregates at higher loading (>1.0 wt%) which cause formation of the concentrated stress sites and deterioration of mechanical characterizations [18].

There are negligible differences between values of the stress at break for composites reinforced with pristine and modified alumina particles (Table 4.3), while significant differences are remarked in comparison to cured UPR resin. The highest increase in σ_t is achieved for 1.0 wt% of filler loading: 59.6, 52.1, 42.2, 56.3, 44.2 and 78.1% for

incorporation of c-Al$_2$O$_3$, Fe-Al$_2$O$_3$, c-Al$_2$O$_3$APTMS, c-Al$_2$O$_3$ATPMS-BD, Fe-Al$_2$O$_3$APTMS and Fe-Al$_2$O$_3$APTMS-BD, respectively.

Generally, lower reinforcing effect, obtained by embedding of APTMS modified alumina, is the result of steric repulsion/interactions and higher particles geometry which hinder the effective approach/diffusion of reactive centers. The observed phenomenon is overcome with the introduction of APTMS-BD modified alumina within the polymer matrix due to myriad ethylenic bonds in flexible structure of BD, efficiently involved in cross-linking reactions [135]. Besides, it is proved that the appropriate ratio of length/functionalities of the fatty acid chains enhances the ductility of the composites through establishing a disordered conformation which enables easier deformation of the materials [136]. On the other hand, it is reported that ethylenic segments disable chains elongation resulting the decrease of the maximum strain [137]. According to values of ε_t and E (Table 4.3), both factors are into play, considering the somewhat higher elongation at break of composites. Moreover, higher ε_t, observed for APTMS-BD reinforced composites, are related to flexibility of BD segments which also manifest an appropriate plasticizing effect [12].

Table 4. 3. Values of σ_t, ε_t, E and VH of UPR/alumina composites

Sample	σ_t [MPa]	ε_t [%]	E [GPa]
UPR	26.10±0.28	3.06±0.13	0.96±0.07
UPR/c-Al$_2$O$_3$(a)	31.14±1.34	3.80±0.14	0.84±0.07
UPR/c-Al$_2$O$_3$(b)	35.09±1.48	4.31±0.15	0.82±0.08
UPR/c-Al$_2$O$_3$(c)	36.59±1.64	3.55±0.14	1.06±0.12
UPR/c-Al$_2$O$_3$(d)	41.65±1.13	4.81±0.13	0.96±0.05
UPR/c-Al$_2$O$_3$(e)	30.54±1.55	3.04±0.13	0.96±0.11
UPR/c-Al$_2$O$_3$APTMS(a)	30.79±1.14	2.61±0.16	1.49±0.16
UPR/c-Al$_2$O$_3$APTMS(b)	34.09±0.30	3.37±0.12	1.07±0.05
UPR/c-Al$_2$O$_3$APTMS(c)	36.43±1.22	3.59±0.23	1.18±0.13
UPR/c-Al$_2$O$_3$APTMS(d)	37.11±1.24	3.12±0.17	1.21±0.19
UPR/c-Al$_2$O$_3$APTMS(e)	27.68±1.16	2.28±0.15	1.39±0.11
UPR/c-Al$_2$O$_3$APTMS-BD(a)	30.78±1.34	3.40±0.14	1.01±0.08
UPR/c-Al$_2$O$_3$APTMS-BD(b)	32.25±1.52	3.64±0.13	0.98±0.09
UPR/c-Al$_2$O$_3$APTMS-BD(c)	38.44±1.73	4.13±0.16	1.02±0.10
UPR/c-Al$_2$O$_3$APTMS-BD(d)	40.79±1.66	4.37±0.19	1.06±0.11
UPR/c-Al$_2$O$_3$APTMS-BD(e)	30.78±1.34	3.40±0.14	1.01±0.08
UPR/Fe-Al$_2$O$_3$(a)	30.85±1.60	3.80±0.13	0.87±0.11
UPR/Fe-Al$_2$O$_3$(b)	36.56±1.42	4.05±0.14	0.99±0.07
UPR/Fe-Al$_2$O$_3$(c)	38.58±1.13	4.56±0.13	1.04±0.06
UPR/Fe-Al$_2$O$_3$(d)	39.69±1.34	4.81±0.17	1.01±0.08
UPR/Fe-Al$_2$O$_3$(e)	23.99±1.85	2.23±0.14	1.08±0.12
UPR/Fe-Al$_2$O$_3$APTMS(a)	32.08±1.21	2.98±0.14	1.41±0.06
UPR/Fe-Al$_2$O$_3$APTMS(b)	33.20±0.99	3.07±0.12	1.23±0.08
UPR/Fe-Al$_2$O$_3$APTMS(c)	35.09±1.63	3.02±0.13	1.07±0.12
UPR/Fe-Al$_2$O$_3$APTMS(d)	37.64±1.47	3.11±0.19	1.51±0.11
UPR/Fe-Al$_2$O$_3$APTMS(e)	31.22±1.26	3.01±0.18	1.06±0.06
UPR/Fe-Al$_2$O$_3$APTMS-BD(a)	32.42±1.28	2.99±0.18	1.00±0.12
UPR/Fe-Al$_2$O$_3$APTMS-BD(b)	36.46±1.28	3.73±0.19	1.12±0.06
UPR/Fe-Al$_2$O$_3$APTMS-BD(c)	41.93±1.35	4.12±0.15	1.01±0.11
UPR/Fe-Al$_2$O$_3$APTMS-BD(d)	46.48±1.47	4.79±0.17	0.97±0.15
UPR/Fe-Al$_2$O$_3$APTMS-BD(e)	30.22±1.15	2.90±0.15	1.18±0.13

4.4.3 Micro Vickers hardness of composites with pristine VTMOEO and MEMO modified alumina particles

Micro Vickers hardness (VH) tests are performed to determine the resistance of a material to the penetration of a foreign body. The results from micro Vickers hardness testing are measured and summarized in Table 4.4. The addition of pristine alumina results in moderate increase of VH (59 and 14% for c-Al$_2$O$_3$(d) and Fe-Al$_2$O$_3$(d), respectively), but still significant if compared to cured UPR resin. This is due to the better adhesion/interactions with the UPR matrix, which is confirmed by the SEM images (Figure 4.10). The standard deviation increases at higher filler loadings, due to the non-homogeneous structure of the composites compared to UPR resin.

The surface modification enhances compatibility of fillers with polymer network, which results in uniform distribution and obtaining the compact materials capable to endure the force originated from the indenter. The greatest HV is found for the UPR/Fe-Al$_2$O$_3$VTMOEO(d), which is for ≈387% higher than for cured UPR resin. Similar trend for changes of the tensile strength and VH properties by increasing the filler loadings, given in Tables 4.2 and 4.4, respectively, confirms the significance of good compatibility of polymer matrix and the fillers. The improved micro Vickers hardness broadens the field of application for such materials since they possess increased resistance to wear, cutting and scratching [19].

Table 4. 4. Micro Vickers hardness of composites strengthened with pristine and VTMOEO/MEMO modified alumina particles

Sample	Particle content, wt. % →	Micro Vickers Hardness (VH)					
		0	0.10	0.25	0.50	1.00	2.50
UPR		31.2±0.7	-	-	-	-	-
UPR/c-Al$_2$O$_3$		-	37.2±0.6	39.2±2.3	41.6±1.0	49.6±3.6	38.4±2.4
UPR/c-Al$_2$O$_3$VTMOEO		-	58.2±4.4	62.9±1.0	73.4±1.6	82.2±0.6	66.6±2.9
UPR/c-Al$_2$O$_3$MEMO		-	64.2±1.0	67.2±1.7	73.7±3.7	74.1±5.9	68.7±6.6
UPR/Fe-Al$_2$O$_3$		-	24.8±0.7	25.9±0.4	27.9±1.7	35.7±0.6	26.9±0.9
UPR/Fe-Al$_2$O$_3$VTMOEO		-	78.9±7.0	110.1±8.0	112.0±7.8	122.8±6.9	89.1±6.2
UPR/Fe-Al$_2$O$_3$MEMO		-	68.1±6.1	70.6±1.3	105.6±6.9	112.0±5.3	82.7±4.2

Table 4.4 shows that the introduction of the commercial alumina has greater influence on increasing of VH in comparison to Fe doped alumina. The myriad hydroxyl groups onto c-Al$_2$O$_3$ surface establish greater interaction with polar sites in UPR matrix than Fe-Al$_2$O$_3$ particles, which possesses reduced OH content. The exceptional improvement of mechanical properties for the addition of MEMO and VTMOEO modified fillers originates from the introduction of reactive groups capable for establishing the covalent bonds with UPR matrix. Besides, the hydrophobic filler surface is designed in such a way, which improves the compatibility between reinforcements and polymer matrix resulting in better mechanical properties. The slightly higher VH remarked for the Fe-Al$_2$O$_3$(VTMOEO, MEMO) reinforced composites, can be due to a presence of hard Fe atom within the corresponding fillers. The remarked trend is in fully accordance with the ones obtained from the tensile measurements (Table 4.2).

4.4.4 Micro Vickers hardness of the composites based on UPR resin and APTMS/APTMS-BD modified alumina

Micro Vickers hardness values, shown in Table 4.5, suggest that embedding of these reinforcements significantly improve VH of the composites based on UPR resin and APTMS/APTMS-BD modified alumina. A slightly higher increase of stress at break and VH for incorporation of the c-Al_2O_3, compared to Fe-Al_2O_3, is a consequence of higher amount of surface hydroxyl sites which participate in intermolecular interaction with polymer matrix, as evidenced by amount of grafted modifiers (see Table 4.7). Higher amount of APTMS and subsequently BD modifier found for c-Al_2O_3 particle reflect forming of thicker layers *via* available hydroxyl groups. Oppositely, at Fe-Al_2O_3 lower quantity of modifiers are homogeneously distributed and tightly bonded to filler surface providing better interfacial filler/matrix adhesion (Figure 4.13 and Table 4.7).

Table 4. 5. Micro Vickers hardness of composites strengthened with pristine and APTMS/APTMS-BD modified alumina particles

Sample Particle content, wt% →	Micro Vickers Hardness (VH)					
	0	0.10	0.25	0.50	1.00	2.50
UPR	31.2±0.7	-	-	-	-	-
UPR/c-Al_2O_3	-	37.2±0.6	39.2±2.3	41.6±1.0	49.6±3.6	38.4±2.4
UPR/c-Al_2O_3APTMS	-	59.9±2.1	62.3±2.9	65.4±1.8	68.3±1.7	50.3±8.2
UPR/c-Al_2O_3APTMS-BD	-	54.6±1.4	56.8±1.3	59.7±1.9	70.5±0.9	52.9±2.2
UPR/Fe-Al_2O_3	-	24.8±0.7	25.9±0.4	27.9±1.7	35.7±0.6	26.9±0.9
UPR/Fe-Al_2O_3APTMS	-	45.8±4.8	55.0±2.6	57.6±3.2	61.1±5.7	42.0±2.3
UPR/Fe-Al_2O_3APTMS-BD	-	65.4±2.3	67.6±4.3	73.4±3.7	82.3±2.2	56.1±4.9

In general, better improvement of mechanical properties is attained by incorporation of APTMS-BD modified alumina. Still, VH significantly increase for incorporation the both functionalized fillers. The highest increase of 119, 126, 96 and 163% for addition of c-Al_2O_3APTMS(d), c-Al_2O_3ATPMS-BD(d), Fe-Al_2O_3APTMS(d) and Fe-Al_2O_3ATPMS-BD(d), respectively, is obtained. Such results indicate that created covalent bonds between ethylenic groups from BD and UPR resin provide an appropriate conditions for a load transfer from polymer matrix to filler particles [133].

4.5 Thermal properties of the pristine and VTMOEO/MEMO modified alumina

Results obtained by TG analysis of pristine and VTMOEO/MEMO modified particles are shown in Table 4.6 and Figure 4.12. The pristine alumina exhibits different thermal behavior depending on the structural and surface properties. The commercial nano-scaled c-Al_2O_3 (γ-form) exhibits a high moisture affinity, which is in accordance with the supplier remark. The Fe-Al_2O_3 particles has poor tendency to absorb ambient moisture due to the lower number of surface hydroxyl groups which participate in forming of hydrogen bonds with water molecules. The high number of surface hydroxyl groups onto the c-Al_2O_3 also provides the establishment of covalent bonds with silane coupling agents. The highest mass loss is remarked for c-Al_2O_3MEMO which indicates the higher amount of attached organic phase originates from coupling agent. Besides, this suggests that the introduction of VTMOEO domains into alumina is obstructed due to steric hindrance induced by presence of three

flexible 2-methoxyethoxy groups within the VTMOEO structure [5]. Thermal dehydration and decomposition at lower temperatures cause the formation of stable condensed structures on the surface of the alumina particles (Figure 4.12c). Further decomposition at higher temperatures is remarked as a broad DTG peak in the range of 250 – 650 °C.
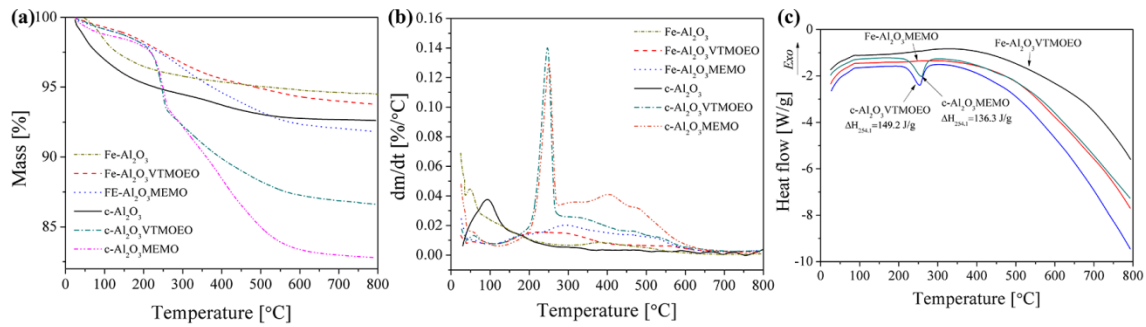
Figure 4. 12. Thermal properties of pristine and VTMOEO/MEMO modified alumina particles

Table 4. 6. TG analysis of pristine and VTMOEO/MEMO functionalized alumina particles

Sample	$T_{0.05}$ [ºC]	Grafted modifier [wt%]	Residual content [wt%]	DTG peaks (°C)
c-Al$_2$O$_3$	230.9	–	94.5	50.5
Fe-Al$_2$O$_3$	516.7	–	92.6	93.3
c-Al$_2$O$_3$VTMOEO	245.8	1.9	93.8	55.0/256.5
c-Al$_2$O$_3$MEMO	249.3	2.7	91.8	55.1/294.0
Fe-Al$_2$O$_3$VTMOEO	486.6	5.6	86.6	58.6/245.7
Fe-Al$_2$O$_3$MEMO	375.8	9.8	82.8	53.8/249.5/404.9

4.6 Thermal properties of the pristine and APTMS/APTMS-BD modified alumina

The thermal properties of pristine and functionalized alumina as well as amount of grafted modifiers are determined using TG, DTG and DSC analysis (Figure 4.13). The amount of grafted modifiers is calculated from the difference between residual content for modified and pristine fillers (higher weight loss of modified particles above 125 °C is attributed to loss of organic modifier) - Table 4.7. The weight loss for all analyzed samples between 25 ºC and 125 ºC is attributed to the loss of moisture/volatile compounds adsorbed at the surface of alumina [138]. TG profile for pristine fillers (Figure 4.13(a)) shows that they are more thermally stable then modified ones, with the weight loss of 7.4% and 5.5% for c-Al$_2$O$_3$ and Fe-Al$_2$O$_3$, respectively (Table 4.7).

The TG profile of pristine alumina is similar, while the degradation pattern for functionalized alumina depends on the surface chemical structure. The weight loss of modified alumina, in the range 125 - 260 ºC, originates from dehydration/thermal transformation of the functional groups bound *via* silanol groups at the alumina surface. Thermal dehydration and conformational rearrangements of BD residues occur at lower temperatures (endothermic peak on Figure 4.13(c)) [135]. This phenomenon is not remarked for Fe-Al$_2$O$_3$ based fillers, probably due to thermal stability of more ordered/tightly bound surface functionalities. At temperatures above 260 ºC conjugated ethylenic domains in linoleic and α-linolenic fatty acids induce decreasing of the thermal stability of corresponding composites [135]. The modification with APTMS-BD shifts the temperature of the highest

decomposition from 460 ℃ to 600 ℃, in comparison to APTMS modified alumina. The highest weight loss, 24.8%, is noticed for c-Al₂O₃APTMS-BD. The both, pristine and functionalized Fe doped alumina exhibit higher thermal stability, compared to c-Al₂O₃ particles, which is attributed to lower amount of attached organic modifiers.
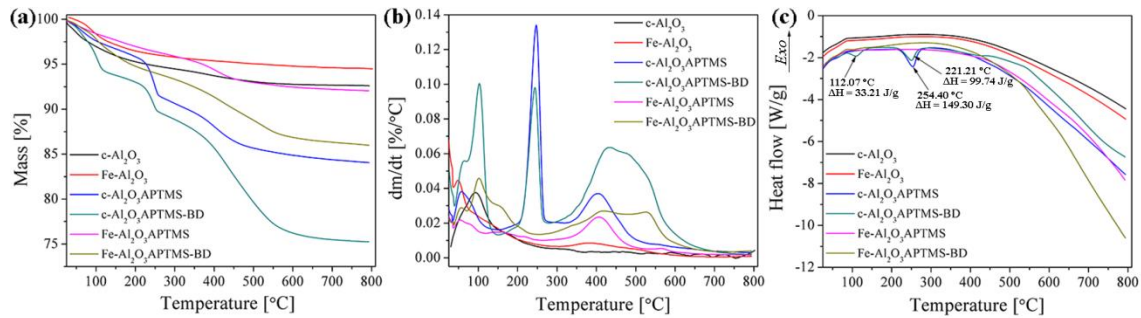
Figure 4. 13. Thermal properties of unmodified and APTMS/APTMS-BD modified alumina particles determined by (a) TG, (b) DTG and (c) DSC analysis

Table 4.7 shows the temperatures where 5 wt% of the materials weight decrease ($T_{0.05}$), residue content at 800 ℃, the amount of grafted modifiers as well as DTG characteristic peaks. Higher thermal stability of Fe doped based alumina indicates relationship between larger weight loss and increased percentage of the thermodegradable organic functionalities in APTMS-BD modified particles.

The DTG peaks of APTMS and APTMS-BD modified alumina (Figure 4.13 (b)) are grouped and, independently on type of particles, show similar pattern within the same group. Introduction of the BD onto the alumina leads to the deeper decomposition where high amount of low molecule weight volatile compounds is obtained, which is reflected in shifted peaks (~103 ℃) compared to APTMS modified particles (~55 ℃). Peaks at about 240 ℃ originate from the partial decomposition and peak at 407/435 ℃ corresponds to the complete thermal degradation of modifying agents and dehydration of silanol group.

Table 4. 7. The $T_{0.05}$, residue content, grafted modifiers and DTG peaks of unmodified/modified alumina particles

Sample	$T_{0.05}$ [ºC]	Residual content [wt%]	Grafted modifier [wt%]	DTG peaks [ºC]
c-Al₂O₃	230.9	92.6	-	94.2
Fe-Al₂O₃	516.7	94.5	-	48.8, 382.7
c-Al₂O₃APTMS	225.9	84.1	8.5	58.2, 247.2, 407.4
c-Al₂O₃APTMS-BD	108.1	75.3	19.2	102.7, 243.9, 434.5
Fe-Al₂O₃APTMS	371.3	92.0	2.5	54.2, 158.9, 406.9, 565.1
Fe-Al₂O₃APTMS-BD	188.0	86.0	8.5	102.7, 243.9, 434.6

4.7 Dynamic-mechanical properties of the composites reinforced with pristine and VTMOEO/MEMO modified alumina

DMA is used for studying the viscoelastic response of the cured UPR resin and UPR/alumina composites. The data obtained from DMA include the temperature dependencies of the storage modulus (G′) and loss modulus (G″), which reflect the elastic and viscous behavior of cured UPR resin and corresponding composites, respectively, and damping factor (tanδ) (Table 4.8). The G′_GS and G′_RP values for glassy state and rubbery plateau are also given in Table 4.8.

It is well known that the incorporation of reinforcement to a polymer matrix increases its moduli [139]. The DMA curve patterns show that the increase in G′ is the greatest above the T_g, in the plateau regions of the viscoelastic spectrum. The temperature dependences of G′ and G″ exhibit similar behavior for all tested specimens and modulus values are generally higher for the composites than for pure UPR resin (Table 4.8). The increased G' in the rubbery state of the composites compared to the pure UPR resin is a result of two combined phenomena: the restriction of free segmental movement by the filler particles and the higher cross-link density of the composites [19]. The data given in Table 4.8 indicate that composites reinforced with c-Al_2O_3 particles have a slightly higher cross-link density compared to the composites with the Fe-Al_2O_3 based particles. The composite with 2.5 wt% c-Al_2O_3 has the highest increase of G' in the rubbery region (84 %), when compared to UPR matrix, and therefore, the highest cross-link density.

Table 4. 8. DMA results of the UPR resin and composites reinforced with VTMOEO/MEMO modified alumina particles

Sample	G'_{GS} [MPa]	G'_{RP} [MPa]	$T_{g(tan\delta peak)}$ [°C]	tanδ height	tan δ width [°C]
UPR	980	24.9	169.2	0.286	60.1
UPR/c-Al_2O_3(a)	967	25.5	182.5	0.248	89.7
UPR/c-Al_2O_3(b)	1202	32.6	185.1	0.236	90.9
UPR/c-Al_2O_3(c)	1107	31.3	185.1	0.234	92.4
UPR/c-Al_2O_3(d)	1093	45.8	197.6	0.197	101.0
UPR/c-Al_2O_3(e)	985	30.2	192.4	0.231	90.8
UPR/c-Al_2O_3VTMOEO(a)	1181	28.2	179.0	0.257	102.1
UPR/c-Al_2O_3VTMOEO(b)	1196	27.2	177.6	0.263	93.3
UPR/c-Al_2O_3VTMOEO(c)	968	23.3	177.8	0.258	91.2
UPR/c-Al_2O_3VTMOEO(d)	1336	36.2	185.1	0.242	90.6
UPR/c-Al_2O_3VTMOEO(e)	1092	25.2	177.4	0.260	92.2
UPR/c-Al_2O_3MEMO(a)	1088	23.6	169.8	0.265	83.8
UPR/c-Al_2O_3MEMO(b)	1062	28.5	186.5	0.241	85.6
UPR/c-Al_2O_3MEMO(c)	1411	41.7	186.8	0.225	86.2
UPR/c-Al_2O_3MEMO(d)	1126	33.5	193.6	0.236	80.2
UPR/c-Al_2O_3MEMO(e)	1245	36.1	188.7	0.225	83.8
UPR/Fe-Al_2O_3(a)	998	26.1	182.4	0.248	92.1
UPR/Fe-Al_2O_3(b)	1095	25.6	183.4	0.246	93.5
UPR/Fe-Al_2O_3(c)	1328	33.0	184.7	0.243	97.8
UPR/Fe-Al_2O_3(d)	1146	30.7	189.5	0.252	84.9
UPR/Fe-Al_2O_3(e)	1173	29.5	181.1	0.251	78.7
UPR/Fe-Al_2O_3VTMOEO(a)	1021	23.4	180.4	0.258	98.1
UPR/Fe-Al_2O_3VTMOEO(b)	1270	29.0	180.1	0.256	104.8
UPR/Fe-Al_2O_3VTMOEO(c)	1168	25.0	181.6	0.257	99.6
UPR/Fe-Al_2O_3VTMOEO(d)	1153	33.0	192.4	0.251	95.6
UPR/Fe-Al_2O_3VTMOEO(e)	1136	25.9	177.7	0.257	101.6
UPR/Fe-Al_2O_3MEMO(a)	961	24.7	179.6	0.254	88.0
UPR/Fe-Al_2O_3MEMO(b)	979	30.6	190.8	0.240	89.7
UPR/Fe-Al_2O_3MEMO(c)	1061	29.2	191.3	0.244	87.3
UPR/Fe-Al_2O_3MEMO(d)	1022	34.4	198.5	0.242	85.0
UPR/Fe-Al_2O_3MEMO(e)	1031	31.9	194.7	0.240	92.0

The low values of the damping factor (tanδ) for the UPR matrix and corresponding composites indicate their high cross-linking densities (Table 4.8). The effect of surface modification of the alumina particles is studied by comparison of the T_g values, determined as the maximum of tanδ(T) curve ($T_{g(tan\delta peak)}$), the height of the peak on the tanδ(T) curve

(tan$\delta_{(height)}$) and the width of the peak on the tan (T) curve (tan$\delta_{(width)}$) (Table 4.8). Alumina reinforcement shifts the tanδ maximum to a higher temperature and it simultaneously broadens. The broadening of the transition region increases as the volume fraction of particles increases or as the particle size of the filler decreases for a given volume fraction [139]. The values of tanδ width suggest that the c-Al$_2$O$_3$ particles have the smallest diameter in the pristine form, while Fe-Al$_2$O$_3$ particles are dissipated to smaller particles after VTMOEO modification. The established interactions between fillers and UPR matrix substantially increase the T_g, decrease the tanδ height and increase the tanδ width as the result of the polymer chain restriction. The incorporation of filler particles promotes restriction of the free segmental movement and so, the peak height is lower than that for the pure UPR [140]. Such trend is observed for all the investigated composites. Thus, the storage modulus of is increased as a measure of elastic response to the external force.

4.8 Dynamic-mechanical properties of the composites reinforced with pristine and APTMS/APTMS-BD modified alumina

To quantify the changes of rheological properties as influenced by adding the pristine and functionalized alumina, some characteristics are given in Table 4.9. The data include temperature dependences of storage modulus in glassy (G'_{GS}) and rubbery (G'_{RP}) regions at 50 and 235 ℃, as well as damping factor (tanδ) height, glass transition temperature determined from tanδ peak position ($T_{g(\tan\delta)}$) and cross-linking density (ν). The cross-linking density is calculated using equation which describes rubbery elasticity theory (Eq. 4.2) assuming the absence of macromolecule entanglements [141]:

$$\nu = \frac{G'_{RP}}{RT} \quad (4.2)$$

where, ν represents cross-linking density, G'_{RP} storage modulus in rubbery plateau at temperature $T = T_g + 50$ ℃ and R is universal gas constant.

The G' value is nearly constant below 50 ℃, and decreases as the temperature increases (Figure 4.14). A slightly different pattern and higher G'_{GS}, observed for UPR/c-Al$_2$O$_3$(c), is related to the strength of intermolecular forces and the way the polymer chains packing [142]. The drop of G' as the temperature goes up is attributed to the higher mobility of polymer segments. With increasing temperature, the composites which contain higher filler amount show a less significant drop in G', manifested as two separate relaxation processes. Hereupon, the remarked broadening of the transition region may be related to heterogeneity in the molecular weight between cross-links [143]. Furthermore, composites containing higher filler loading exhibit a higher rubbery modulus since rigidity of the filler and the filler/matrix interface are less affected by the temperature than the rigidity of the bulk matrix. That causes the restriction in macromolecule segments mobility at the filler/matrix interface which is reflected in higher cross-linking density of the corresponding composites [18].

Generally, the maximum G' values are found for the composites with 1 wt% filler loading for all samples (Figure 4.14). The UPR/c-Al$_2$O$_3$ exhibits the highest increase of $G'_{(RP)}$ and cross-linking density, 93.6 and 88.3% in comparison to neat UPR resin. Besides, the presence of 1.0 wt% of c-Al$_2$O$_3$APTMS-BD filler leads to 67.9 and 61.7% increasing of G'_{RP} and ν. At filler addition above 1 wt%, the G' tends to decrease markedly. Nevertheless, shifted rubbery plateau (T from Eq. 1) of composites ($T > 235$ ℃) indicates higher cross-linking density compared to neat UPR resin ($T > 220$ ℃) [5].

As the G' of all composites is higher than the neat UPR, the extent of reinforcing is evaluated using the coefficient of reinforcement (C), calculated by Eq. 4.3. The obtained results are given in Table 4.9 [144]:

$$C = \frac{\left(G^{'}_{GS}/G^{'}_{RP}\right)_{composite}}{\left(G^{'}_{GS}/G^{'}_{RP}\right)_{resin}} \ (4.3)$$

Generally, the C value decreases as filler loadings increase which implies higher strengthening effect in composites containing more incorporated alumina particles. These results follow the ones obtained for ν value proving that higher restriction of polymer segment movements is occurred for composites with c-Al_2O_3 and Fe-Al_2O_3APTMS-BD particles. Moreover, cross-linking density of samples which contain APTMS modified particles is in accordance with trend obtained for mechanical properties of corresponding composites which is a result of previously discussed phenomena (see Chapter 4.4.2).

Table 4. 9. DMA results of UPR and corresponding composites

Sample	$G^{'}_{GS}$ [MPa]	$G^{'}_{RP}$ [MPa]	T_g(tanδ peak) [ºC]	tanδ peak height	$\nu \cdot 10^3$ [mol/dm^3]	Constant [C]
UPR	971	24.4	168.7	0.29	6.0	-
UPR/c-Al$_2$O$_3$(a)	901	26.2	182.1	0.25	6.2	0.87
UPR/c-Al$_2$O$_3$(b)	890	30.0	189.9	0.23	7.0	0.82
UPR/c-Al$_2$O$_3$(c)	1081	35.8	185.3	0.24	8.5	0.77
UPR/c-Al$_2$O$_3$(d)	959	48.9	197.3	0.20	11.3	0.50
UPR/c-Al$_2$O$_3$(e)	999	32.6	185.7	0.23	7.7	0.78
UPR/c-Al$_2$O$_3$APTMS(a)	1009	23.4	170.3	0.25	5.7	1.10
UPR/c-Al$_2$O$_3$APTMS(b)	1085	22.3	171.3	0.27	5.4	1.24
UPR/c-Al$_2$O$_3$APTMS(c)	1071	25.5	175.1	0.26	6.2	1.07
UPR/c-Al$_2$O$_3$APTMS(d)	1021	28.7	175.8	0.22	6.9	0.90
UPR/c-Al$_2$O$_3$APTMS(e)	953	27.9	172.7	0.25	6.8	0.87
UPR/c-Al$_2$O$_3$APTMS-BD(a)	951	21.4	169.0	0.27	5.1	1.13
UPR/c-Al$_2$O$_3$APTMS-BD(b)	1052	25.2	174.0	0.27	6.1	1.06
UPR/c-Al$_2$O$_3$APTMS-BD(c)	1148	35.1	184.4	0.24	8.3	0.83
UPR/c-Al$_2$O$_3$APTMS-BD(d)	1216	41.8	193.6	0.22	9.7	0.74
UPR/c-Al$_2$O$_3$APTMS-BD(e)	1285	31.4	167.0	0.27	7.7	1.04
UPR/Fe-Al$_2$O$_3$(a)	882	26.5	182.8	0.25	6.3	0.85
UPR/Fe-Al$_2$O$_3$(b)	956	29.8	182.5	0.25	7.1	0.82
UPR/Fe-Al$_2$O$_3$(c)	1020	32.7	184.2	0.25	7.7	0.79
UPR/Fe-Al$_2$O$_3$(d)	1173	35.2	189.8	0.26	8.3	0.85
UPR/Fe-Al$_2$O$_3$(e)	1061	30.5	180.8	0.25	7.3	0.88
UPR/Fe-Al$_2$O$_3$APTMS(a)	1036	23.8	175.0	0.25	5.7	1.11
UPR/Fe-Al$_2$O$_3$APTMS(b)	966	25.0	175.4	0.26	6.0	0.98
UPR/Fe-Al$_2$O$_3$APTMS(c)	1071	28.5	185.6	0.25	6.7	0.96
UPR/Fe-Al$_2$O$_3$APTMS(d)	1010	29.9	189.5	0.25	7.0	0.86
UPR/Fe-Al$_2$O$_3$APTMS(e)	923	28.3	172.5	0.26	6.9	0.83
UPR/Fe-Al$_2$O$_3$APTMS-BD(a)	871	31.0	175.7	0.22	7.5	0.71
UPR/Fe-Al$_2$O$_3$APTMS-BD(b)	836	33.1	176.0	0.22	8.0	0.64
UPR/Fe-Al$_2$O$_3$APTMS-BD(c)	871	35.0	177.2	0.22	8.4	0.63
UPR/Fe-Al$_2$O$_3$APTMS-BD(d)	915	36.3	181.5	0.22	8.6	0.64
UPR/Fe-Al$_2$O$_3$APTMS-BD(e)	884	35.3	175.5	0.22	8.5	0.64

Figure 4. 14. Temperature dependences of storage modulus for UPR resin and composites reinforced with pristine and APTMS/APTMS-BD modified alumina particles

The broadening of the G'' peak of analyzed composites in comparison to the neat UPR resin indicates the influence of filler incorporation (Figure 4.15). It is related to the inhibition of the relaxation process within the composites as a consequence of higher number of chain segments upon filler addition. Other factor potentially originates from the heterogeneous structure of the composites caused by phase separation during copolymerization with styrene and different intramolecular interactions [145]. The heterogeneity is mainly related to the formation of tighter microgel structures composed of distinct regions of densely cross-linked network distributed among a loosely cross-linked matrix [146]. Great dynamic heterogeneities of a thermosetting resins established *via* formation of a complex structure are also reported, where a bimodal distribution of local relaxation times due to slow and fast relaxing regions is found [147].

Figure 4. 15. Temperature dependences of loss modulus for UPR resin and composites reinforced with pristine and APTMS/APTMS-BD modified alumina particles

The peak of tanδ, positioned between 175 °C and 200 °C, is attributed to the T_g, *i.e.* relaxation corresponding to the neat polyester matrix (Figure 4.16). The addition of filler causes the appearance of two relaxation regions remarked at lower temperatures. Maximum damping occurs in a region where the most of the chain segments take part in a cooperative movements caused by applied force. The transition observed at 75 °C can be related to the motion of the phenyl groups in the styrene domains. The transition about 120 °C mainly originates from local modes of polyester units remote from the cross-link junctions. The main segmental relaxation of UPR represents the glass transition of the whole network, while the minor relaxation, at a lower temperature is ascribed to the polyester segments between cross-links [148]. The complexity of the transition region is due to multiple relaxations, occurred as a consequence of the heterogeneous network structure of cross-linked polyesters. The peak intensity of the main relaxation decreases as the transition becomes progressively broader. The introduction of cross-links leads to a decrease in the conformational freedom for the macromolecule segments and results in restricted mobility in the vicinity of the cross-link junctions. The constraint imposed by the cross-links typically manifests itself by increase in T_g with increasing cross-link density [149]. The temperature of remarked relaxation is shifted to higher temperatures in the composite as a consequence of the mobility reduction caused by filler incorporation. Temperature shifts ranging from 10 to 25 °C are the reflection of high cross-link densities, where the average distance between cross-link junctions approaches the characteristic length scale of local segmental rearrangement.

Composites with pristine alumina exhibit higher T_g values compared to neat UPR and other composites. The maximum increase of T_g is 16.9% and 12.5% for composites with c-Al_2O_3 and Fe-Al_2O_3, respectively. This indicates the establishment of dipolar/hydrogen bonds between filler and polymer matrix which contributes in restricted macromolecule segments motions. Although modification processes design filler surface reactivity, steric hindrance caused by presence of voluminous modifiers plays significant role, reflecting in higher mobility of polymer segments. Moreover, flexible BD segments in participate in overall segment motions which are reflected in lower T_g values of corresponding composites (plasticizing effect).

Generally, the incorporation of the both two-step modified alumina, leads to further improvement of dynamical-mechanical properties of the corresponding composites. Availability of the NH_2 and OH surface groups within APTMS modified particles, which participate in creation of hydrogen/dipole-dipole bonding interactions with polymer matrix, is limited as a result of the steric hindrance of APTMS segments (Figure 4.7). Conversely, this phenomenon is overcome by introducing the fatty acid segments with ethylenic bonds (BD) suitable for establishing covalent bonds with UPR matrix [125].
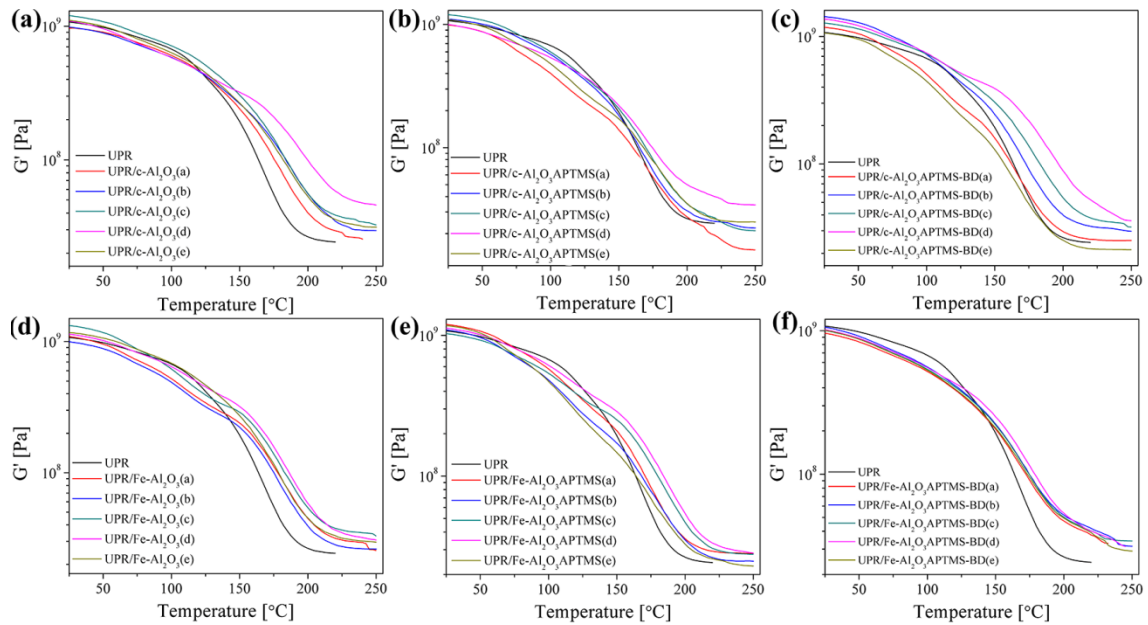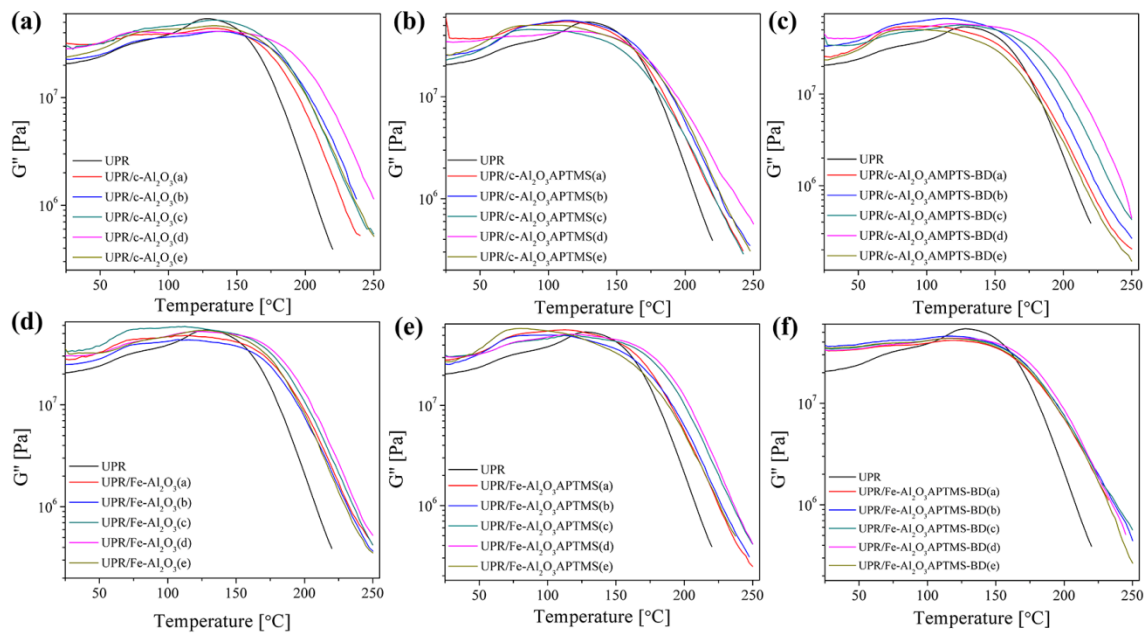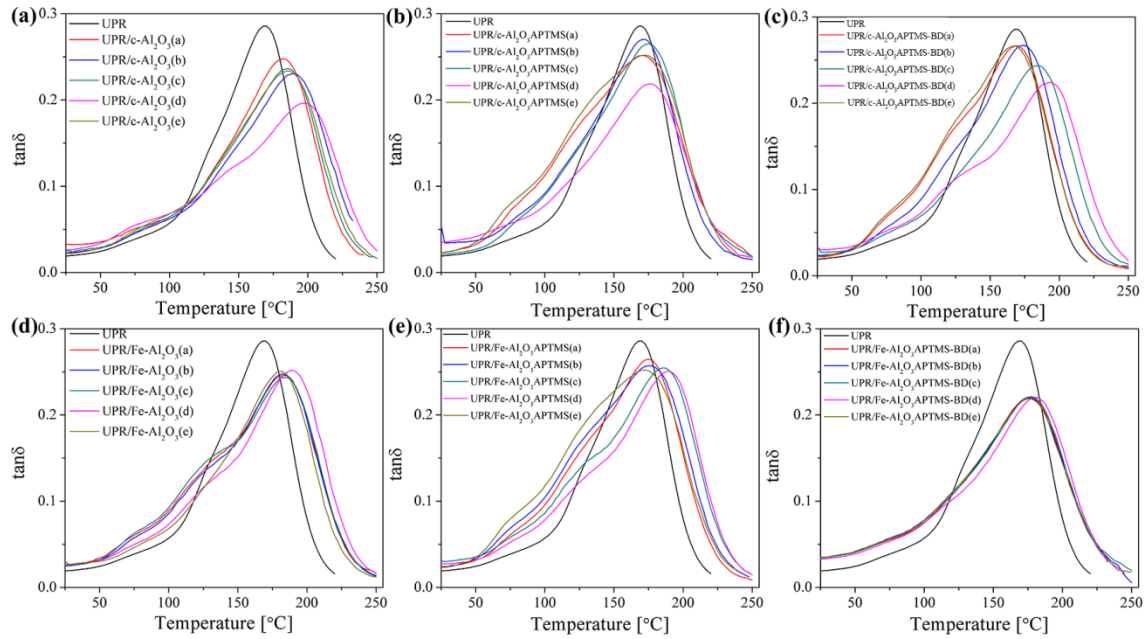
Figure 4. 16. Temperature dependences of damping factor for UPR resin and composites reinforced with pristine and APTMS/APTMS-BD modified alumina particles

4.9 Comparative analysis of mechanical properties of composites reinforced with alumina based fillers

DMA and tensile test provide the information about the composite behavior at the macro-level under different test conditions. Tensile test provides data about the material response to uniaxial mechanical stress which is manifested through the fracture mechanism. The micro indentation test enables the obtaining of the hardness at the micro-level, and gives the information about the uniformity of the specimen. In that sense, such properties for two basically different systems are analyzed in the light of the structural reinforcing effect.

The results presented in Table 4.10 provide insight into the influence of the crystalline structure, surface properties, shape and amount of added alumina fillers to the mechanical properties of PMMA and UPR based composites. The PMMA based composite reinforced with 3 wt% of spherical alumina nanoparticles, whiskers and fibers has an increased storage modulus for 9%, 63% and 100%, respectively. The elastic modulus of PMMA composites reinforced with spherical alumina whiskers and fibers, *i.e.* the stiffness of the composite, is significantly increased compared to neat PMMA [150,151].

The presence of higher content of transition phases of alumina (γ, η and κ) causes improved composite toughness, while α phase significantly increases the hardness. It is also found the relation between processing of alumina and obtained properties. Increase of the calcination temperature causes a decrease of surface area, from 96.4 m^2 g^{-1} for Fe-Al$_2$O$_3$ (700 °C) to 89.7 m^2 g^{-1} for Fe-Al$_2$O$_3$ (900 °C), with concomitant decrease of surface hydroxyl groups [109] and increase of α phase content. All of these factors contribute to increase of composites hardness, *i.e.* 36% (PMMA+3 wt% Fe-Al$_2$O$_3$ (700 °C)) *versus* 99% (PMMA+3 wt% Fe-Al$_2$O$_3$ (900 °C)) (Table 4.10). Contrary to this, decrease of fracture toughness from 1.887 J to 1.495 J, respectively is remarked. Such behavior depends on content of η and κ phases [109]. Utilization of the Fe-Al$_2$O$_3$ particles as a reinforcement in UPR resin, which contain 25.5% of α phase, does not contribute to significant increase in hardness and toughness of corresponding composites due to the weak interfacial adhesion polymer matrix. To retrieve the composite toughness, without sacrificing hardness, the most effective method

presented here is subjection the alumina to vinyl surface modification to achieve an excellent combination of mechanical properties of the UPR based composite.

Table 4. 10. Percentage change of mechanical properties of composite reinforced with alumina fillers compared to matrix used

Sample	Crystal structure	σ_t, [%]	E, [%]	HV, [%]	Ref.
UPR/Fe-Al$_2$O$_3$VTMOEO(d)	η, κ, α	+62 [a]	-63 [a]	+387 [c]	[152]
PMMA+3 wt% Al$_2$O$_3$ nanofibers	α	–	+134 [b]	+158 [b]	[151]
PMMA+3 wt% Al$_2$O$_3$ particles	γ	–	+10 [b]	+8 [b]	[151]
PMMA+3 wt% Al$_2$O$_3$ wiskers	–	–	+96 [b]	+64 [b]	[151]
PMMA+3 wt% Fe-Al$_2$O$_3$ (900 °C [d])	η, κ, α	-55 [a]	-3 [a]	+99 [c]	[109]
PMMA+3 wt% Fe-Al$_2$O$_3$ (700 °C [d])	η and κ	-48 [a]	+2 [a]	+36 [c]	[109]
PMMA+3 wt% Al$_2$O$_3$ (700 °C [d])	η	-33 [a]	+11 [a]	+26 [c]	[109]

4.10 Alumina/PMMA composites as adsorbents for Pb^{2+}, Cd^{2+} and Ni^{2+} removal

4.10.1 Structural characterization of alumina/PMMA composite constituents

The chemical structure of synthesized monodisperse PMMA microspheres, alumina precursor, the calcined highly-ordered alumina and the γ-alumina after the adsorption test is examined by FTIR spectroscopy (Figure 4.17). The intensive ethylene C-H stretch bands for PMMA at 2840, 2953 and 2998 cm^{-1} are remarked [153]. These peaks within the alumina precursor are overlapped with broad OH stretching vibrations at about 3400 cm^{-1} (Figure 4.20a). The characteristic band originates from C=O from ester group within the PMMA is displayed at 1731 cm^{-1}. It can be remarked the typical peak at 1352 cm^{-1}, attributed to O–CH$_3$ deformation vibration. There are also two peaks noted in 1140–1160 cm^{-1} area which originates from methyl ester groups. The other bands present in the spectrum of PMMA are a doublet in the region 1500-1425 cm^{-1}, a medium-to-strong band near 1150 cm^{-1} and a medium intensity band at 750-725 cm^{-1}. The FTIR spectra of atactic and syndiotactic PMMA are qualitatively identical containing band at 1063 cm^{-1}, which is absent within the isotactic PMMA [154].

FTIR spectrum of the alumina precursor, which contains PMMA microbeads shows a substantial increase of a typical absorption at ≈3440 cm^{-1} associated with the presence of H-bonding interactions between the water molecules and the OH groups from the hydroxide-based layers (Figure 4.17a) [155]. The presence of water in these materials is also approved by the medium-intensity bending absorption peak at 1641 cm^{-1} [156,157]. The bands, between 740 and 500 cm^{-1}, could be related to vibrational modes associated with the [M^{II,III}(OH)$_6$]$^{4-,3-}$ complexes distributed along the layered double hydroxide (LDH) layers [158].

The FTIR spectrum of the highly ordered alumina shows the tetrahedral and octahedral vibrations bands of the Al–O at ≈600 and ≈800 cm^{-1}, respectively, which indicates that the synthesized alumina has a γ crystalline structure (Figure 4.20b) [159–161]. The Al–O stretching mode is remarked at 630 cm^{-1} while the torsional mode can be noted at 736 cm^{-1} [162]. The bands at 1121 cm^{-1} and 1074 cm^{-1} represent the δ_{as}(Al–O–H) and δ_s(Al–O–H) modes of boehmite, respectively [163].

The ATR-FTIR spectra of the γ-alumina, after Pb^{2+}, Ni^{2+}, and Cd^{2+} adsorption, are shown in Figure 4.20b. The bands remarked at 1520-1570 cm^{-1} and/or 1350-1410 cm^{-1} can be

attributed to adsorption of CO_2 and NO_3^- onto γ-alumina surfaces. The CO_2 is probably the part of bicarbonate anion, which is the most abundant specie present onto alumina surface. [164]. Besides, according to intensity of CO_2 peak, it can be concluded the presence of an impurities identified on the alumina surface which enhance the ability for CO_2 absorption [165]. Such impurities include Na^+ ion which amplifies the intensity of the area about 3500 cm^{-1} which generally represents the series of the peaks of different origin.

The peak at 1639 cm^{-1}, related to the bending vibration of OH groups, is significantly changed after adsorption: severe intensity drop is found after Pb^{2+} adsorption, while it is moderate for Ni^{2+} and Cd^{2+}. The broad bands at ≈ 112 cm^{-1}, assigned to the $\delta_{as}(Al–O–H)/\delta_s(Al–O–H)$ modes of boehmite, are increased after cation adsorption. Moreover, the ion adsorption causes the appearance of the absorbed bands belonging to new species which are recorded at 500-1250 cm^{-1}. They are considered as cation association with the Al–O bond, whereas those vibrations depend on the cation type. The previous study claims that hydrated γ-Al_2O_3 surface contains no tetrahedral AlO_4, while both phases, octahedral AlO_6 and tetrahedral AlO_4, are present in the bulk [166]. Creation of metal-Al complexes require appropriate geometrical adaption, which makes a change in intensity and peak shifting. The structural transformation of the surface geometry of γ-Al_2O_3 after cation attaching is markedly remarked in the FTIR spectra in the form of different contributions, defined by deconvolution, in the spectral region 500-1000 cm^{-1} (Figure 4.20 c)-f)).
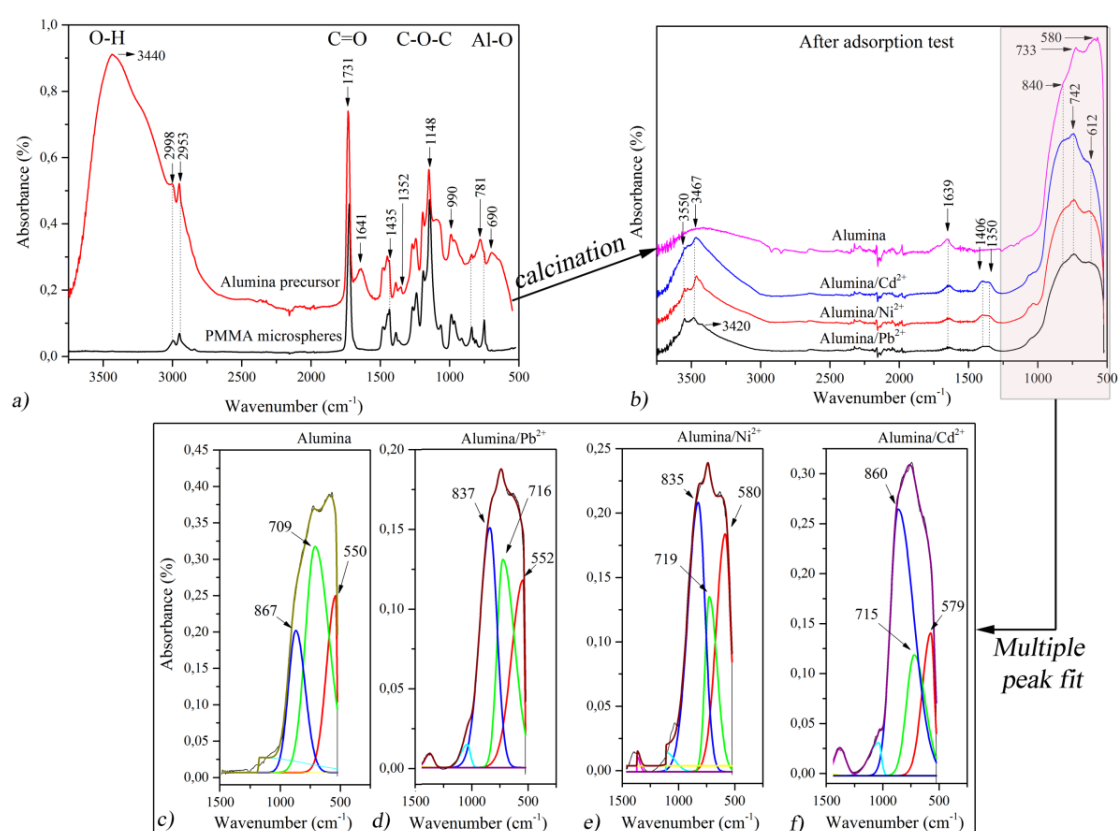
Figure 4. 17. FTIR spectra of: a) monodisperse PMMA microspheres and alumina precursor, b) pure 3DOM γ-alumina, and after cation adsorption; a multiple peak fit of the γ-alumina spectra in the region of bands 500-1200 cm^{-1}: c) pure alumina, and after d) Pb^{2+}, e) Ni^{2+}, and f) Cd^{2+} removal

4.10.2 Molecular weight determination of the PMMA microspheres by viscosimetry measurements

The molecular weight of the PMMA microspheres is calculated according to Eq. (4.4) [167], using the Mark-Houwink parameters for PMMA at 25 °C in chloroform: $K \cdot 10^3 = 4.8$ g/mL, $a = 0.8$ [168] and $[\eta] = 71.33$ dm^3/kg:

$$\overline{M}_V = \left(\frac{[\eta]}{K}\right)^{1/a} \qquad (4.4)$$

The synthesized monodisperse PMMA microspheres have a molecular weight, determined by the previous equation, of 16400 g/mol.

4.10.3 SEM analysis of PMMA microspheres and highly ordered γ-alumina

The Figure 4.18a) shows SEM micrograph of PMMA microspheres organized in well-ordered hexagonal close-packed pattern. The alumina displays a highly ordered macroporous structure formed by the thermal degradation of the PMMA microspheres. The surface of the 3DOM γ-alumina allows insight into the layers below the one at the top (Figure 4.21b). Well-ordered, regularly shaped pores and interconnected walls create an "inverse-opal" structure in three dimensions. The obtained ordered structure is established due to the high monodispersity of the PMMA microspheres, sufficient to attain an appropriate degree of crystallization [169]. The main parameters extracted by the image analysis of the SEM micrograph are presented in Table 4.11. The difference between the average radius of the PMMA microspheres and the pore size of the 3DOM alumina, is a result of the shrinkage of the PMMA template (8.77%) during the calcination. This result shows a significantly lower extent of shrinkage compared to ones obtained by a similar method (26-34%) [104,170]. Low shrinkage and retained 3DOM structure indicate good thermal and structural stability of the samples.
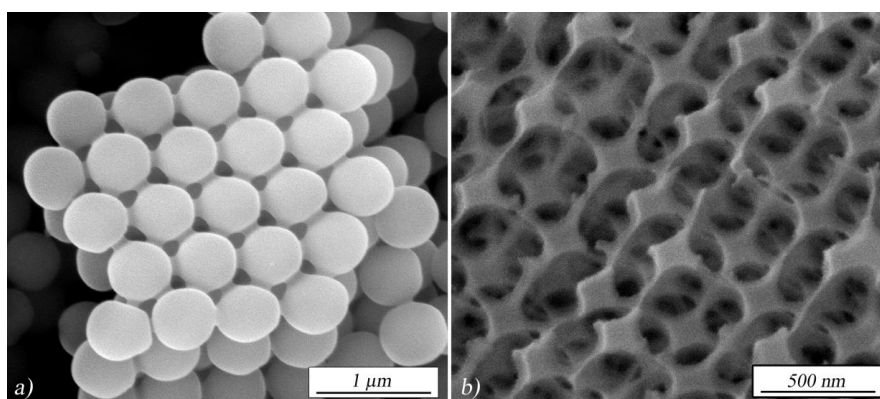
Figure 4. 18. SEM images of: a) CCT based on PMMA microspheres, b) highly ordered γ-alumina

Table 4. 11. SEM image analysis of PMMA microspheres and the highly ordered γ-alumina

PMMA microsphere radius [nm]	Distance between the centers of PMMA microspheres [nm]	Distance between the PMMA spheres [nm]	Wall thickness of alumina [nm]	Pore radius [nm]	Specific surface area of γ-alumina [m^2 g^{-1}]	pH$_{PZC}$
250.9 (10.0)	573.1 (27.8)	69.2 (4.9)	21.3 (4.7)	228.9 (2.3)	77.3	6.4

4.10.4 Thermal analysis of PMMA, alumina precursor and calcinated alumina

The TG/DTG curves of the PMMA, alumina precursor and alumina after calcination at 800 °C are shown in Figure 4.19. Small gradual decrease in weight of 9.1 wt% (Figure 4.19a) is attributed to PMMA decomposition where the easy volatile products are obtained. This change is recorded at 175 °C (Figure 4.19b) on the DTG temperature dependency curve. Further on, the severe weigh loss of 86.6 wt% is occurred at 376 °C (Figure 4.19b) whereas the main bonds within the PMMA are deteriorated. The residue after 800 °C (0.6 wt%) indicates that the decomposition of PMMA template is fully completed. The alumina precursor displays three decomposition steps during the calcination. The first one at 85 °C is attributed to the removal of remained solvent (6.3 wt%) used for dissolving of $Al_2Cl(OH)_5$ and PEG during the alumina preparation. Two significant weight losses (24.2 and 38.6 wt%) at 256 and 376 °C (Figure 4.19b), are assigned to the decomposition of starting materials for alumina synthesis and PMMA template [170]. The results obtained in the TG/DTG analysis indicate that used calcination temperature is appropriate for the formation of single-phase γ-alumina crystallites [171]. The reached yield for 3DOM γ-alumina is higher than the one reported by Han and co-workers [170], which is due to the consequence of used precursor.
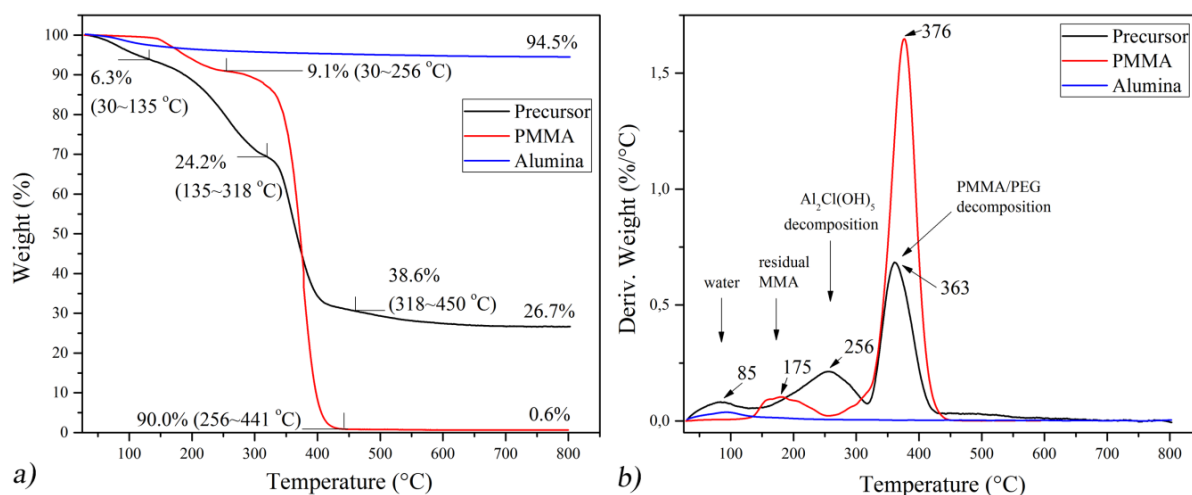
Figure 4. 19. a) Thermogravimetric (TG) and b) derivate thermogravimetric (DTG) curves of the PMMA colloidal crystal template, alumina precursor before calcination and alumina after calcination at 800 °C

4.10.5 Textural properties and pH$_{PZC}$ of the highly-ordered macroporous γ-alumina

The pH of the point of zero charge, pH$_{PZC}$, is the measure of the negatively charge present onto γ-alumina surface, and is measured by the method of pH drift. Regarding the knowing the pH$_{PZC}$ of γ-alumina, the surface sites could be protonated and positively charged by its mixing with solution having a pH value lower than pH$_{PZC}$ of γ-alumina. At pH>pH$_{PZC}$ the adsorption process takes place *via* electrostatic interactions, while at pH values bellow pH$_{PZC}$ the adsorption of metal ions occurs *via* chemisorptions or precipitation [172]. The textural properties of highly ordered macroporous γ-alumina were determined using BET, *i.e.* specific surface area, and given in Table 4.11.

4.10.6 Influence of pH on the adsorption capability of γ-alumina

The solubility of metal ions, the concentration of counter ions on the functional groups of the adsorbent and the degree of ionization of the adsorbent are affected by the pH of the aqueous medium. That is the reason why the effectiveness of pollutant removal *vs* initial pH (pH_i) is studied whereas the obtained results are presented in Figure 4.20.
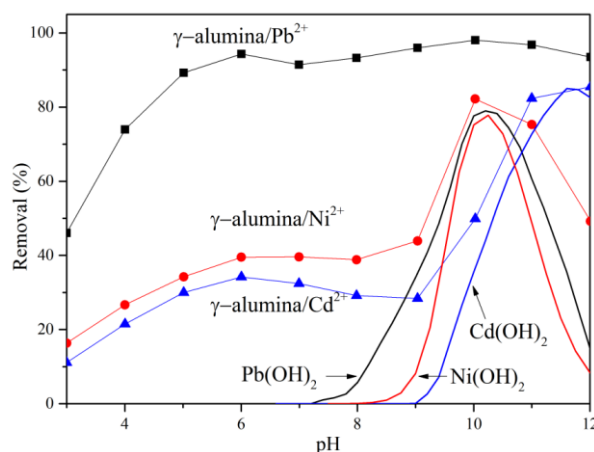
Figure 4. 20. Influence of pH on Pb^{2+}, Ni^{2+} and Cd^{2+} removal by 3DOM γ-alumina ($C_i = 5$ mg/mL, $m/V = 200$ mg/L, $t = 25$ °C)

It could be observed from Figure 4.20 that the percentage of cation adsorption onto 3DOM γ-alumina is almost independent of pH in the range 5-7 where the process efficacy for removal of Pb^{2+} is 90%, while for Ni^{2+} and Cd^{2+} is quite lower, 25-40%. A subsequent gradual increase of Ni^{2+} and Cd^{2+} removal is observed at pH > 8, which is not in accordance to published results, where the similar effect is obtained at pH = 2–7 [173]. This phenomenon is thoroughly explained by metal speciation as shown in Figure 4.21.

At pH>pH_{PZC}, the negatively charged surface of 3DOM γ-alumina attracts positively charged ions by electrostatic interactions. The contrary is true for the system at pH<pH_{PZC}. The goal is avoiding the low pH of environment which hinders the metal ions adsorption due to presence of protons which also have the great affinity towards surface active sites. The increasing the pH value to above 6 leads to hydrolysis of Pb^{2+} species with a known equilibrium constant (Figure 4.21) [174]. Considering the region about pH=7, the concentration of H^+ ions is low and the adsorption capability for Pb^{2+} ions is optimum at $pH_{PZC} = 6.4$. According to the literature about the hydrolysis of Cd^{2+} and Ni^{2+} species (Figure 4.21), obtained using MINTEQ 3.0 software [175], high removal degree is expected at higher pH values [108]. Higher adsorption at pH>8 could be a consequence of the precipitation of insoluble metal hydroxides [176]. Thus, the removal adsorption curves for studied cations represent the sum of adsorption and precipitation at pH>8. According to this, at pH<8, it is certain that removals of Pb^{2+}, Cd^{2+} and Ni^{2+} are not affected by hydroxide/salt precipitation. In this sense, the selection of pH 6 for Cd^{2+} and Ni^{2+} removal and pH 6.5 for Pb^{2+} are an adequate choice to attain high adsorption capacities. Such a conclusion is in accordance with previous findings that the maximum removal of cations is observed at pH values near the pH_{PZC} [177].

The adsorption of bivalent metal ions at the alumina/electrolyte interface is followed by the exchange of hydrogen from surface hydroxyl groups forming outer or inner sphere complex given by Eq. (4.5) and (4.6):

$$AlOH + M^{2+} \rightarrow (AlO^-)M^+ + H^+ \quad (4.5)$$
$$2AlOH + M^{2+} \rightarrow (AlO^-)_2M^+ + 2H^+ \quad (4.6)$$

As the pH of the solution increases, the concentration of H^+ ions decrease favoring the adsorption of metal ions. The bonding of ions onto alumina surface creates a double-layered structure where cations are more tightly bound to hydroxyl groups present in the inner sphere of the double layer as a result of a geometric transition triggered by the protonation/deprotonation processes. In addition, experimental results and modeling, using MINTEQ software, show a slight increase in the adsorption of cations with increasing ionic strength (sodium nitrate at 0.05, 0.1 and 0.5 mg/mL). These results could be explained by the higher activity of the counter ions at the outer surface that compensates accumulation of the surface charge generated by specific cation adsorption. In general, the distribution of the charge on the γ-alumina surface is formed due to the reaction of both surface groups with the electrolyte ions and protonation/deprotonation and adsorption of the cations of interest.
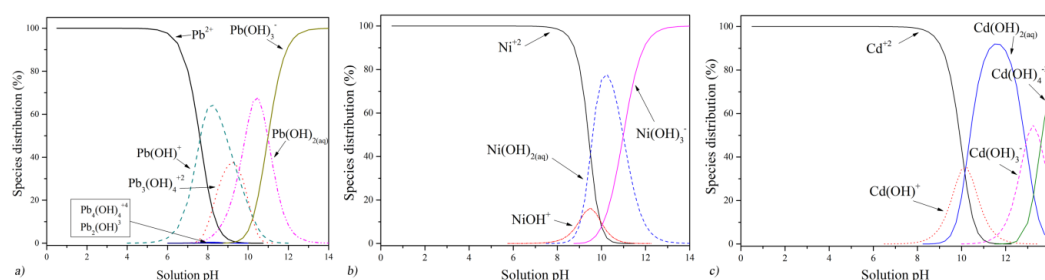
Figure 4. 21. Speciation of: a) Pb^{2+}, b) Ni^{2+} and c) Cd^{2+} obtained using MINTEQ 3.0 software ($C = 25$ mg/mL, $t = 25$ °C)

4.10.6.1 Effects of contact time on the solution pH change

To investigate the effect of contact time on pH change of the solution in the course of Pb^{2+}, Ni^{2+} and Cd^{2+} removal from water, experiments were conducted with different contact times in the range 0-24 h. The results of this study are presented in Figure 4.22, where the maximal removal of Pb^{2+}, Ni^{2+} and Cd^{2+} ions is obtained after 24 h for an adsorption system containing 2 g/L of the studied cation.
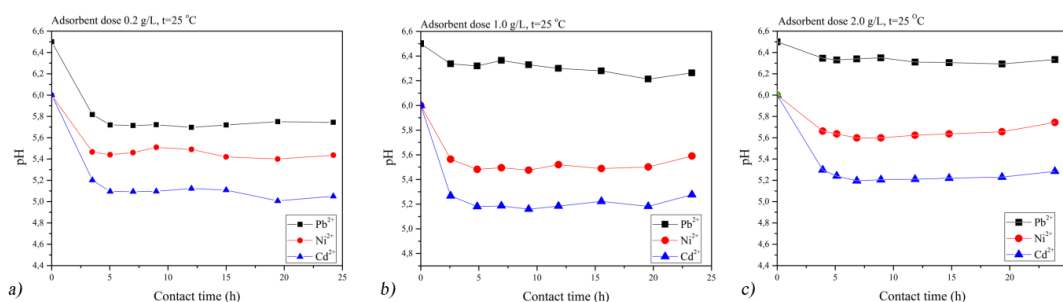
Figure 4. 22. pH value change *versus* contact time for adsorbent dose: a) 0.2 g/L, b) 1.0 g/L, c) 2.0 g/L

The time-dependent change in pH during adsorption, shown in Figure 4.22a)-c), is attributed to the release/consumption of hydrogen ions from/by surface functional groups and the cation adsorption processes (Eq. 4.5). The observed change in pH is a consequence of two contributing factors: more intensive exchange with surface OH groups and the attachment of the adsorbate. Generally, cation adsorption on 3DOM γ-alumina takes place *via* the the sorption processes: adsorption, ion-exchange, surface complexation and co-precipitation, whereby complexation plays the main role in the surface protonation/deprotonation processes.

4.10.6.2 Effect of adsorbent dose and temperature on the removal efficiency and solution pH

To investigate the effect of adsorbent dosage, the amount of adsorbent is varied in the range of 200-2000 mg/mL and the results are presented in Figure 4.23. Higher removal efficiencies of Pb^{2+}, Ni^{2+} and Cd^2 ions are obtained at higher adsorbent dosages and temperatures. Increasing the quantity of adsorbent enhances the number of active surface sites resulting in higher ions removal efficiency [173]. As the adsorbent dosage increases, the competition between present ions for binding sites decreases.

The adsorbent dose-dependent pH change exhibits similar trend as time-dependent change of pH during adsorption, showing the severe pH decrease as the quantity of adsorbent goes down (Figure 4.23d)–f)). This result indicates a higher coverage of the adsorbent surface which causes the higher hydrogen release as a consequence.
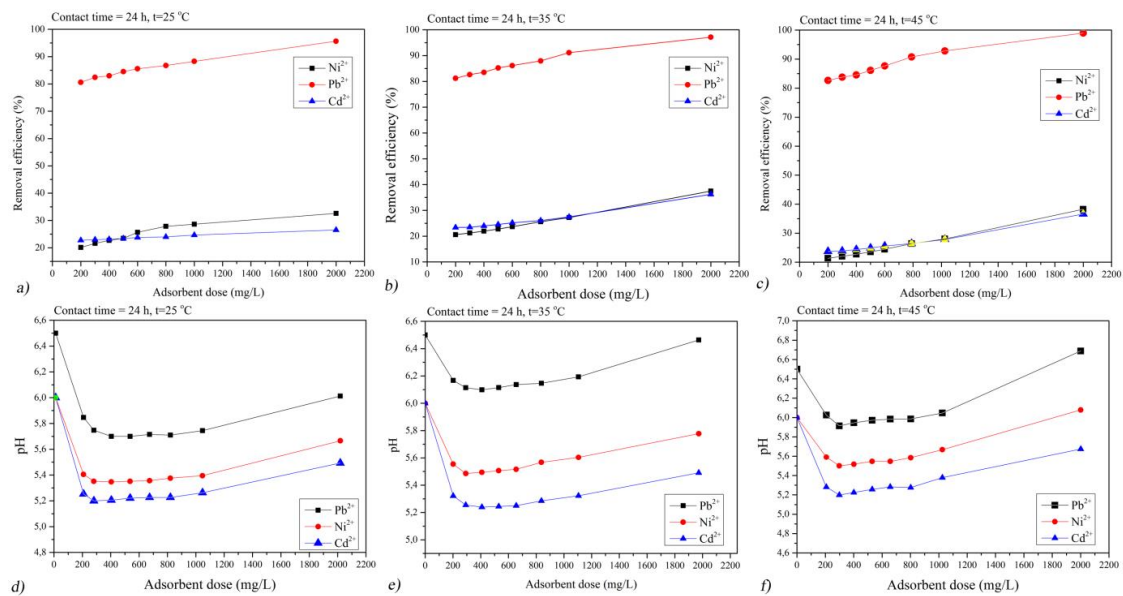
Figure 4. 23. Removal efficiency of highly ordered γ-alumina *versus* adsorbent dose ($t = $ 24 h) and temperature: a) 25 °C, b) 35 °C and c) 45 °C; pH value change *versus* adsorbent dose ($t = $ 24 h) and temperature: d) 25 °C, e) 35 °C and f) 45 °C

4.10.6.3 Equilibrium study of Pb^{2+}, Ni^{2+} and Cd^{2+} adsorption on γ-alumina

Isotherm studies were conducted to calculate the adsorption capacity of the highly ordered γ-alumina for Pb^{2+}, Ni^{2+} and Cd^{2+} ions removal. For this purpose, three commonly isotherm models were used, *i.e.* the Langmuir, Freundlich and Dubinin-Radushkevich isotherms. The equation of the Langmuir isotherm model is [95]:

$$\frac{C_e}{q_e} = \frac{1}{q_m K_L} + \frac{C_e}{q_m} \quad (4.7)$$

where q_e is the adsorbed amount of metal ions per mass of the adsorbent at equilibrium (mg/g); C_e is the equilibrium concentration of metal ions (mg/L); q_m (mg/g) is the maximum theoretical Pb^{2+}, Ni^{2+} and Cd^{2+} capacity and K_L (L/mg) is Langmuir constant related to the affinity of the binding sites. The constant related to Langmuir isotherm model is calculated from the slope and intercept of the plot of $1/q_e$ *versus* $1/C_e$.

The equation for the Freundlich model is represented by Eq. (4.8) [108]

$$\log q_e = \log K_F + \frac{1}{n} \log C_e \quad (4.8)$$

where the K_F is Freundlich constant, n is a constant that gives information about the degree of heterogeneity of the surface sites. The constants of this model are calculated by the slope and intercept of a plot of log q_e versus log C_e.

The Dubinine-Radushkevich (D-R) isotherm model was used to predict the nature of the adsorption processes as physical or chemical by calculating the sorption energy. The linear form of this model is described by Eq. (4.9) [178]:

$$\ln q_e = \ln Q_0 - K_{DR} \left[RT \ln \left(1 + \frac{1}{C_e} \right) \right]^2 \quad (4.9)$$

where K_{DR} (mol^2/kJ^2) is the D-R constant, which is determined as the slope of $\ln q_e$ versus $\left[RT \ln \left(1 + \frac{1}{C_e} \right) \right]^2$, and the intercept yields the adsorption capacity Q_0 (mg/g).

Results from Table 4.12 indicate that the Freundlich isotherm model fitted well Pb^{2+} adsorption on γ-alumina while the D-R isotherm model gave the best fitting for Ni^{2+} and Cd^{2+}.

Table 4. 12. Adsorption isotherm parameters ($C_i = 25$ mg/mL, $t = 24$ h, $m/V = 200$ mg/L, $m_{ads}=1, 2, 3, 4, 5, 7$ and 10 mg, pH = 6.5 for Pb^{2+} and pH = 6 for Ni^{2+} and Cd^{2+})

Isotherm model and model parameters		Ni^{2+}			Cd^{2+}			Pb^{2+}		
		25 °C	35 °C	45 °C	25 °C	35 °C	45 °C	25 °C	35 °C	45 °C
Langmuir isotherm	q_m	21.15	22.88	25.39	19.22	20.98	23.32	93.99	94.75	95.39
	K_L	1251	1216	1176	2493	2322	2131	41822	48592	53307
	K_L	0.021	0.021	0.020	0.022	0.021	0.019	0.202	0.234	0.257
	R^2	0.934	0.912	0.937	0.947	0.937	0.924	0.980	0.987	0.986
Freundlich isotherm	K_F	0.234	0.273	0.294	0.196	0.227	0.266	15.24	17.28	18.55
	$1/n$	1.390	1.348	1.339	1.442	1.381	1.317	0.754	0.731	0.734
	R^2	0.941	0.926	0.955	0.956	0.941	0.922	**0.986**	**0.987**	**0.987**
Dubinin-Radushkevich isotherm	q_m	23.47	23.69	23.96	21.52	22.49	23.47	47.29	49.42	50.70
	K_{ad}	7.82	7.82	7.80	8.56	8.52	8.47	8.39	8.34	8.32
	E_a	7.993	7.998	8.00	7.64	7.66	7.58	7.72	7.74	7.75
	R^2	**0.992**	**0.990**	**0.997**	**0.984**	**0.991**	**0.995**	0.738	0.766	0.773

4.10.6.4 The thermodynamics of the adsorption process

The influence of temperature on the adsorption process was examined at the three different temperatures 298, 308 and 318 K. The Gibbs free energy, enthalpy (ΔH^0) and entropy (ΔS^0) for Pb^{2+}, Ni^{2+} and Cd^{2+} ions adsorption was calculated according to Eq. (4.10) and (4.11):

$$\Delta G^0 = -RT \ln(K_{L1}) \quad (4.10)$$

$$\ln(K_{L1}) = \frac{\Delta S^0}{R} - \frac{\Delta H^0}{RT} \quad (4.11)$$

where ΔG^0 is the Gibbs free energy change (kJ/mol), T is the absolute temperature (K), R is the universal gas constant (8.314 Jmol/K) and K_L is a non-dimensional constant derived from Eq. (4.6).

The negative values of ΔG^0 indicate the feasibility and spontaneity of Pb^{2+}, Ni^{2+} and Cd^{2+} adsorption on γ-alumina (Table 4.13) [113]. Due to the endothermic character of Pb^{2+}, Ni^{2+} and Cd^{2+} ions adsorption on γ-alumina the beneficial processes take place at higher

temperature (Table 4.12). The value of ΔH^0 give an information about the type of Pb^{2+}, Ni^{2+} and Cd^{2+} adsorption onto γ-alumina as follows [178,179]: ΔH^0 in the range from 2.1 to 20.9 kJ/mol for physical adsorption and from 80 to 200 kJ/mol for chemical adsorption. It can be deduced that the adsorption of the ions of interest represents the physical process. The positive values of ΔS^0 reflect an increase in the randomness between solid and solution interface during the uptake of Pb^{2+}, Ni^{2+}, and Cd^{2+} onto γ-alumina. The higher value of ΔS^0 found for Pb^{2+} ions points to a more spontaneous adsorption process.

Table 4. 13. Calculated Gibbs free energy, enthalpy and entropy for γ-alumina

	ΔG^0 (kJ/mol)			ΔH^0 (kJ/mol)	ΔS^0 (J/mol K)	R^2
	298 K	308 K	318 K			
Ni^{2+}	-27.48	-28.49	-29.49	2.45	100.40	0.999
Cd^{2+}	-28.95	-30.15	-31.31	6.20	117.92	0.998
Pb^{2+}	-36.33	-37.94	-39.41	9.59	154.09	0.986

An additional criterium used to assess the feasibility of the studied adsorption processes on the given adsorbent, *i.e.*, the separation factor (R_L), is calculated using Eq. (4.12):

$$R_L = \frac{1}{\left(1 + K_L C_0\right)} \quad (4.12)$$

where C_0 (mol/dm^3) is the initial adsorbent concentration and K_L (dm^3/mol) is the Langmuir constant. The value of R_L indicates the type of an isotherm: irreversible ($R_L = 0$), favorable ($0 < R_L < 1$), linear ($R_L = 1$) or unfavorable ($R_L > 1$). The R_L values obtained for the adsorption of Ni^{2+}, Cd^{2+} and Pb^{2+} on γ-alumina are in the range 0.824 to 0.980, 0.818 to 0.981 and 0.279 to 0.832, respectively, which indicate that the studied adsorption are favorable processes.

4.10.6.5 Kinetics study of γ-alumina adsorption

Kinetic studies were performed to determine the rate of the adsorption process. The kinetic models used for this purpose include pseudo-first order kinetics (Eq. (4.13)) [108]:

$$\log(q_e - q_t) = \log(q_e) - \frac{k_{s1}}{2.303}t \quad (4.13)$$

and pseudo-second order (PSO) kinetics (Eq. (4.14)) [108]

$$\frac{t}{q_t} = \frac{1}{k_{s2}q_e^2} + \frac{1}{q_e}t \quad (4.14)$$

where q_e and q_t are the adsorption equilibrium capacity (mg/g) at time t, respectively. The rate of adsorption uptake is generally considered as one general step, as described by the pseudo-first order and PSO equations.

Second order equation used for adsorption is given by Eq. (4.15):

$$\frac{1}{C_t} = k_2 t + \frac{1}{C_e} \quad (4.15)$$

where C_e and C_t are the adsorbent equilibrium concentrations (mg/mL) at time t, respectively.

More elaborated modeling is achieved using the inter-particle diffusion model, *i.e.* the Weber–Morris model, which is calculated as follows [108]:

$$q_t = k_w t^{0.5} \quad (4.16)$$

where k_w (mg/g min$^{1/2}$) represents the intra-particle diffusion rate constant and t denotes contact time (min). The Weber-Morris model considers four consecutive steps: pollutant transport in the bulk, diffusion through the liquid film surrounding the particle surface (film diffusion), diffusion through the pores inside of particles (intra-particle diffusion) and chemical reaction (adsorption/desorption). The variable and constant of each kinetic model

are calculated and presented in Tables 4.14-4.16. The correlation coefficient (R^2) values of the second order kinetics are the highest for Ni^{2+} and Cd^{2+} while ones for Pb^{2+} indicate that experimental data could be better described by a pseudo-second order kinetic model.

Table 4. 14. Kinetic parameters for Pb^{2+}, Ni^{2+}, and Cd^{2+} onto γ-alumina (C_i =25 mg/mL, m_{ads} = 10 mg, V = 5 mL, pH = 6)

Sorbat/kinetic law order		Pseudo-first	Pseudo-second	Second order
Ni^{2+}	q_e	11.686	10.337	10.337
	k (k_{S1}, k_{S2}, k_2)	0.0368	0.00796	0.002099
	R^2	0.963	0.947	**0.972**
Cd^{2+}	q_e	11.362	12.471	12.471
	k (k_{S1}, k_{S2}, k_2)	0.030	0.004	0.001822
	R^2	0.935	0.876	**0.968**
Pb^{2+}	q_e	5.278	13.187	13.187
	k (k_{S1}, k_{S2}, k_2)	0.1282	0.0397	0.057813
	R^2	0.946	**0.999**	0.944

According to obtained kinetic results, the activation energies are calculated using the Arrhenius equation, (Eq. (4.17)) [113]:

$$k_2 = k_0 \exp\left(\frac{-E_a}{RT}\right) \quad (4.17)$$

where k_2 (g/(mg min)) is the pseudo-second order rate adsorption constant, k_0 (g/(mmol·min)) is the temperature independent factor, E_a (kJ/mol) is the activation energy.

Table 4. 15. Pseudo-second order kinetic model parameters for Ni^{2+}, Cd^{2+} and Pb^{2+} adsorption on γ-alumina at 25 °C, 35 °C and 45 °C

	Adsorbate	k_2 [g /mg min]	Δq [%]	R^2
Ni^{2+}	25 °C	0.002099	3.36	0.972
	35 °C	0.001974	3.68	0.971
	45 °C	0.001867	3.87	0.970
Cd^{2+}	25 °C	0.001822	3.91	0.967
	35 °C	0.001809	4.04	0.942
	45 °C	0.001796	5.19	0.905
Pb^{2+}	25 °C	0.057813	3.35	0.944
	35 °C	0.062165	3.33	0.945
	45 °C	0.066844	3.21	0.946

Calculated results are as follows E_a = 4.60 kJ/mol for Ni^{2+} ions, E_a = 0.58 kJ/mol for Cd^{2+} ions and E_a = 5.71 kJ/mol for Pb^{2+} ions. In the physical adsorption the equilibrium is usually quickly achieved and easily reversible, due to the energy requirement is small (E_a = 0-40 kJ/mol) [178]. The values of activation energy for Pb^{2+}, Ni^{2+} and Cd^{2+} confirm that the adsorption of all three metal ions onto γ-alumina is a physical adsorption process.

The consideration of adsorption process as consecutive/competitive stepwise process is satisfactorily described by the use of Weber-Morris (W-M) model and results are given in Table 4.16.

The W–M fitting reveal that two successive linear steps well describe adsorption process: fast kinetics in the first step followed by very slow reaching the equilibrium in the second stage. A larger intercept found for the γ-alumina indicates higher resistance, *i.e.* slower ionic transport due to hindered intra-particle diffusion. The first linear step describes the external mass transfer from the bulk solution to the most available adsorption sites, while the second step represents processes which highly depend on adsorbent porosity, *i.e.* pore geometry and

network density. The intra-particle and film diffusion resistance slow down adsorbate transport. The adsorption takes place at low rate at the final stage of the process, until saturation of all available surface sites is achieved.

Table 4. 16. The rate constants of intra-particle diffusion kinetic modeling (C_i=25 mg/mL, m_{ads}=10 mg, V=10 mL, pH=6)

Step	Constants	Ni^{2+}	Cd^{2+}	Pb^{2+}
Step 1	k_{p1} (mg/g min$^{-0.5}$)	1.539	1.903	3.094
(Intra-particle diffusion)	C (mg/g)	-0.5969	-1.4989	2.347
	R^2	0.995	0.997	0.999
Step 2	k_{p2} (mg/g min$^{-0.5}$)	0.6510	0.797	0.466
(Equilibrium)	C (mg/g)	3.671	2.534	9.860
	R^2	0.997	0.993	0.996

4.10.7 Comparative analysis of the adsorption performance of γ-alumina

Comparison of adsorption capacity of highly ordered γ-alumina with PMMA microspheres template was difficult to perform due to insufficient literature data for application of such materials in such purpose. Only, 3DOM γ-alumina supported CoMo-based catalyst significantly enhances the hydrodesulfurization activity of dibenzothiophene in striking contrast to commercial mesoporous alumina supported catalyst [170]. Hence, the comparison of adsorption performance of synthesized highly ordered γ-alumina and available literature data is performed to recognize benefits of the possible use of synthesized adsorbent in a water purification processes (Table 4.17).

Table 4. 17. Material properties and adsorption capacities of γ-alumina

Ion	Adsorbent	pH_{PZC}	Capacity [mg/g]	Reference
Pb^{2+}	3DOM γ-alumina	6.4	95.39 (pH 6.5)	[180]
	γ-alumina	-	65.67 (pH 7.0)	[173]
	nanostructured γ-alumina		109.04 (pH 4.5)	[181]
Ni^{2+}	3DOM γ-alumina	6.4	25.39 (pH 6.0)	[180]
	γ-alumina NP*	-	38.14 (pH 10)	[108]
	alumina/humic acid	7.0	21.0 (pH 7.0)	[177]
	alumina/walnut shell	6.0	6.8 (pH 7.0)	[177]
Cd^{2+}	3DOM γ-alumina	6.4	23.32 (pH 6.0)	[180]
	alumina/humic acid	7.0	13.9 (pH 7.0)	[177]
	alumina/walnut shell	6.0	9.3 (pH 7.0)	[177]

Comparison of the q_{max} values of materials based on γ-alumina, with similar pH_{PZC} and regardless to the applied synthesis conditions, indicates that three-dimensional ordered structure contributes to improved absorption capability of γ-alumina. The results obtained for the capacity of 3DOM γ-alumina compared to those for γ-alumina [173] show higher potential for Pb^{2+} removal, as results of structure itself, *i.e.* higher number of available adsorption surface sites for pollutant removal. Higher capacity of 3DOM γ-alumina with respect to Cd^{2+}, comparing to hybrid alumina/humic acid adsorbent [177], proves the superb adsorption performance of material present in this study. Also, results presented in Table 4.17, show that adsorption capacity of 3DOM γ-alumina with respect to Ni^{2+} is comparable with literature data found for hybrid material based on alumina [177], while is lower to those found for alumina nanoparticle [108].

Presented study is performed with a goal to obtain scientific results useful for consideration of possible application in macroscopic/realistic system for water purification. Conversely, the adsorption properties of 3DOM γ-alumina could be improved by changing surface properties by introducing the iron oxide deposit/layer in a controlled procedure [99]. The development of new modification approaches, must be justified by an appropriate increase in adsorption capacity. This goal will be achieved through the synthesis of modified 3DOM γ-alumina adsorbents to manufacturing the novel material suitable for removal of heavy metals from natural water.

5 CONCLUSION AND FURTHER RESEARCH PERSPECTIVE

The primary purpose of the research described in this dissertation is to use commercial industrial waste (PET) to produce new eco-friendly and multifunctional materials for potential use in industry, construction and mining. Waste PET was used to synthesize UPR resin that served as a polymeric matrix for the incorporation of alumina nano- and micro-scaled particles. UPR resins was synthesized by a stepwise polycondensation process from two-function products of catalytic depolymerization of PET and maleic anhydride. The relatively poor mechanical and thermal properties of pure cross-linked UPR resin limit its application in high performance materials. The aforementioned disadvantages can be compensated by the addition of inorganic or organic fillers of appropriate dimensions, textural features and surface functionality.

The UPR resin was synthesized by a two-step process: 1) catalytic glycolysis of PET using propylene glycol and 2) polycondensation of the obtained intermediate (polyol) with maleic anhydride. NMR qualitative analysis showed that the predominant products of PET glycolysis are the symmetric and asymmetric glycol esters of terephthalic acid and glycols.

Commercial nano-scaled and synthesized Fe doped submicro-scaled alumina were completely characterized and used as reinforcement in UPR based composites. Mechanical test results indicate that the tensile strength micro Vickers hardness of the composites are higher than the pure UPR resin for both types of alumina particles and its loadings. Somewhat better results were obtained for composites strengthened with commercial nano-scaled alumina, as expected. Since alumina particles posses hydrophilic nature, which is incompatible with hydrophobic segments of polymeric matrices, some actions were required to be done to additionally enhance mechanical properties of corresponding composites. To address this issue, alumina was modified using organosilanes capable to anchor to filler surface via myriad of available hydroxyl groups. Such obtained particles are suitable for establishment of a great linkage with polymeric matrices, such as UPR.

Dynamic-mechanical, tensile properties and hardness of nominally brittle, thermosetting UPR and UPR/alumina composites was studied in relation to quantity, structure and surface properties, and extent/type functionalities of added c-Al_2O_3 and Fe-Al_2O_3 filler. The obtained results showed that the critical concentration of filler loading was 1 wt%, above it dramatic decline in mechanical properties of composites was remarked. A greater increase of σ_t, 33.4%, for UPR/c-Al_2O_3(d) in comparison to 27.1% for UPR/Fe-Al_2O_3(d) was found. Also, low increase, 34.6% and 26.9%, for UPR/c-Al_2O_3VTMOEO(d) and UPR/c-Al_2O_3MEMO(d) composites, respectively, were found. Contrary to this, significant increase, 62.5% and 50.5%, for Fe-UPR/Al_2O_3(VTMOEO, MEMO)(d), respectively, showed that extent/type of alumina surface modification significantly influences σ_t change. Obtained results indicated two contributing factors of main reinforcing effect: physical interactions (intermolecular interactions) and chemical cross-linking (covalent bonding) to system reactivity and change of mechanical properties. First phenomenon was main operative in both, UPR/c-Al_2O_3 and UPR/Fe-Al_2O_3 composites, higher in the first one, while covalent bonding had the highest contribution in UPR/Fe-Al_2O_3VTMOEO composites. Higher accessibility of vinyl groups, bound at a lower extent in the inner interfacial layers of UPR/Fe-Al_2O_3(VTMOEO, MEMO)(d), efficiently participate in a cross-linking reactions. Additionally, SEM analysis of UPR/Al_2O_3 indicated that the structured aggregates with embedded polymeric chains created an inner interface between UPR macromolecules/filler increasing effectiveness of intermolecular interactions and increase of the tensile strength was a consequence.

Similar reinforcing phenomena operative in both, UPR/c-Al_2O_3(VTNOEO, MEMO) and UPR/Fe-Al_2O_3(VTMOEO, MEMO), clearly showed the significance of the optimal alumina modification to achieve higher performances of produced composites. Vinyl functionalized

alumina, *i.e.* Fe-Al$_2$O$_3$VTMOEO, contributed to significant improvement of the fracture toughness and VH. Besides, increased T_g confirmed the improvement of storage and loss modulus, and dynamical-mechanical properties of UPR based composites.

Using the APTMS and APTMS-BD modified alumina contributed in somewhat lower improving of mechanical properties of UPR resin. Obtained results showed that better reinforcing effect was obtained with embedding pristine alumina particles into UPR matrix. Somewhat better mechanical improvement was achieved by incorporation of the APTMS-BD modified alumina into UPR matrix.

Dynamical-mechanical properties of the composites strengthened with APTMS and APTMS-BE modified alumina were significantly improved which was mostly reflected in elevated T_g. T_g showed lower values for functionalized alumina due to steric hindrance exhibited by modifiers segments attached onto filler particles. Moreover, free BD segments in composites with APTMS-BD modified particles additionally lowering the T_g values (plasticizing effect).

The obtained eco/multi-functional materials are potentially suitable for application in industry, mining and construction. According to mechanical properties, composites with embedded pristine alumina are more suitable for materials which will be subjected to dynamic loadings, while the ones containing modified fillers are better for the materials which will be undergone to high static loadings.

Further research plans will focus on finding an adequate styrene replacement as a monomer for cross-linking of UPR resins. Since alumina is well known material used as flame retardant, the goal is to modify/combine it with, a reactive substance containing phosphorus, nitrogen or silicon, to additionally improve this characteristic. In this manner, environmental friendly flame retarders will be obtained. In addition, the idea is to utilize melamine, siloxane and/or bio-renewable resources (glycerol, fatty acids from natural oils) that would be liquid to maintain compatibility and processing during the preparation of UPR resin and appropriate composite. Incorporation of long, flexible fatty acid chains to the formulation of these products will plasticize, while presence of a rigid aromatic ring from PET will retain partial rigidity of end-products. Introduced unsaturation or reactive groups within the products thus obtained would react with the previously synthesized acrylic or methacryloyl chloride, thereby producing a replacement for styrene as a cross-linking monomer. Styrene replacement would be done gradually until an adequate composite formulation will be found that would give a product that is as satisfying as a flame retarder (the target achieved a V-0 standard according to the UL-94 standard method) and could provide means for completely styrene substitution.

Three-dimensionally ordered macroporous (3DOM) γ-alumina was synthesized using PMMA as porogen agent. XRD measurements confirmed the γ-alumina crystal phase, while SEM confirmed macro and micro porosity. Synthesized adsorbent was used for Pb^{2+}, Ni^{2+}, and Cd^{2+} removal, and the results showed that pH is an important parameter which control effectiveness of pollutant removal.

The quality of the isotherm modelling of adsorption data was judged by the correlation coefficients and error functions, and the best adsorption model was found to be Freundlich isotherm for Pb^{2+} removal and Dubinin-Radushkevich isotherm for Ni^{2+} and Cd^{2+} removal. The ΔH^0 value of 9.59 kJ/mol for Pb^{2+}, 2.45 kJ/mol for Ni^{2+} and 6.20 kJ/mol for Cd^{2+} adsorption onto γ-alumina indicated the dominance of physical adsorption. The positive values of ΔS^0 reflect suggest high spontaneity of adsorption processes. Time dependent studies showed that the best fitting kinetic model is parabolic or Weber-Morris model giving the highest values of correlation coefficients compared to the other investigated models. The kinetic data of the adsorption on all the investigated adsorbents were well fitted with the pseudo-second-order kinetic and Weber-Morris models, suggesting that the rate-limiting step

was diffusion rather than chemical sorption. Calculated activation energies, E_a, of 4.60 kJ/mol for Ni^{2+}, 0.58 kJ/mol for Cd^{2+} and 5.71 kJ/mol for Pb^{2+} indicate that the adsorption of all three ions onto γ-alumina is a mainly physical adsorption process.

6 LITERATURE

[1]   Vilaplana F, Karlsson S. Quality Concepts for the Improved Use of Recycled Polymeric Materials: A Review. Macromol Mater Eng 2008;293:274–97. https://doi.org/10.1002/mame.200700393.

[2]   Oromiehie A, Mamizadeh A. Recycling PET beverage bottles and improving properties. Polym Int 2004;53:728–32. https://doi.org/10.1002/pi.1389.

[3]   Al-Sabagh AM, Yehia FZ, Eshaq G, Rabie AM, ElMetwally AE. Greener routes for recycling of polyethylene terephthalate. Egypt J Pet 2016;25:53–64. https://doi.org/10.1016/j.ejpe.2015.03.001.

[4]   Khoonkari M, Haghighi AH, Sefidbakht Y, Shekoohi K, Ghaderian A. Chemical Recycling of PET Wastes with Different Catalysts. Int J Polym Sci 2015;2015:1–11. https://doi.org/10.1155/2015/124524.

[5]   Rusmirovic JD, Trifkovic KT, Bugarski B, Pavlovic VB, Dzunuzovic J, Tomic M, et al. High performances unsaturated polyester based nanocomposites: Effect of vinyl modified nanosilica on mechanical properties. Express Polym Lett 2016;10:139–59. https://doi.org/10.3144/expresspolymlett.2016.14.

[6]   Czub P. Synthesis and modification of epoxy resins using recycled poly(ethylene terephthalate). Polym Adv Technol 2009;20:183–93. https://doi.org/10.1002/pat.1251.

[7]   Rusmirovic J, Bozic A, Stamenovic M, Spasojevic P, Rancic M, Stojiljkovic I, et al. Alkyd nanocomposite coatings based on waste pet glicolyzates and modified silica nanoparticles. Zast Mater 2016;57:47–54. https://doi.org/10.5937/ZasMat1601047R.

[8]   Kovačević TM. The influence of modified micro-particles obtained from nonmetallic fraction of printed circuit boards on mechanical and thermal properties of polyester resin synthesized from waste poly(ethylene trephthalate). University of Belgrade, 2018.

[9]   Haghdan S, Smith GD. Natural fiber reinforced polyester composites: A literature review. J Reinf Plast Compos 2015;34:1179–90. https://doi.org/10.1177/0731684415588938.

[10]   Varga C, Miskolczi N, Bartha L, Lipóczi G. Improving the mechanical properties of glass-fibre-reinforced polyester composites by modification of fibre surface. Mater Des 2010;31:185–93. https://doi.org/10.1016/j.matdes.2009.06.034.

[11]   Marinkovic A, Radoman T, Dzunuzovic E, Dzunuzovic J, Spasojevic P, Isailovic B, et al. Mechanical properties of composites based on unsaturated polyester resins obtained by chemical recycling of poly(ethylene terephthalate). Hem Ind 2013;67:913–22. https://doi.org/10.2298/HEMIND130930077M.

[12]   Rusmirović JD, Rančić MP, Pavlović VB, Rakić VM, Stevanović S, Djonlagić J, et al. Cross-Linkable Modified Nanocellulose/Polyester Resin-Based Composites: Effect of Unsaturated Fatty Acid Nanocellulose Modification on Material Performances. Macromol Mater Eng 2018;303:1700648. https://doi.org/10.1002/mame.201700648.

[13]   Tasić A, Rusmirović JD, Nikolić J, Božić A, Pavlović V, Marinković AD, et al. Effect of the vinyl modification of multi-walled carbon nanotubes on the performances of waste poly(ethylene terephthalate)-based nanocomposites. J Compos Mater 2017;51:491–505. https://doi.org/10.1177/0021998316648757.

[14]   Rusmirović JD, Radoman T, Džunuzović ES, Džunuzović J V., Markovski J, Spasojević P, et al. Effect of the modified silica Nanofiller on the Mechanical Properties of Unsaturated Polyester Resins Based on Recycled Polyethylene Terephthalate. Polym Compos 2017;38:538–54. https://doi.org/10.1002/pc.23613.

[15]   Mallakpour S, Khadem E. Recent development in the synthesis of polymer nanocomposites based on nano-alumina. Prog Polym Sci 2015;51:74–93. https://doi.org/10.1016/j.progpolymsci.2015.07.004.

[16] Chaeichian S, Pourmahdian S, Afshar Taromi F. Synthesis of Unsaturated Polyester Resins from PET Wastes: Effect of a Novel Co-catalytic System on Glycolysis and Polyesterification Reactions. Des Monomers Polym 2008;11:187–99. https://doi.org/10.1163/156855508X298080.

[17] Fink JK. Reactive polymers fundamentals and applications. In: Ebnesajjad S, editor. React. Polym. Fundam. Appl. Second, William Andrew, Inc., 13 Eaton Avenue Norwich, NY 13815; 2005, p. 809.

[18] Kovačević T, Rusmirović J, Tomić N, Mladenović G, Milošević M, Mitrović N, et al. Effects of oxidized/treated non-metallic fillers obtained from waste printed circuit boards on mechanical properties and shrinkage of unsaturated polyester-based composites. Polym Compos 2019;40:1170–86. https://doi.org/10.1002/pc.24827.

[19] Kovačević T, Rusmirović J, Tomić N, Marinović-Cincović M, Kamberović Ž, Tomić M, et al. New composites based on waste PET and non-metallic fraction from waste printed circuit boards: Mechanical and thermal properties. Compos Part B Eng 2017;127:1–14. https://doi.org/10.1016/j.compositesb.2017.06.020.

[20] Vlad S, Oprea S, Stanciu A, Ciobanu C, Bulacovschi V. Polyesters based on unsaturated diols. Eur Polym J 2000;36:1495–501. https://doi.org/10.1016/S0014-3057(99)00211-6.

[21] Rusmirović JD. Dynamic-mechanical and thermal properties of composites based on unsaturated polyester resins and modified silicon-dioxide and cellulose nanoparticles. Belgrade, 2016.

[22] Cardona F, Rogers D, Davey S, Van Erp G. Investigation of the Effect of Styrene Content on the Ultimate Curing of Vinylester Resins by TGA-FTIR. J Compos Mater 2007;41:137–52. https://doi.org/10.1177/0021998306063357.

[23] Simitzis JC, Zoumpoulakis LT, Soulis SK, Mendrinos LN. Influence of Residual Polyesterification Catalysts on the Curing of Polyesters. Microchim Acta 2001;136:171–4. https://doi.org/10.1007/s006040170049.

[24] Dholakiya B. Unsaturated polyester resin for specialty applications. Polyester, Intech; 2012, p. 167–202. https://doi.org/doi.org/10.5772/48479.

[25] Kim J, Jeong D, Son C, Lee Y, Kim E, Moon I. Synthesis and applications of unsaturated polyester resins based on PET waste. Korean J Chem Eng 2007;24:1076–83. https://doi.org/10.1007/s11814-007-0124-5.

[26] Siddiqui MN, Redhwi HH, Achilias DS. Recycling of poly(ethylene terephthalate) waste through methanolic pyrolysis in a microwave reactor. J Anal Appl Pyrolysis 2012;98:214–20. https://doi.org/10.1016/j.jaap.2012.09.007.

[27] Sinha V, Patel MR, Patel J V. Pet Waste Management by Chemical Recycling: A Review. J Polym Environ 2010;18:8–25. https://doi.org/10.1007/s10924-008-0106-7.

[28] Karayannidis GP, Achilias DS. Chemical Recycling of Poly(ethylene terephthalate). Macromol Mater Eng 2007;292:128–46. https://doi.org/10.1002/mame.200600341.

[29] Abdelaal MY, Sobahi TR, Makki MSI. Chemical transformation of PET waste through glycolysis. Constr Build Mater 2011;25:3267–71. https://doi.org/10.1016/j.conbuildmat.2011.03.013.

[30] López-Fonseca R, Duque-Ingunza I, de Rivas B, Arnaiz S, Gutiérrez-Ortiz JI. Chemical recycling of post-consumer PET wastes by glycolysis in the presence of metal salts. Polym Degrad Stab 2010;95:1022–8.

[31] Rusmirović JD. Dynamic-mechanical and thermal properties of composites based on unsaturated polyester resins and modified silicon-dioxide and cellulose nanoparticles. University of Belgrade, 2016.

[32] Lu M, Kim S. Unsaturated polyester resins based on recycled PET: Preparation and curing behavior. J Appl Polym Sci 2001;80:1052–7. https://doi.org/10.1002/app.1189.

[33] Zahedi AR, Rafizadeh M, Taromi FA. Optimizing synthesis of PET oligomers end capped with phthalic/maleic anhydride via recycling of off grade PET using design of experiments. J Thermoplast Compos Mater 2014;27:1256–77. https://doi.org/10.1177/0892705712470266.

[34] Duque-Ingunza I, López-Fonseca R, de Rivas B, Gutiérrez-Ortiz JI. Synthesis of unsaturated polyester resin from glycolysed postconsumer PET wastes. J Mater Cycles Waste Manag 2013;15:256–63. https://doi.org/10.1007/s10163-013-0117-x.

[35] Lu M, Kim S. Unsaturated polyester resins based on recycled PET: Preparation and curing behavior. J Appl Polym Sci 2001;80:1052–7. https://doi.org/10.1002/app.1189.

[36] Santos PS, Santos HS, Toledo SP. Standard transition aluminas. Electron microscopy studies. Mater Res 2000;3:104–14. https://doi.org/10.1590/S1516-14392000000400003.

[37] Behera PS, Sarkar R, Bhattacharyya S. Nano Alumina: A Review of the Powder Synthesis Method. Interceram - Int Ceram Rev 2016;65:10–6. https://doi.org/10.1007/BF03401148.

[38] Soleimani E, Zamani N. Surface Modification of Alumina Nanoparticles: A Dispersion Study in Organic Media. Acta Chim Slov 2017;64:644–53. https://doi.org/10.17344/acsi.2017.3459.

[39] Marthe J, Meillot E, Jeandel G, Enguehard F, Ilavsky J. Enhancement of scattering and reflectance properties of plasma-sprayed alumina coatings by controlling the porosity. Surf Coatings Technol 2013;220:80–4. https://doi.org/10.1016/j.surfcoat.2012.05.048.

[40] Elsen SR, Ramesh T. Optimization to develop multiple response hardness and compressive strength of zirconia reinforced alumina by using RSM and GRA. Int J Refract Met Hard Mater 2015;52:159–64. https://doi.org/10.1016/j.ijrmhm.2015.06.007.

[41] Kovačević T, Drah A, Božić A, Stamenović M, Rusmirović J, Tomić N, et al. The surface modification of alumina particles for its application in unsaturated polyester resins. 26th Int. Conf. Ecol. Truth Envirotal Res., 2018, p. 338–42.

[42] Miranda-Hernández JG, Moreno-Guerrero S, Soto-Guzmán AB, Rocha-Rangel E. Production and characterization of Al2O3-Cu composite materials. Ournal Ceram Process Res 2006;7:311–4.

[43] Isfahani TD, Javadpour J, Khavandi A, Dinnebier R, Goodarzi M, Rezaie HR. Mechanochemical synthesis of alumina nanoparticles: Formation mechanism and phase transformation. Powder Technol 2012;229:17–23. https://doi.org/10.1016/j.powtec.2012.05.034.

[44] Suchanek WL, Garcés JM. Hydrothermal synthesis of novel alpha alumina nano-materials with controlled morphologies and high thermal stabilities. CrystEngComm 2010;12:2996. https://doi.org/10.1039/b927192a.

[45] Thiruchitrambalam M, Palkar V., Gopinathan V. Hydrolysis of aluminium metal and sol–gel processing of nano alumina. Mater Lett 2004;58:3063–6. https://doi.org/10.1016/j.matlet.2004.05.043.

[46] Li J, Pan Y, Xiang C, Ge Q, Guo J. Low temperature synthesis of ultrafine α-Al2O3 powder by a simple aqueous sol–gel process. Ceram Int 2006;32:587–91. https://doi.org/10.1016/j.ceramint.2005.04.015.

[47] Rogojan R, Andronescu E, Ghiţulică C, Ştefan Vasile B. Synthesis and characterization of alumina nano-powder obtained by sol-gel method. UPB Sci Bull Ser B Chem Mater Sci 2011;73:67–76.

[48] Shojaie-Bahaabad M, Taheri-Nassaj E. Economical synthesis of nano alumina powder using an aqueous sol–gel method. Mater Lett 2008;62:3364–6. https://doi.org/10.1016/j.matlet.2008.03.012.

[49] Li J, Pan Y, Xiang C, Ge Q, Guo J. Low temperature synthesis of ultrafine α-Al2O3 powder by a simple aqueous sol–gel process. Ceram Int 2006;32:587–91. https://doi.org/10.1016/j.ceramint.2005.04.015.

[50] Mirjalili F, Hasmaliza M, Abdullah LC. Size-controlled synthesis of nano α-alumina particles through the sol–gel method. Ceram Int 2010;36:1253–7. https://doi.org/10.1016/j.ceramint.2010.01.009.

[51] Bagherpour S. Fibre Reinforced Polyester Composites. Polyester, InTech; 2012, p. 135–66. https://doi.org/10.5772/48697.

[52] Mohammad N. Synthesis, characterization and properties of of the new unsaturated polyester resins for composite applications. 2007.

[53] Kumar AP, Depan D, Singh Tomer N, Singh RP. Nanoscale particles for polymer degradation and stabilization—Trends and future perspectives. Prog Polym Sci 2009;34:479–515. https://doi.org/10.1016/j.progpolymsci.2009.01.002.

[54] Cong H, Radosz M, Towler B, Shen Y. Polymer–inorganic nanocomposite membranes for gas separation. Sep Purif Technol 2007;55:281–91. https://doi.org/10.1016/j.seppur.2006.12.017.

[55] Johan MR, Shy OH, Ibrahim S, Mohd Yassin SM, Hui TY. Effects of Al2O3 nanofiller and EC plasticizer on the ionic conductivity enhancement of solid PEO–LiCF3SO3 solid polymer electrolyte. Solid State Ionics 2011;196:41–7. https://doi.org/10.1016/j.ssi.2011.06.001.

[56] Bhimaraj P, Burris DL, Action J, Sawyer WG, Toney CG, Siegel RW, et al. Effect of matrix morphology on the wear and friction behavior of alumina nanoparticle/poly(ethylene) terephthalate composites. Wear 2005;258:1437–43. https://doi.org/10.1016/j.wear.2004.09.077.

[57] Naderi N, Sharifi-Sanjani N, Khayyat-Naderi B, Faridi-Majidi R. Preparation of organic–inorganic nanocomposites with core-shell structure by inorganic powders. J Appl Polym Sci 2006;99:2943–50. https://doi.org/10.1002/app.22990.

[58] Zhao S, Zhang J, Zhao S, Li W, Li H. Effect of inorganic–organic interface adhesion on mechanical properties of Al2O3/polymer laminate composites. Compos Sci Technol 2003;63:1009–14. https://doi.org/10.1016/S0266-3538(02)00317-2.

[59] Ash BJ, Siegel RW, Schadler LS. Glass-transition temperature behavior of alumina/PMMA nanocomposites. J Polym Sci Part B Polym Phys 2004;42:4371–83. https://doi.org/10.1002/polb.20297.

[60] Guo Z, Pereira T, Choi O, Wang Y, Hahn HT. Surface functionalized alumina nanoparticle filled polymeric nanocomposites with enhanced mechanical properties. J Mater Chem 2006;16:2800. https://doi.org/10.1039/b603020c.

[61] Wang Y-P, Zhou P, Luo S-Z, Guo S, Lin J, Shao Q, et al. In situ polymerized poly(acrylic acid)/alumina nanocomposites for Pb 2+ adsorption. Adv Polym Technol 2018;37:2981–96. https://doi.org/10.1002/adv.21969.

[62] Oliveira M, Nogueira R, Machado AV. Synthesis of aluminium nanoparticles in a PP matrix during melt processing: Effect of the alkoxide organic chain. React Funct Polym 2012;72:703–12. https://doi.org/10.1016/j.reactfunctpolym.2012.06.022.

[63] Li M, Zhou S, You B, Wu L. Study on Acrylic Resin/Alumina Hybrid Materials Prepared by the Sol-Gel Process. J Macromol Sci Part B 2005;44:481–94. https://doi.org/10.1081/MB-200064772.

[64] Oliveira M, Nogueira R, Machado AV. Synthesis of aluminium nanoparticles in a PP matrix during melt processing: Effect of the alkoxide organic chain. React Funct Polym 2012;72:703–12. https://doi.org/10.1016/j.reactfunctpolym.2012.06.022.

[65] Bi Q, Hao L, Zhang Q, Wang P, Xu P, Ding Y. Study on the effect of amino-functionalized alumina on the curing kinetics of epoxy composites. Thermochim Acta

2019;678:178302. https://doi.org/10.1016/j.tca.2019.178302.

[66]   Rashid ESA, Rasyid MFA, Akil HM, Ariffin K, Kooi CC. Effect of (3-aminopropyl) triethylsilane treatment on mechanical and thermal properties of alumina-filled epoxy composites. Proc Inst Mech Eng Part L J Mater Des Appl 2011;225:160–9. https://doi.org/10.1177/0954420711403214.

[67]   Chung D. Polymer-Matrix Composites: Structure and processing. Second Edi. Elsevier Inc.; 2017.

[68]   Almasi H, Ghanbarzadeh B, Dehghannya J, Entezami AA, Asl AK. Novel nanocomposites based on fatty acid modified cellulose nanofibers/poly(lactic acid): Morphological and physical properties. Food Packag Shelf Life 2015;5:21–31.

[69]   Radoman TS, Dzunuzovic J V., Trifkovic KT, Palija T, Marinkovic AD, Bugarski B, et al. Effect of surface modified TiO2 nanoparticles on thermal, barrier and mechanical properties of long oil alkyd resin-based coatings. Express Polym Lett 2015;9:916–31. https://doi.org/10.3144/expresspolymlett.2015.83.

[70]   Radoman T, Terzic N, Spasojevic P, Dzunuzovic J, Marinkovic A, Jeremic K, et al. Synthesis and characterization of the surface modified titanium dioxide/epoxy nanocomposites. Adv Technol 2015;4:7–15. https://doi.org/10.5937/savteh1501007R.

[71]   Bagwe RP, Hilliard LR, Tan W. Surface Modification of Silica Nanoparticles to Reduce Aggregation and Nonspecific Binding. Langmuir 2006;22:4357–62. https://doi.org/10.1021/la052797j.

[72]   Abdelmouleh M, Boufi S, Belgacem MN, Dufresne A, Gandini A. Modification of cellulose fibers with functionalized silanes: Effect of the fiber treatment on the mechanical performances of cellulose-thermoset composites. J Appl Polym Sci 2005;98:974–84. https://doi.org/10.1002/app.22133.

[73]   Xie Y, Hill CAS, Xiao Z, Militz H, Mai C. Silane coupling agents used for natural fiber/polymer composites: A review. Compos Part A Appl Sci Manuf 2010;41:806–19. https://doi.org/10.1016/j.compositesa.2010.03.005.

[74]   He H, Jing W, Xing W, Fan Y. Improving protein resistance of α-Al2O3 membranes by modification with POEGMA brushes. Appl Surf Sci 2011;258:1038–44. https://doi.org/10.1016/j.apsusc.2011.08.121.

[75]   Jin B, Zhang W, Sun G, Gu H-B. Fabrication and characterization of ethylene-vinyl acetate copolymer/Al2O3 nanocomposites. J Ceram Process Res 2007;8:336–40.

[76]   Zunjarrao SC, Singh RP. Characterization of the fracture behavior of epoxy reinforced with nanometer and micrometer sized aluminum particles. Compos Sci Technol 2006;66:2296–305. https://doi.org/10.1016/j.compscitech.2005.12.001.

[77]   Mallakpour S, Dinari M. Investigating the nanostructure and thermal properties of chiral poly(amide-imide)/Al2O3 compatibilized with 3-aminopropyltriethoxysilane. Mater Res Bull 2013;48:3865–72. https://doi.org/10.1016/j.materresbull.2013.05.095.

[78]   Rashid ESA, Rasyid MFA, Akil HM, Ariffin K, Kooi CC. Effect of (3-aminopropyl) triethylsilane treatment on mechanical and thermal properties of alumina-filled epoxy composites. Proc Inst Mech Eng Part L J Mater Des Appl 2011;225:160–9. https://doi.org/10.1177/0954420711403214.

[79]   Lins SAB, Rocha MCG, D'Almeida JRM. Mechanical and thermal properties of high-density polyethylene/alumina/glass fiber hybrid composites. J Thermoplast Compos Mater 2018:089270571879739. https://doi.org/10.1177/0892705718797391.

[80]   Mohanty A, Srivastava VK. Effect of alumina nanoparticles on the enhancement of impact and flexural properties of the short glass/carbon fiber reinforced epoxy based composites. Fibers Polym 2015;16:188–95. https://doi.org/10.1007/s12221-015-0188-5.

[81]   Mohanty A, Srivastava VK. Effect of alumina nanoparticles on the enhancement of

impact and flexural properties of the short glass/carbon fiber reinforced epoxy based composites. Fibers Polym 2015;16:188–95. https://doi.org/10.1007/s12221-015-0188-5.

[82]   Baskaran R, Sarojadevi M, Vijayakumar CT. Unsaturated polyester nanocomposites filled with nano alumina. J Mater Sci 2011;46:4864–71.

[83]   Golgoon A, Aliofkhazraei M, Toorani M, Moradi MH, Sabour Rouhaghdam A. Corrosion and wear behavior of alumina-polyester nanocomposite coatings. Polym Eng Sci 2017;57:846–56. https://doi.org/10.1002/pen.24461.

[84]   Golgoon A, Aliofkhazraei M, Toorani M, Moradi MH, Sabour Rouhaghdam A. Corrosion and wear behavior of alumina-polyester nanocomposite coatings. Polym Eng Sci 2017;57:846–56. https://doi.org/10.1002/pen.24461.

[85]   Sudirman, Anggaravidya M, Budianto E, Gunawan I. Synthesis and Characterization of Polyester-Based Nanocomposite. Procedia Chem 2012;4:107–13. https://doi.org/10.1016/j.proche.2012.06.016.

[86]   Jovanović S, Jeremić K. Characterization of polymers (in Serbian). Belgrade, Serbia: Faculty of Technology and Metallurgy, University of Belgrade; 2007.

[87]   Baskaran R, Sarojadevi M, Vijayakumar CT. Unsaturated polyester nanocomposites filled with nano alumina. J Mater Sci 2011;46:4864–71. https://doi.org/10.1007/s10853-011-5398-7.

[88]   Mallakpour S, Dinari M. Investigating the nanostructure and thermal properties of chiral poly(amide-imide)/Al2O3 compatibilized with 3-aminopropyltriethoxysilane. Mater Res Bull 2013;48:3865–72. https://doi.org/10.1016/j.materresbull.2013.05.095.

[89]   Adhikari J, Biswas B, Chabri S, Bandyapadhyay NR, Sawai P, Mitra BC, et al. Effect of functionalized metal oxides addition on the mechanical, thermal and swelling behaviour of polyester/jute composites. Eng Sci Technol an Int J 2017;20:760–74. https://doi.org/10.1016/j.jestch.2016.10.016.

[90]   Brzić SJ. Influence of tris(2,3-epoxypropyl)isocyanurate as bonding agent on composite rocket propellant characteristics. University of Belgrade, 2016.

[91]   Fox TG, Flory PJ. Second-Order Transition Temperatures and Related Properties of Polystyrene. I. Influence of Molecular Weight. J Appl Phys 1950;21:581–91. https://doi.org/10.1063/1.1699711.

[92]   Lu H, Xu X, Li X, Zhang Z. Morphology, crystallization and dynamic mechanical properties of PA66/nano-SiO2 composites. Bull Mater Sci 2006;29:485–90. https://doi.org/10.1007/BF02914079.

[93]   Arimatéia RR, Hanken RB, Oliveira AD, Agrawal P, Freitas NL, Silva ES, et al. Effect of alumina on the properties of poly(methyl methacrylate)/alumina composites obtained by melt blending. J Thermoplast Compos Mater 2019:1–21. https://doi.org/10.1177/0892705719843167.

[94]   Ghaffari A, Husain SW, Tehrani MS, Anbia M, Azar PA. Highly efficient adsorption of hexavalent chromium from the aqueous system using nanoporous carbon modified with tetraethylenepentamine. Int J Environ Sci Technol 2015;12:1835–44. https://doi.org/10.1007/s13762-014-0734-5.

[95]   Obradović N, Filipović S, Marković S, Mitrić M, Rusmirović J, Marinković A, et al. Influence of different pore-forming agents on wollastonite microstructures and adsorption capacities. Ceram Int 2017;43:7461–8. https://doi.org/10.1016/j.ceramint.2017.03.021.

[96]   Veličković ZS, Bajić ZJ, Ristić MD, Djokić VR, Marinković AD, Uskoković PS, et al. Modification of multi-wall carbon nanotubes for the removal of cadmium, lead and arsenic from wastewater. Dig J Nanomater Biostructures 2013;8:501–11.

[97]   Bajić ZJ, Djokić VR, Veličković ZS, Vuruna MM, Ristić MD, Issa N Ben, et al.

Equilibrium, kinetic and thermodynamic studies on removal of Cd(II), Pb(II) AND As(V) from wastewater using carp (cyprinus carpio) scales. Dig J Nanomater Biostructures 2013;8:1581–90.

[98]   Shang JG, Kong XR, He LL, Li WH, Liao QJH. Low-cost biochar derived from herbal residue: characterization and application for ciprofloxacin adsorption. Int J Environ Sci Technol 2016;13:2449–58. https://doi.org/10.1007/s13762-016-1075-3.

[99]   Taleb K, Rusmirovic J, Rancic M, Nikolic J, Drmanic S, Velickovic Z, et al. Efficient pollutants removal by amino-modified nanocellulose impregnated with iron oxide. J Serbian Chem Soc 2016;81:1199–213. https://doi.org/10.2298/JSC160529063T.

[100]   Taleb K, Markovski J, Veličković Z, Rusmirović J, Rančić M, Pavlović V, et al. Arsenic removal by magnetite-loaded amino modified nano/microcellulose adsorbents: effect of functionalization and media size. Arab J Chem 2016. https://doi.org/10.1016/j.arabjc.2016.08.006.

[101]   Vuković GD, Marinković AD, Škapin SD, Ristić MĐ, Aleksić R, Perić-Grujić AA, et al. Removal of lead from water by amino modified multi-walled carbon nanotubes. Chem Eng J 2011;173:855–65. https://doi.org/10.1016/j.cej.2011.08.036.

[102]   Veličković Z, Karkalić R, Bajić ZJ, Marinković A, Nikolić A, Otrisal P, et al. Cerium supported on high porous carbon from fich scales carp, as a novel low cost adsorbent to remove As(V) ions from water. Mater Methods Technlogies 2018;12:110–22.

[103]   Markovski JS, Marković DD, Đokić VR, Mitrić M, Ristić MĐ, Onjia AE, et al. Arsenate adsorption on waste eggshell modified by goethite, α-MnO2 and goethite/α-MnO2. Chem Eng J 2014;237:430–42. https://doi.org/10.1016/j.cej.2013.10.031.

[104]   Sasahara K, Hyodo T, Shimizu Y, Egashira M. Macroporous and nanosized ceramic films prepared by modified sol-gel method with PMMA microsphere templates. J Eur Ceram Soc 2004;24:1961–7. https://doi.org/10.1016/S0955-2219(03)00518-1.

[105]   Wang D, Caruso RA, Caruso F. Synthesis of Macroporous Titania and Inorganic Composite Materials from Coated Colloidal SpheresA Novel Route to Tune Pore Morphology. Chem Mater 2001;13:364–71. https://doi.org/10.1021/cm001184j.

[106]   Hudson LK, Misra C, Perrotta AJ, Wefers K, Williams FS. Aluminum Oxide. Ullmann's Encycl. Ind. Chem., Weinheim, Germany: Wiley-VCH Verlag GmbH & Co. KGaA; 2000, p. 255–71. https://doi.org/10.1002/14356007.a01_557.

[107]   Camacho LM, Ponnusamy S, Campos I, Davis TA, Deng S. Evaluation of Novel Modified Activated Alumina as Adsorbent for Arsenic Removal. Handb. Arsen. Toxicol., Elsevier; 2015, p. 121–36. https://doi.org/10.1016/B978-0-12-418688-0.00005-8.

[108]   Agarwal S, Tyagi I, Gupta VK, Dehghani MH, Jaafari J, Balarak D, et al. Rapid removal of noxious nickel (II) using novel γ-alumina nanoparticles and multiwalled carbon nanotubes: Kinetic and isotherm studies. J Mol Liq 2016;224:618–23. https://doi.org/10.1016/j.molliq.2016.10.032.

[109]   Lazouzi G, Vuksanović MM, Tomić NZ, Mitrić M, Petrović M, Radojević V, et al. Optimized preparation of alumina based fillers for tuning composite properties. Ceram Int 2018;44:7442–9. https://doi.org/10.1016/j.ceramint.2018.01.083.

[110]   Truong LT, Larsen Å, Holme B, Diplas S, Hansen FK, Roots J, et al. Dispersibility of silane-functionalized alumina nanoparticles in syndiotactic polypropylene. Surf Interface Anal 2010;42:1046–9. https://doi.org/10.1002/sia.3166.

[111]   Shim SE, Kim K, Oh S, Choe S. Preparation of ultra fine poly(methyl methacrylate) microspheres in methanol-enriched aqueous medium. Macromol Res 2004;12:240–5. https://doi.org/10.1007/BF03218394.

[112]   Brzic S, Bogosavljevic M, Uscumlic G, Jelisavac L. Effect of tris (2,3-epoxypropyl) isocyanurate on dynamic modulus of CTBN-based composite rocket propellant. Sci

Tech Rev 2016;66:18–27. https://doi.org/10.5937/STR1602018B.

[113] Budimirović D, Veličković ZS, Djokić VR, Milosavljević M, Markovski J, Lević S, et al. Efficient As(V) removal by α -FeOOH and α -FeOOH/ α -MnO 2 embedded PEG-6-arm functionalized multiwall carbon nanotubes. Chem Eng Res Des 2017;119:75–86. https://doi.org/10.1016/j.cherd.2017.01.010.

[114] Cava S, Tebcherani SM, Souza IA, Pianaro SA, Paskocimas CA, Longo E, et al. Structural characterization of phase transition of Al2O3 nanopowders obtained by polymeric precursor method. Mater Chem Phys 2007;103:394–9. https://doi.org/10.1016/j.matchemphys.2007.02.046.

[115] Zec J, Tomić N, Zrilić M, Marković S, Stojanović D, Jančić-Heinemann R. Processing and characterization of UHMWPE composite fibres with alumina particles in poly(ethylene-vinyl acetate) matrix. J Thermoplast Compos Mater 2018;31:689–708. https://doi.org/10.1177/0892705717718240.

[116] Bača L, Lipka J, Toth I, Pach L. Study of crystallisation of Al_2O_3-Fe_2O_3 gels by Mossbauer spectroscopy. Ceram − Silikáty 2001;45:9–14.

[117] Wang Y, Eli W, Zhang L, Gao H, Liu Y, Li P. A new method for surface modification of nano-CaCO3 and nano-Al2O3 at room temperature. Adv Powder Technol 2010;21:203–5. https://doi.org/10.1016/j.apt.2009.12.006.

[118] Jin B, Zhang W, Sun G, Gu H-B. Fabrication and characterization of ethylenevinyl acetate copolymer Al2O3 nanocomposites. J Ceram Process Res 2007;8:336–40.

[119] Prabhu S, Cheirmadurai K, Raghava Rao J, Thanikaivelan P. Glycine functionalized alumina nanoparticles stabilize collagen in ethanol medium. Bull Mater Sci 2016;39:223–8.

[120] Ahangaran F, Hassanzadeh A, Nouri S. Surface modification of Fe3O4@SiO2 microsphere by silane coupling agent. Int Nano Lett 2013;3:23.

[121] Kovačević T, Rusmirović J, Tomić N, Mladenović G, Milošević M, Mitrović N, et al. Effects of oxidized/treated non-metallic fillers obtained from waste printed circuit boards on mechanical properties and shrinkage of unsaturated polyester-based composites. Polym Compos 2017.

[122] Palimi MJ, Rostami M, Mahdavian M, Ramezanzadeh B. Surface modification of Fe2O3 nanoparticles with 3-aminopropyltrimethoxysilane (APTMS): An attempt to investigate surface treatment on surface chemistry and mechanical properties of polyurethane/Fe2O3 nanocomposites. Appl Surf Sci 2014;320:60–72. https://doi.org/10.1016/j.apsusc.2014.09.026.

[123] Kurth DG, Bein T. Thin Films of (3-Aminopropyl)triethoxysilane on Aluminum Oxide and Gold Substrates. Langmuir 1995;11:3061–7. https://doi.org/10.1021/la00008a035.

[124] Cao X, Lee LJ. Control of shrinkage and residual styrene of unsaturated polyester resins cured at low temperatures: I. Effect of curing agents. Polymer (Guildf) 2003;44:1893–902. https://doi.org/10.1016/S0032-3861(03)00014-4.

[125] Wypych G. Handbook of fillers. Toronto, Ontario, Canada: ChemTec Publishing; 2016.

[126] Gogoi P, Boruah R, Dolui SK. Jatropha curcas oil based alkyd/epoxy/graphene oxide (GO) bionanocomposites: Effect of GO on curing, mechanical and thermal properties. Prog Org Coatings 2015;84:128–35. https://doi.org/10.1016/j.porgcoat.2014.09.022.

[127] Lu M, Shim M, Kim S. Reaction mechanism of an unsaturated polyester system containing thickeners. Eur Polym J 2001;37:1075–8.

[128] Wypych G. Handbook of fillers. ChemTec Publishing; 2016.

[129] Gogoi P, Boruah R, Dolui SK. Jatropha curcas oil based alkyd/epoxy/graphene oxide (GO) bionanocomposites: Effect of GO on curing, mechanical and thermal properties. Prog Org Coatings 2015;84:128–35.

[130] Ramirez D, Gómez G, Jaramillo F. Gel time and polymerization kinetics of unsaturated polyester resin/clay montmorillonite nanocomposites. Polym Compos 2015;36:1931–40. https://doi.org/10.1002/pc.23101.

[131] Szczurek A, Barcikowski M, Leluk K, Babiarczuk B, Kaleta J, Krzak J. Improvement of interaction in a composite structure by using a sol-gel functional coating on carbon fibers. Materials (Basel) 2017;10:990. https://doi.org/10.3390/ma10090990.

[132] Ibrahim MS, Sapuan SM, Faieza AA. Mechanical and thermal properties of composites from unsaturated polyester filled with oil palm ash. J Mech Eng Sci 2012;2:133–47. https://doi.org/http://dx.doi.org/10.15282/jmes.2.2012.1.0012.

[133] Muthu J, Dendere C. Functionalized multiwall carbon nanotubes strengthened GRP hybrid composites: Improved properties with optimum fiber content. Compos Part B Eng 2014;67:84–94. https://doi.org/10.1016/j.compositesb.2014.06.012.

[134] Zhang M, Singh RP. Mechanical reinforcement of unsaturated polyester by Al2O3 nanoparticles. Mater Lett 2004;58:408–12. https://doi.org/10.1016/S0167-577X(03)00512-3.

[135] Rusmirović JD, Ivanović JZ, Pavlović VB, Rakić VM, Rančić MP, Djokić V, et al. Novel modified nanocellulose applicable as reinforcement in high-performance nanocomposites. Carbohydr Polym 2017;164:64–74. https://doi.org/10.1016/j.carbpol.2017.01.086.

[136] Kulomaa T, Matikainen J, Karhunen P, Heikkilä M, Fiskari J, Kilpeläinen I. Cellulose fatty acid esters as sustainable film materials – effect of side chain structure on barrier and mechanical properties. RSC Adv 2015;5:80702–8.

[137] Crépy L, Chaveriat L, Banoub J, Martin P, Joly N. Synthesis of cellulose fatty esters as plastics-influence of the degree of substitution and the fatty chain length on mechanical properties. ChemSusChem 2009;2:165–70.

[138] Costa TMH, Gallas MR, Benvenutti E V., da Jornada JAH. Study of Nanocrystalline γ-Al 2 O 3 Produced by High-Pressure Compaction. J Phys Chem B 1999;103:4278–84. https://doi.org/10.1021/jp983791o.

[139] Menczel JD, Prime RB. Thermal Analysis of Polymers: Fundamentals and Applications. John Wiley & Sons, Inc.; 2009.

[140] Lavoratti A, Scienza LC, Zattera AJ. Dynamic-mechanical and thermomechanical properties of cellulose nanofiber/polyester resin composites. Carbohydr Polym 2015;136:955–63.

[141] Džunuzović J V., Pergal M V., Poręba R, Vodnik V V., Simonović BR, Špírková M, et al. Analysis of dynamic mechanical, thermal and surface properties of poly(urethane-ester-siloxane) networks based on hyperbranched polyester. J Non Cryst Solids 2012;358:3161–9. https://doi.org/10.1016/j.jnoncrysol.2012.09.013.

[142] Ornaghi HL, Bolner AS, Fiorio R, Zattera AJ, Amico SC. Mechanical and dynamic mechanical analysis of hybrid composites molded by resin transfer molding. J Appl Polym Sci 2010;118:876–96. https://doi.org/10.1002/app.32388.

[143] Nielsen E, Landel R. Mechanical Properties of Polymers and Composites. 2nd Editio. New York: Marcel Dekker; 1994.

[144] Devi LU, Bhagawan SS, Thomas S. Dynamic mechanical analysis of pineapple leaf/glass hybrid fiber reinforced polyester composites. Polym Compos 2010;31:956–65. https://doi.org/10.1002/pc.20880.

[145] Hsu CP, Lee LJ. Free-radical crosslinking copolymerization of styrene/unsaturated polyester resins: 1. Phase separation and microgel formation. Polymer (Guildf) 1993;34:4496–505. https://doi.org/10.1016/0032-3861(93)90156-5.

[146] Qazvini NT, Mohammadi N. Dynamic mechanical analysis of segmental relaxation in unsaturated polyester resin networks: Effect of styrene content. Polymer (Guildf)

2005;46:9088–96. https://doi.org/10.1016/j.polymer.2005.06.118.

[147] Wang C-Y, Ediger MD. Spatially heterogeneous dynamics in thermoset resins below the glass-transition temperature. J Polym Sci Part B Polym Phys 2000;38:2232–9. https://doi.org/10.1002/1099-0488(20000901)38:17<2132::AID-POLB30>3.0.CO;2-J.

[148] Yang Y-S. Viscosities of unsaturated polyester resins: Combining effects of prepolymer structure, resin composition, and temperature. J Appl Polym Sci 1996;60:2387–95. https://doi.org/10.1002/(SICI)1097-4628(19960627)60:13<2387::AID-APP10>3.0.CO;2-2.

[149] Kalakkunnath S. Viscoelastic relaxation characteristics of rubbery polymer networks and engineering polyesters. University of Kentucky, US, 2007.

[150] Ben H, Dimitrijevic M, Kojovic A, Stojanovic D, Obradovic-Djuricic K, Jancic-Heinemann R, et al. The effect of alumina nanofillers size and shape on mechanical behavior of PMMA matrix composite. J Serbian Chem Soc 2014;79:1295–307. https://doi.org/10.2298/JSC140121035B.

[151] Alzarrug FA, Dimitrijević MM, Jančić Heinemann RM, Radojević V, Stojanović DB, Uskoković PS, et al. The use of different alumina fillers for improvement of the mechanical properties of hybrid PMMA composites. Mater Des 2015;86:575–81. https://doi.org/10.1016/j.matdes.2015.07.069.

[152] Drah A, Tomić N, Kovačević T, Đokić V, Tomić M, Jančić-Heinemann R, et al. Structural and surface modified alumina particles used as reinforcement in polymer based composites with improved toughness. Mech Compos Mater 2019;In Press.

[153] Pracella M, Haque MM-U, Alvarez V. Compatibilization and Properties of EVA Copolymers Containing Surface-Functionalized Cellulose Microfibers. Macromol Mater Eng 2010;295:949–57. https://doi.org/10.1002/mame.201000175.

[154] Hummel D. Infrared Analysis of Polymers, Resins and Additives: Plastics, Elastomers, Fibers and Resins, Part 1. New York: John Wiley & Sons, Inc.; 1971.

[155] Ulibarri MA, Hernandez MJ, Cornejo J. Hydrotalcite-like compounds obtained by anion exchange reactions. J Mater Sci 1991;26:1512–6. https://doi.org/10.1007/BF00544660.

[156] Grey IE, Ragozzini R. Formation and characterization of new magnesium aluminum hydroxycarbonates. J Solid State Chem 1991;94:244–53. https://doi.org/10.1016/0022-4596(91)90189-O.

[157] Abellán G, Coronado E, Martí-Gastaldo C, Pinilla-Cienfuegos E, Ribera A. Hexagonal nanosheets from the exfoliation of Ni2+-Fe3+ LDHs: a route towards layered multifunctional materials. J Mater Chem 2010;20:7451. https://doi.org/10.1039/c0jm01447h.

[158] Busca G, Trifiro F, Vaccari A. Characterization and catalytic activity of cobalt-chromium mixed oxides. Langmuir 1990;6:1440–7. https://doi.org/10.1021/la00099a002.

[159] Rodríguez M, Sifontes ÁB, Méndez FJ, Díaz Y, Cañizales E, Brito JL. Template synthesis and characterization of mesoporous γ-Al2O3 hollow nanorods using Stevia rebaudiana leaf aqueous extract. Ceram Int 2013;39:4499–506. https://doi.org/10.1016/j.ceramint.2012.11.044.

[160] Macêdo MIF, Osawa CC, Bertran CA. Sol-Gel Synthesis of Transparent Alumina Gel and Pure Gamma Alumina by Urea Hydrolysis of Aluminum Nitrate. J Sol-Gel Sci Technol 2004;30:135–40. https://doi.org/10.1023/B:JSST.0000039497.46154.8f.

[161] Macêdo MIF, Bertran CA, Osawa CC. Kinetics of the γ → α-alumina phase transformation by quantitative X-ray diffraction. J Mater Sci 2007;42:2830–6. https://doi.org/10.1007/s10853-006-1364-1.

[162] Li D-Y, Lin Y-S, Li Y-C, Shieh D-L, Lin J-L. Synthesis of mesoporous

pseudoboehmite and alumina templated with 1-hexadecyl-2,3-dimethyl-imidazolium chloride. Microporous Mesoporous Mater 2008;108:276–82. https://doi.org/10.1016/j.micromeso.2007.04.009.

[163] Liu C, Shih K, Gao Y, Li F, Wei L. Dechlorinating transformation of propachlor through nucleophilic substitution by dithionite on the surface of alumina. J Soils Sediments 2012;12:724–33. https://doi.org/10.1007/s11368-012-0506-0.

[164] Wijnja H, Schulthess CP. ATR–FTIR and DRIFT spectroscopy of carbonate species at the aged γ-Al2O3/water interface. Spectrochim Acta Part A Mol Biomol Spectrosc 1999;55:861–72. https://doi.org/10.1016/S1386-1425(98)00236-4.

[165] Lee DH, Condrate RA. An FTIR spectral investigation of the structural species found on alumina surfaces. Mater Lett 1995;23:241–6. https://doi.org/10.1016/0167-577X(95)00039-9.

[166] Yoshida T, Yamaguchi T, Ilda Y, Nakayama S. XPS Study of Pb(II) Adsorption on γ-Al 2 O 3 Surface at High pH Conditions. J Nucl Sci Technol 2003;40:672–8. https://doi.org/10.1080/18811248.2003.9715405.

[167] Wagner HL. The Mark–Houwink–Sakurada Relation for Poly(Methyl Methacrylate). J Phys Chem Ref Data 1987;16:165–73. https://doi.org/10.1063/1.555776.

[168] Bischoff J, Desreux V. Etude des solutions diluées de polyméthacrylate de méthyle I. Bull Des Sociétés Chim Belges 2010;61:10–32. https://doi.org/10.1002/bscb.19520610103.

[169] Klein SM, Manoharan VN, Pine DJ, Lange FF. Preparation of monodisperse PMMA microspheres in nonpolar solvents by dispersion polymerization with a macromonomeric stabilizer. Colloid Polym Sci 2003;282:7–13. https://doi.org/10.1007/s00396-003-0915-0.

[170] Han D, Li X, Zhang L, Wang Y, Yan Z, Liu S. Hierarchically ordered meso/macroporous γ-alumina for enhanced hydrodesulfurization performance. Microporous Mesoporous Mater 2012;158:1–6. https://doi.org/10.1016/j.micromeso.2012.03.022.

[171] Li H, Zhang L, Dai H, He H. Facile Synthesis and Unique Physicochemical Properties of Three-Dimensionally Ordered Macroporous Magnesium Oxide, Gamma-Alumina, and Ceria−Zirconia Solid Solutions with Crystalline Mesoporous Walls. Inorg Chem 2009;48:4421–34. https://doi.org/10.1021/ic900132k.

[172] Phuengprasop T, Sittiwong J, Unob F. Removal of heavy metal ions by iron oxide coated sewage sludge. J Hazard Mater 2011;186:502–7. https://doi.org/10.1016/j.jhazmat.2010.11.065.

[173] Bhat A, Megeri GB, Thomas C, Bhargava H, Jeevitha C, Chandrashekar S, et al. Adsorption and optimization studies of lead from aqueous solution using γ-Alumina. J Environ Chem Eng 2015;3:30–9. https://doi.org/10.1016/j.jece.2014.11.014.

[174] Kovačević D, Pohlmeier A, Özbaş G, Narres H-D, Kallay MJN. The adsorption of lead species on goethite. Colloids Surfaces A Physicochem Eng Asp 2000;166:225–33. https://doi.org/10.1016/S0927-7757(99)00449-5.

[175] Gustafsson J. Visual MINTEQ 2011.

[176] Yang S, Li J, Shao D, Hu J, Wang X. Adsorption of Ni(II) on oxidized multi-walled carbon nanotubes: Effect of contact time, pH, foreign ions and PAA. J Hazard Mater 2009;166:109–16. https://doi.org/10.1016/j.jhazmat.2008.11.003.

[177] Mahdavi S, Jalali M, Afkhami A. Heavy metals removal from aqueous solutions by Al2O3 nanoparticles modified with natural and chemical modifiers. Clean Technol Environ Policy 2015;17:85–102. https://doi.org/10.1007/s10098-014-0764-1.

[178] Mahmoud MA. Kinetics and thermodynamics of aluminum oxide nanopowder as adsorbent for Fe (III) from aqueous solution. Beni-Suef Univ J Basic Appl Sci

2015;4:142–9. https://doi.org/10.1016/j.bjbas.2015.05.008.

[179] Mahmoud MA. Adsorption of Cadmium onto Orange Peels: Isotherms, Kinetics, and Thermodynamics. J Chromatogr Sep Tech 2014;05. https://doi.org/10.4172/2157-7064.1000238.

[180] Drah A, Tomić NZ, Veličić Z, Marinković AD, Radovanović Ž, Veličković Z, et al. Highly ordered macroporous γ-alumina prepared by a modified sol-gel method with a PMMA microsphere template for enhanced Pb2+, Ni2+ and Cd2+ removal. Ceram Int 2017;43:13817–27. https://doi.org/10.1016/j.ceramint.2017.07.102.

[181] Saadi Z, Saadi R, Fazaeli R. Dynamics of Pb(II) adsorption on nanostructured γ - alumina: calculations of axial dispersion and overall mass transfer coefficients in the fixed-bed column. J Water Health 2015;13:790–800. https://doi.org/10.2166/wh.2015.271.

PRILOG

Biografija

Abdusalam Mohamed Ali Alhemali Drah je rođen 01.01.1961. godine u Zlitenu, Libija. Završio je Engleski jezik i Pomorske studije 1989. godine na Arapskoj Pomorskoj Akademiji (Arab Maritime Academy) u Sharjahu u Ujedinjenim Arapsim Emiratima (UAE). Tokom studija obučavao se na različitim tipovima brodova radi sticanja iskustva. Tokom 2002. godine dobio je Uverenje o osposebljnosti za glavnog inženjera (Chief Engineering Certificate) na temi „The influence of the thermal stresses on marine water tube boilers under normal and maximum water working pressures" sa prosečnom ocenom 72%, od strane Libijske Akademije za pomorska ispitivanja u Tripoliju. Istovremeno, kandidat je završio diplomske studije u oblasti mašinskog i industrijskog inženjerstva na temi „Comparing of ductile iron and austempered ductile iron mechanical properties", sa prosečnom ocenom 78%. Nakon toga kandidat se upisao na Školu za Tehničke studije i ispitivanja, Fakulteta za inženjerstvo na Univerzitetu Alfateh gde je tokom 2009. godine završio master studije odbranivši tezu pod naslovom„ The influence of laser surface hardening on austempered ductile iron" sa prosečnom ocenom 82%. Tokom 2015. godine kandidat je upisao doktorske studije na Tehnološko-metalurškom fakultetu, Univerziteta u Beogradu, Katedra za Konstrukcione i specijalne materijale, smer Inženjerstvo materijala, položio sve ispite, kao i završni ispit predviđene planom i programom. Kandidat tečno govori engleski jezik, poznaje metodologiju za ispitivanje materijala i rad na računaru.

Radno iskustvo:

- 1984-1987–mlađi inženjer na brodu - General National Maritime Transport Company (GNMTC),
- 1990-2002–pomorski inženjer kod iste kompanije,
- 2004-2014–učitelj i instruktor za studente smera mašinsko inženjerstvo na master studijama na Institutu za poslovne studije, Zliten, Libya.

Oblast naučno-istraživačkog rada Abdusalam Draha obuhvata tercijarnu reciklažu otpadne PET ambalaže radi dobijanja nezasićene poliestarske smole, koja služi kao matrica za dobijanje novih kompozitnih materijala poboljšanih dinamičko-mehaničkih i termičkih svojstava. Pored toga ispitana je upotreba kompozita na bazi alumine i PMMA za uklanjanje jona teških metala iz vode.

Abdusalam Drah je kao koautor i autor učestvovao u izradi i publikaciji 8 naučnih radova u kategorijama: M21 - 1, M22 - 1, M23 - 1, M24 - 1, M33 - 4. Iz oblasti istraživanja kojoj pripada tema doktorske disertacije, kandidat je autor 1 rada objavljenog u međunarodnom časopisu izuzetnih vrednosti (oznaka grupe M20: vrsta rezultata M21a), 1 rada objavljenog u istaknutom međunarodnom časopisu (oznaka grupe M20: vrsta rezultata M22), 1 rada objavljenog u međunarodnom časopisu (oznaka grupe M20: vrsta rezultata M23), 1 rada objavljenog u nacionalnom časopisu međunarodnog značaja koji nije na SCI listi (oznaka grupe M20: vrsta rezultata M24). Pored toga, kandidat je u oblasti istraživanja kojoj pripada tema doktorske disertacije) kao koautor objavio 1 saopštenje prikazano na međunarodnom skupu (oznaka grupe M30: vrsta rezultata M33).

Spisak objavljenih radova i saopštenja vezanih za doktorsku disertaciju

Kategorija M21:

A. Drah, N. Tomić, Z. Veličić, A. Marinković, Ž. Radovanović, Z. Veličković, R. Jančić-Heinemann, Highly ordered macroporousγ-alumina prepared by modified sol-gel method with PMMA microsphere template for enhanced Pb^{2+}, Ni^{2+} and Cd^{2+} removal, *Ceramic International*, 43, (2017) 13817-13827; ISSN 0272-8842; IF(2016)=2.986 (M21a); DOI: 10.1016/j.ceramint.2017.07.102

Kategorija M22:

1. **Abdusalam Drah**, Tihomir Kovačević, Jelena Rusmirović, Nataša Tomić, Saša Brzić, Marica Bogosavljavić, Aleksandar Marinković, Effect of surface activation of alumina particles on the performances of thermosetting-based composite materials, *Journal of Composite Materials* 53(19) (2019), 2727-2742, ISSN: 0021-9983, IF: 1.755, DOI: 10.1177/0021998319839133

Kategorija M23:

1. **Abdusalam Drah**, Nataša Tomić, Tihomir Kovačević, Veljko Đokić, Miloš Tomić, Radmila Jančić-Heinemann, Aleksandar Marinković, Structural and surface modified alumina particles used as reinforcement in polymer based composites with improved toughness, *Mechanics of Composite Materials*, In press, (2019), ISSN: 0191-5665, IF: 0,703

Kategorija M33:

1. Tihomir Kovačević, **A. Drah**, A. Božić, M. stamenović, J. Rusmirović, N. Tomić, V. Alivojvodić, A. Marinković, The surface modification of alumina particles for its application in unsaturated polyester resins, 26th International Conference Ecological Truth & Environmental Research 12-15 June 2018, 338-342, Bor Lake, Bor, Serbia, ISBN: 978-86-6305-076-1

Prilog 1

Izjava o autorstvu

Ime i prezime autora: Abdusalam Drah
Broj indeksa:

Izjavljujem
da je doktorska disertacija pod naslovom
„Funkcionalizacija čestica aluminijum-oksida za kompozite na bazi nezasićenih poliestarskih smola dobijenih iz reciklovanog poli(etilentereftalata)"

- rezultat sopstvenog istraživačkog rada;
- da disertacija u celini ni u delovima nije bila predložena za sticanje druge diplome prema studijskim programima drugih visokoškolskih ustanova;
- da su rezultati korektno navedeni i
- da nisam kršio/la autorska prava i koristio/la intelektualnu svojinu drugih lica.

Potpis autora

U Beogradu, _____

_____

Prilog 2

Obrazac 6.

Izjava o istovetnosti štampane i elektronske verzije doktorskog rada

Ime i prezime autora: Abdusalam Drah
Broj indeksa:
Studijski program: Inženjerstvo materijala
Naslov rada: „Funkcionalizacija čestica aluminijum-oksida za kompozite na bazi nezasićenih poliestarskih smola dobijenih iz reciklovanog poli(etilentereftalata)"
Mentor: Aleksandar Marinković

Izjavljujem da je štampana verzija mog doktorskog rada istovetna elektronskoj verziji koju sam predao/la radi pohranjena u **Digitalnom repozitorijumu Univerziteta u Beogradu.**
Dozvoljavam da se objave moji lični podaci vezani za dobijanje akademskog naziva doktora nauka, kao što su ime i prezime, godina i mesto rođenja i datum odbrane rada.
Ovi lični podaci mogu se objaviti na mrežnim stranicama digitalne biblioteke, u elektronskom katalogu i u publikacijama Univerziteta u Beogradu.

Potpis autora

U Beogradu, _____

_____

Prilog 3

Obrazac 7.

Izjava o korišćenju

Ovlašćujem Univerzitetsku biblioteku „Svetozar Marković" da u Digitalni repozitorijum Univerziteta u Beogradu unese moju doktorsku disertaciju pod naslovom:
„Funkcionalizacija čestica aluminijum-oksida za kompozite na bazi nezasićenih poliestarskih smola dobijenih iz reciklovanog poli(etilentereftalata)"
koja je moje autorsko delo.

Disertaciju sa svim prilozima predao/la sam u elektronskom formatu pogodnom za trajno arhiviranje.

Moju doktorsku disertaciju pohranjenu u Digitalnom repozitorijumu Univerziteta u Beogradu i dostupnu u otvorenom pristupu mogu da koriste svi koji poštuju odredbe sadržane u odabranom tipu licence Kreativne zajednice (Creative Commons) za koju sam se odlučio/la.

1. Autorstvo (CC BY)
2. Autorstvo – nekomercijalno (CC BY-NC)
3. Autorstvo – nekomercijalno – bez prerada (CC BY-NC-ND)
4. Autorstvo – nekomercijalno – deliti pod istim uslovima (CC BY-NC-SA)
5. Autorstvo – bez prerada (CC BY-ND)
6. Autorstvo – deliti pod istim uslovima (CC BY-SA)

(Molimo da zaokružite samo jednu od šest ponuđenih licenci.

Kratak opis licenci je sastavni deo ove izjave).

Potpis autora

U Beogradu, _____

_____

1. **Autorstvo**. Dozvoljavate umnožavanje, distribuciju i javno saopštavanje dela, i prerade, ako se navede ime autora na način određen od strane autora ili davaoca licence, čak i u komercijalne svrhe. Ovo je najslobodnija od svih licenci.

2. **Autorstvo – nekomercijalno**. Dozvoljavate umnožavanje, distribuciju i javno saopštavanje dela, i prerade, ako se navede ime autora na način određen od strane autora ili davaoca licence. Ova licenca ne dozvoljava komercijalnu upotrebu dela.

3. **Autorstvo – nekomercijalno – bez prerada**. Dozvoljavate umnožavanje, distribuciju i javno saopštavanje dela, bez promena, preoblikovanja ili upotrebe dela u svom delu, ako se navede ime autora na način određen od strane autora ili davaoca licence. Ova licenca ne dozvoljava komercijalnu upotrebu dela. U odnosu na sve ostale licence, ovom licencom se ograničava najveći obim prava korišćenja dela.

4. **Autorstvo – nekomercijalno – deliti pod istim uslovima**. Dozvoljavate umnožavanje, distribuciju i javno saopštavanje dela, i prerade, ako se navede ime autora na način određen od strane autora ili davaoca licence i ako se prerada distribuira pod istom ili sličnom licencom. Ova licenca ne dozvoljava komercijalnu upotrebu dela i prerada.

5. **Autorstvo – bez prerada**. Dozvoljavate umnožavanje, distribuciju i javno saopštavanje dela, bez promena, preoblikovanja ili upotrebe dela u svom delu, ako se navede ime autora na način određen od strane autora ili davaoca licence. Ova licenca dozvoljava komercijalnu upotrebu dela.

6. **Autorstvo – deliti pod istim uslovima**. Dozvoljavate umnožavanje, distribuciju i javno saopštavanje dela, i prerade, ako se navede ime autora na način određen od strane autora ili davaoca licence i ako se prerada distribuira pod istom ili sličnom licencom. Ova licenca dozvoljava komercijalnu upotrebu dela i prerada. Slična je softverskim licencama, odnosno licencama otvorenog koda.